



1 Search for Double Beta Decay to Excited States

2 I. Guinn

3 University of Washington, Seattle, WA,
4 USA

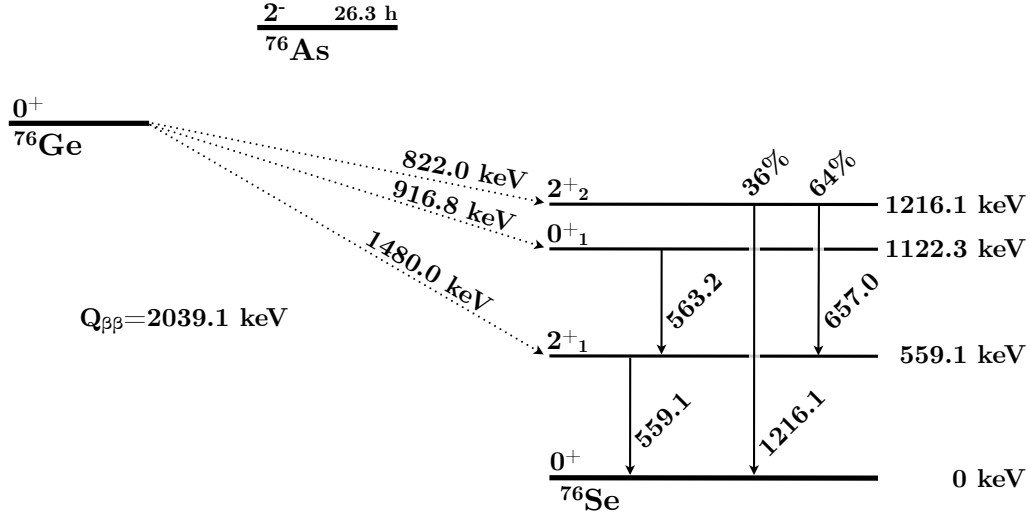
5 CONTENTS

6	I. Introduction	2
7	II. Simulation of Excited State Decays	2
8	A. Comparing <code>decay0</code> to the Kotila and Iachello generator	3
9	III. Background Model Simulation	4
10	IV. Multi-detector events Selection	5
11	A. Variation in Detector Configuration	5
12	B. Dead Layer Effects	8
13	C. Dead Time Effects	8
14	D. Additional Effects	9
15	V. Region of Interest Selection	11
16	A. Signal ROI Optimization	12
17	B. Background ROI Selection	12
18	C. ROI Detection Efficiency and Uncertainty	12
19	D. Detector Crosstalk	13
20	VI. Background Cuts	15
21	A. Enriched Source Detector Cut	15
22	B. Coincident and Sum Energy Cuts	15
23	C. Muon Veto Cut	17
24	VII. Final Efficiency Measurements	17
25	VIII. Double Beta Decay to Excited States Results	18
26	IX. Validation	18
27	A. Data Rate	18
28	B. Background Cut Evaluation	18
29	X. Results	19
30	A. Statistical Methods	19
31	B. Limits and Sensitivities	21
32	References	21
33	A. Detailed Results for All Decay Modes	21
34	B. $2\nu\beta\beta$ to 0_1^+	22
35	C. $2\nu\beta\beta$ to 2_1^+	40
36	D. $2\nu\beta\beta$ to 2_2^+	47
37	1. 559 keV peak	47
38	2. 657 keV peak	54
39	3. 1216 keV peak	60
40	E. $0\nu\beta\beta$ to 0_1^+	66
41	F. $0\nu\beta\beta$ to 2_1^+	73
42	G. $0\nu\beta\beta$ to 2_2^+	80
43	1. 559 keV peak	80
44	2. 657 keV peak	87
45	3. 1216 keV peak	93

46 I. INTRODUCTION

47 ^{76}Se has 3 excited states that ^{76}Ge can decay into in addition to the ground state, as shown in figure 13. While the
 48 ground state decay has been observed, none of the decays to excited states have been yet. Each excited state decay
 49 will have a $\beta\beta$ -decay with a reduced Q -value compared to the ground state decay. The excited state decays will also
 50 promptly produce one or two γ -rays at known energies. These γ s will typically travel several cms before absorption
 51 and will often hit a different detector from the $\beta\beta$ -decay site, meaning that we can search for peaks at these energies.

52



53 FIG. 1 Energy level diagram for $\beta\beta$ -decay of ^{76}Ge to ^{76}Se , including excited states. The Q -values for each decay branch and
 54 the energies and branching ratios for the deexcitation γ s are shown next to their corresponding lines.

55 Furthermore, since these *gammas* hit separate detectors, this signal is inherently multi-site event. As shown in
 56 figure 2, by searching for the peak only in events with high hit multiplicity, i.e. events that involve 2 or more detectors
 57 hit, $\sim 85\%$ of backgrounds can be cut, while only sacrificing $\sim 25\%$ of the signal. Furthermore, the coincident detector
 58 hit(s) can provide additional observables that can be used to further discriminate excited state signals from multi-site
 59 backgrounds. This chapter will describe the various background reduction data cuts and how they are implemented.
 60 It will also evaluate the detection efficiency and systematic error associated with each cut based on simulations of the
 61 MAJORANA DEMONSTRATOR.

62 II. SIMULATION OF EXCITED STATE DECAYS

63 Simulations of the ^{76}Ge decay to excited states of ^{76}Se are used to evaluate the detection efficiency of the analysis
 64 presented in this document. Two different event generators are used to generate ^{76}Ge $\beta\beta$ -decay within MAGE. The
 65 first generator uses calculations of the phase space factors from J. Kotila and F. Iachello[1]. It is implemented in the
 66 mage class `MGGeneratorDoubleBeta` using data tables with the distribution of both electron energies and angular
 67 correlations. These data tables are provided for the $2\nu\beta\beta$ and $0\nu\beta\beta$ decays to the ground state of ^{76}Se , but not for the
 68 decays to any excited state of ^{76}Se . This calculation is an improvement over other phase space calculations thanks to
 69 an exact evaluation of the Dirac wave functions of the electrons involving a finite nuclear size and electron screening.
 70 A second event generator packaged with MAGE is `decay0`[2], a fortran program that generates a wide variety of $\beta\beta$ -
 71 and β -decays. `decay0` is capable of generating $2\nu\beta\beta$ and $0\nu\beta\beta$ for ^{76}Ge to ^{76}Se 0^+ and 2^+ excited states using a
 72 variety of physics mechanisms. For the excited state decays, the deexcitation γ s and conversion electrons are also
 73 generated. Several modifications were made to `decay0` for this analysis. First, the precision of the excited state
 74 deexcitation energies was increased from 1 keV to 0.001 keV (The γ energies changed from 559 to 559.101 keV, from
 75 563 to 563.178 keV, from 657 to 657.041 keV, and from 1216 to 1216.104 keV). Second, angular correlations were
 76 added for the $2_2^+-2_1^+-0_+^{g.s.}$ deexcitation γ cascade which involves a 657 keV γ with multipolarity E2+M1 and mixing

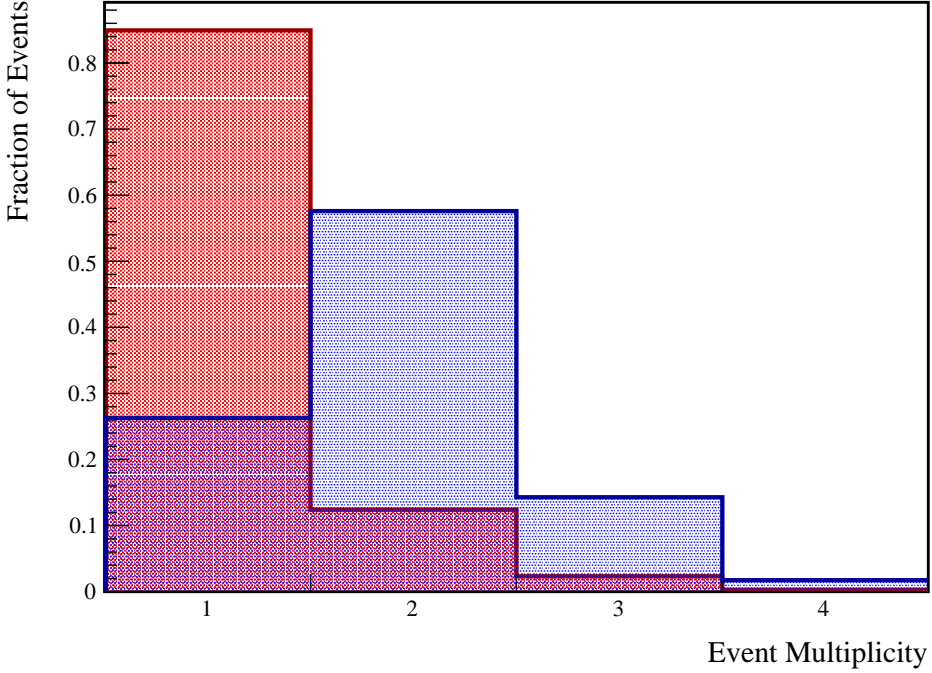


FIG. 2 The simulated distribution of ROI event multiplicities in the background model and $\beta\beta$ E.S.to 0_1^+ decay. These simulations use the DS6 detector configuration.

ratio of +5.2 followed by a 559 keV γ with multipolarity E2[3]. The angular distribution between the γ s is[4]

$$P(\theta) \propto 1 - 0.372 \cdot \cos^2(\theta) + 0.0439 \cdot \cos^4(\theta) \quad (1)$$

The angular correlation for the $0_1^+ - 2_1^+ - 0_{g.s.}^+$ deexcitation was previously included in `decay0`, and is represented by the angular distribution

$$P(\theta) \propto 1 - 3 \cdot \cos^2(\theta) + 4 \cdot \cos^4(\theta) \quad (2)$$

Running `decay0` produces data files with the initial momenta of the generated particles. The MAGE class `MGGeneratorDecay0` reads these datafiles and generates initial positions for these events.

Simulations were run for ${}^{76}\text{Ge}$ $2\nu\beta\beta$ and $0\nu\beta\beta$ to the ${}^{76}\text{Se}$ 0_1^+ , 2_1^+ and 2_2^+ excited states using the `decay0` generator. For each decay mode, 5000000 event primaries were generated in the bulk of the enriched detectors and 500000 primaries were generated in the bulk of the natural detectors. These events were skimmed with the relative activities set equal to the total isotopic mass in each set of detectors: 26.2538 kg in enriched detectors, and 1.1232 kg in natural detectors. These simulations were additionally post-processed with the dead layer thickness set to 0, and skim files were produced both with and without a dead layer, and with and without dead times. Figure 3 shows an energy spectrum of multiplicity 2 events produced by the simulation of the ${}^{76}\text{Ge}$ decay to the 0_1^+ excited state of ${}^{76}\text{Se}$.

90

91 A. Comparing `decay0` to the Kotila and Iachello generator

92 The Kotila and Iachello generator performs a more calculation of phase space than `decay0` and is used for the
 93 MAJORANA DEMONSTRATOR's measurement of $2\nu\beta\beta$ and $0\nu\beta\beta$ to the ground state. Because Kotila and Iachello
 94 present only the phase space integral for the excited state decays, and do not include the energy and angular dis-
 95 tributions, `decay0` is used for this analysis. To evaluate the accuracy of `decay0`, we can compare the spectrum of
 96 the $2\nu\beta\beta$ to the ground state it generates to that of Kotila and Iachello; this comparison will reflect the error with

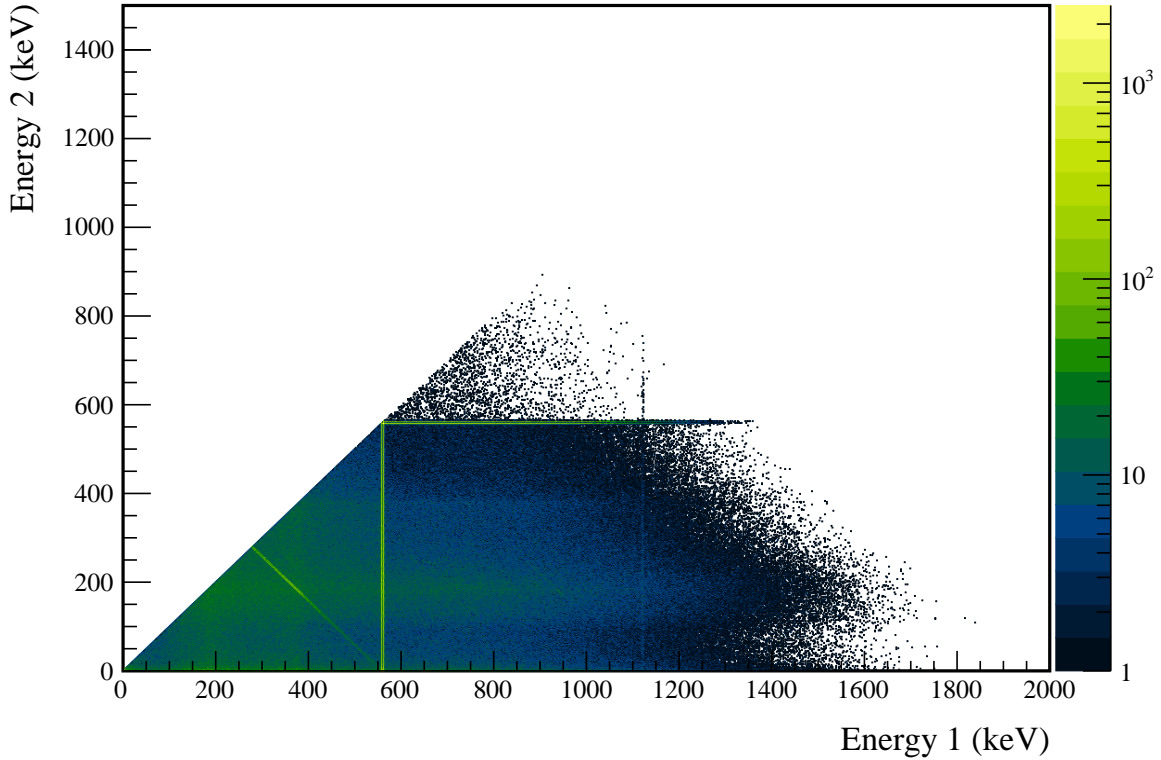


FIG. 3 Multiplicity 2 energy spectrum produced by a decay0 simulation of $2\nu\beta\beta$ of ^{76}Ge to the 0_1^+ state of ^{76}Se .

respect to the true value if we assume that the error on the latter spectrum is much smaller than that of decay0. This comparison is performed using a Kolmogorov-Smirnov (KS) test. The KS test statistic is the maximum difference between the CDF of each normalized energy spectrum. As we will see in chapter ??, this test is useful in evaluating the uncertainties in the measurement presented in this thesis. The CDF difference is shown in figure 4, with a KS statistic of 0.00081. While this error is statistically significant at a level of 97%, we will see that the systematic error generated is subdominant.

III. BACKGROUND MODEL SIMULATION

A simulation of the background spectrum measured by the MAJORANA DEMONSTRATOR will be used to optimize the search for $\beta\beta$ E.S.. MAGE simulations of a variety of decay chains, including ^{232}Th , ^{238}U , ^{40}K , ^{60}Co , ^{222}Rn and ^{68}Ge , have been run using event generators internal to GEANT4. Geometries of large number of component groups have been defined encompassing one or more physical component of the experiment. Decays can be generated in either the bulk of a component group, or on the surface. The activity of each isotope from each component group is determined by fitting a linear combination of the simulated energy spectra to the measured background spectrum. An incomplete version of this fit is used for this thesis, producing the spectra in figures 5 and 6. ^{68}Ge decays with a half-life of 271 days, so its activity is scaled to represent the activity of each major dataset. ^{210}Pb in the lead shield is simulated using a special generator that samples bremsstrahlung x-rays emitted from the surface of a thick lead shield [5].

The background model used for this analysis is known to be inaccurate. Since it is only used for optimizing the search for $\beta\beta$ E.S. and is not important for the detection efficiency calculation, this does not affect the accuracy of the result presented. For future versions of this analysis, a complete and more accurate background model will be used, which will result in small improvements to the optimization.

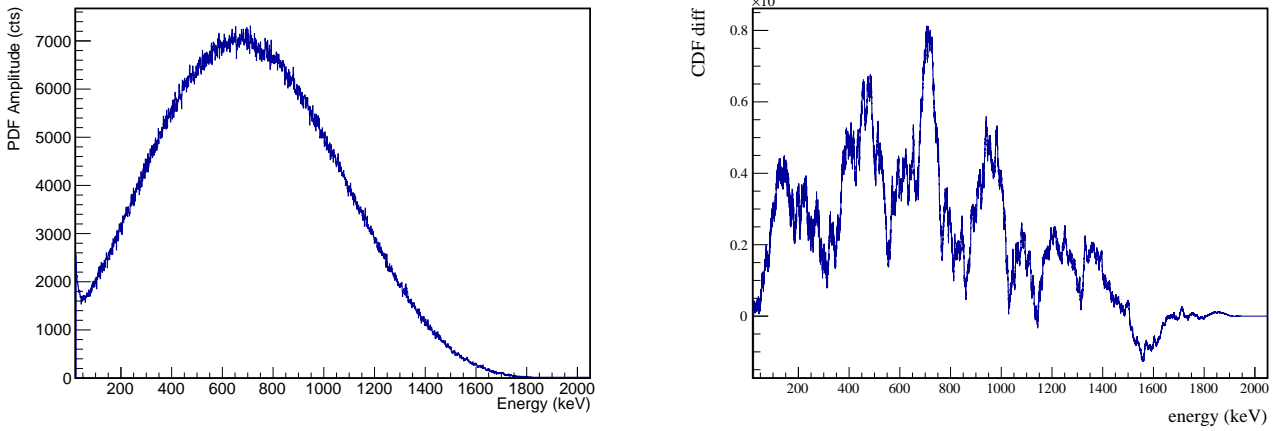


FIG. 4 A KS test is performed comparing the `decay0` $2\nu\beta\beta$ to the ground state energy spectrum to that of Kotila and Iachello. The `decay0` spectrum is shown, along with the difference between the CDF of each spectrum.

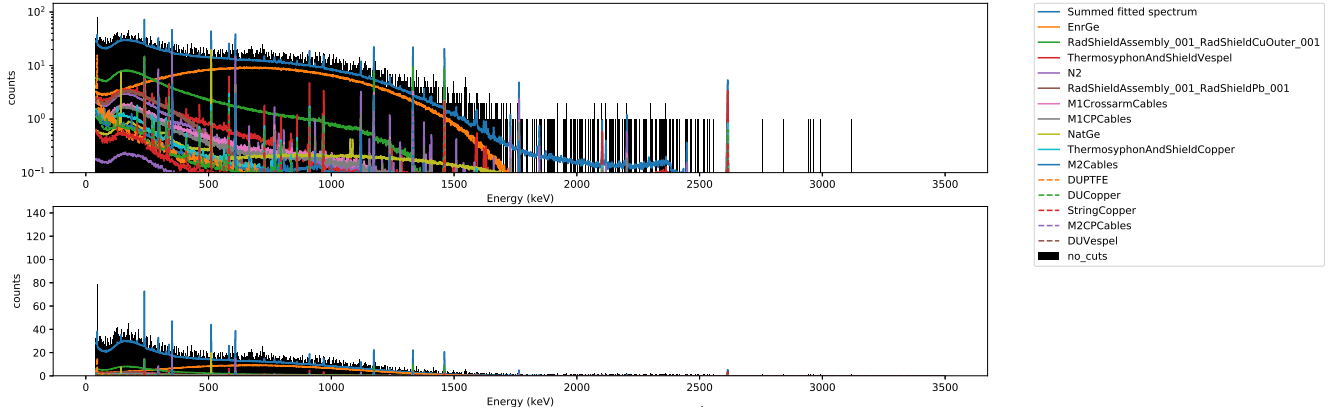


FIG. 5 Energy spectrum of multiplicity 1 events produced from a simulation of the background model, with most common source components labelled.

120 IV. MULTI-DETECTOR EVENTS SELECTION

121 Simultaneous detector hits are combined into events by the event builder (see section ?? and appendix app:eventbuilder).
 122 Events are combined in a 4 μ s rolling window. This window is expected to accept virtually all true coincidence events
 123 (see figure 7. In a small number of runs, clocks between different Gretina cards were desyncronized. For these runs,
 124 the clocks were resynchronized by applying a timing offset during event building that is measured by seeking the time
 125 offset that aligns pulser events. With a typical overall rate between both modules of < 1 Hz, < .4% of all multi-site
 126 events are expected to originate from accidental coincidence, making this a negligible background. Once all the data
 127 has gone through the processing chain described in section ??, the skim files from all good runs in datasets 16a are
 128 collected into a single skim file containing a TTree with only multi-site events by `es_skimdata`.
 129

131 A. Variation in Detector Configuration

132 Throughout the runtime of the MAJORANA DEMONSTRATOR, not all detectors were simultaneously active, and
 133 within each dataset, the set of active detectors varied significantly. Because we are looking at multi-site event events,
 134 the detection efficiency for $\beta\beta$ E.S. events in any detector depends on which other detectors are enabled. For this
 135 reason, detection efficiency is computed for each module in its entirety rather than for individual detectors. To account

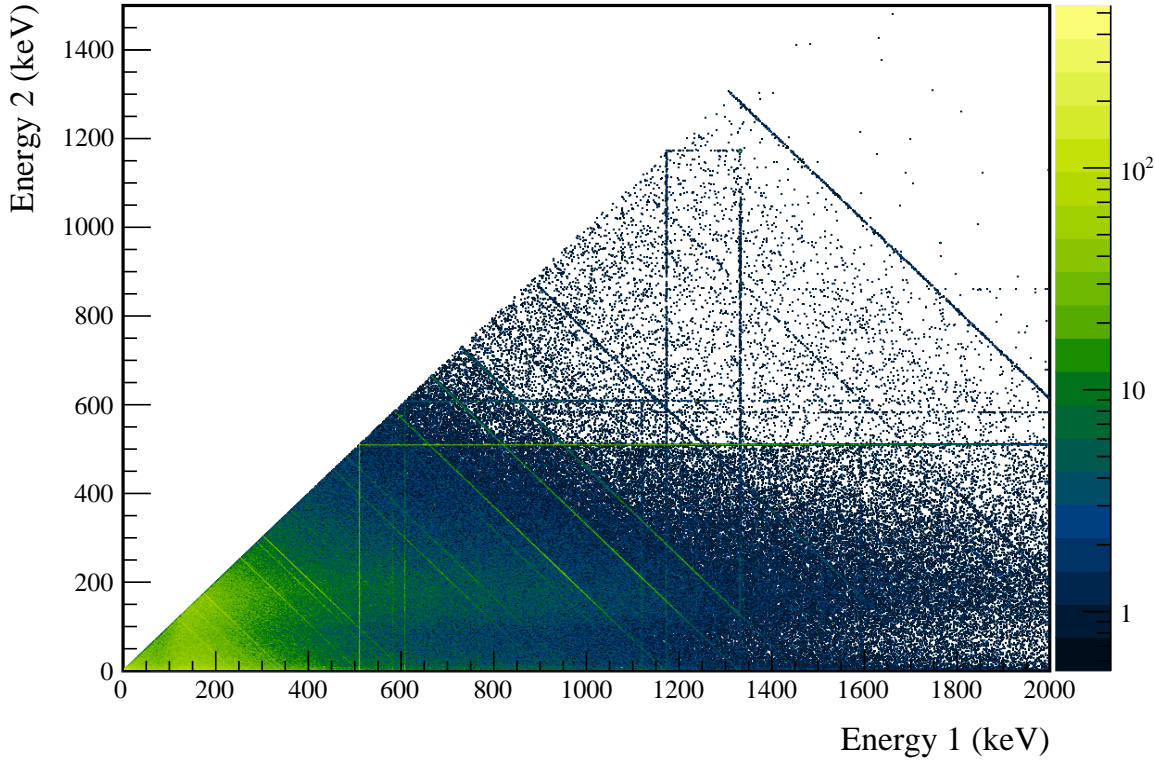


FIG. 6 Multiplicity 2 energy spectrum produced by a simulation of a preliminary version of the MAJORANA DEMONSTRATOR background model.

for changes in detector configuration, each dataset is divided into subdatasets based on which detectors are active. The subdatasets are described by a pair of 64-bit masks, one for each module, with each bit representing a single detector's state. To decode the bitmask, the b 'th least significant bit represents string position P , detector position D if

$$b = 8 \cdot P + D \quad (3)$$

The set of runs and active channels for each run were determined by the run selection and data cleaning committee, and the procedures are outlined in [6]. The program `es_getdatasets` uses these selections to sort each run into a subdataset.

The detection efficiency is defined as the probability of a signal event in any detector, including inactive detectors. Detection efficiency is calculated individually for each subdataset and for each module by creating a separate skim file for each subdataset as outlined in section ???. The final efficiency is then computed as a isotopic exposure weighted average of the efficiency within each subdataset. Any efficiency uncertainties are assumed to be totally correlated between subdatasets, meaning they are added linearly instead of in quadrature. The livetime of each subdataset is calculated by the program `es_livetimes` by totalling the run time in each run, and subtracting any deadtime that affects the entire module, including deadtime caused by the muon veto system and by liquid nitrogen fills. Additional sources of deadtime that affect individual detectors are calculated as inefficiencies rather than being subtracted from the livetime, as discussed in section ???. This is done because deadtime in any individual detector affects the detection efficiency of all other detectors. The isotopic exposure is computed by multiplying the livetime of each module of the total isotopic mass in each module, including mass in inactive detectors and dead layers. Table I lists each subdataset along with its livetime and exposure.



TABLE I List of each subdataset with its livetime, detection efficiency measured for the $\beta\beta$ E.S.to 0_1^+ decay, and total isotopic exposure. Note the large amount of variance in the detection efficiency.

DS	M1 Detector Mask	M2 Detector Mask	Run Time (days)	M1 L.T. (days)	M1 Eff.	M2 L.T. (days)	M2 Eff.	Exposure (kg·y)
DS1	061a08001e0e1c00	0000000000000000	2.64	2.60	1.693%	0.00	0.000%	0.109
DS1	161a08341e0e1c00	0000000000000000	0.02	0.02	1.978%	0.00	0.000%	0.001
DS1	161a0c341e0e1c00	0000000000000000	4.51	4.48	1.915%	0.00	0.000%	0.188
DS1	161a0c361e0e1c00	0000000000000000	3.49	3.48	1.449%	0.00	0.000%	0.146
DS1	1e1a00001e0e1c00	0000000000000000	7.82	7.73	2.015%	0.00	0.000%	0.324
DS1	1e1a08001e0e1c00	0000000000000000	25.49	25.19	2.202%	0.00	0.000%	1.057
DS1	1e1a08041e0e1c00	0000000000000000	2.95	2.93	2.277%	0.00	0.000%	0.123
DS1	1e1a08141e0e1c00	0000000000000000	0.26	0.25	2.297%	0.00	0.000%	0.011
DS1	1e1a08301e0e1c00	0000000000000000	1.40	1.37	2.305%	0.00	0.000%	0.057
DS1	1e1a08341e0e1c00	0000000000000000	7.58	7.50	2.095%	0.00	0.000%	0.315
DS1	1e1a0c001e0e1c00	0000000000000000	1.96	1.93	2.226%	0.00	0.000%	0.081
DS1	1e1a0c341e0e1c00	0000000000000000	0.67	0.67	2.296%	0.00	0.000%	0.028
DS2	1e1a08001e0e1c00	0000000000000000	9.58	9.51	2.248%	0.00	0.000%	0.399
DS3	1e1a0c31e0e1c00	0000000000000000	29.88	29.67	2.566%	0.00	0.000%	1.245
DS4	0000000000000000	1c061a16060e1e00	19.15	0.00	0.000%	18.85	1.811%	0.622
DS5a	08000020040e1c00	18060a02040e1e00	1.49	1.48	0.703%	1.46	1.111%	0.110
DS5a	08080020040e1c00	18060a16060e1e00	2.51	2.49	0.842%	2.47	1.484%	0.186
DS5a	08080030040e1c00	18060a02040e1e00	0.01	0.01	0.888%	0.01	1.094%	0.001
DS5a	0e1a04321e0e1c00	08020a16060e1e00	2.69	2.71	2.265%	2.66	1.165%	0.201
DS5a	0e1a0c321e0e1c00	0000000000000000	0.65	0.63	2.522%	0.00	0.000%	0.026
DS5a	0e1a0c321e0e1c00	08060a16060e1e00	1.24	1.24	2.513%	1.21	1.451%	0.092
DS5a	0e1a0c321e0e1c00	18060a02040e1e00	2.94	2.92	2.288%	2.89	1.098%	0.218
DS5a	0e1a0c321e0e1c00	18060a14060e1600	0.04	0.04	2.487%	0.04	0.906%	0.003
DS5a	0e1a0c321e0e1c00	18060a16060e6000	3.19	3.15	2.452%	3.16	0.774%	0.237
DS5a	0e1a0c321e0e1c00	18060a16060e0600	3.30	3.28	2.458%	3.29	0.793%	0.246
DS5a	0e1a0c31e0e1c00	1806020606081800	1.75	1.73	2.703%	1.73	0.726%	0.129
DS5a	0e1a0c31e0e1c00	180602160601c00	6.84	6.77	2.698%	6.74	1.068%	0.507
DS5a	0e1a0c31e0e1c00	18060216060e1e00	13.48	13.30	2.677%	13.27	1.189%	0.996
DS5a	0e1a0c31e0e1c00	18060816060e1c00	0.05	0.05	2.502%	0.05	1.247%	0.004
DS5a	0e1a0c31e0e1c00	18060a0606060c00	2.16	2.12	2.670%	2.12	0.982%	0.159
DS5a	0e1a0c31e0e1c00	18060a16040e1e00	0.76	0.76	2.668%	0.74	1.222%	0.056
DS5a	0e1a0c31e0e1c00	18060a1606060c00	0.25	0.25	2.682%	0.25	1.060%	0.019
DS5a	0e1a0c31e0e1c00	18060a1606061800	1.88	1.86	2.686%	1.86	0.998%	0.140
DS5a	0e1a0c31e0e1c00	18060a1606061c00	9.20	9.13	2.657%	9.06	1.353%	0.682
DS5a	0e1a0c31e0e1c00	18060a16060e1c00	7.89	7.79	2.688%	7.79	1.350%	0.584
DS5a	0e1a0c31e0e1c00	18060a16060e6000	11.68	11.53	2.340%	11.51	1.357%	0.864
DS5a	0e1a0c31e0e1c00	18060a16060e1e00	5.21	5.15	2.665%	5.13	1.486%	0.386
DS5a	0e1a0c31e0e1c00	18061216060e1e00	2.39	2.37	2.676%	2.37	1.266%	0.178
DS5b	1e1a0c31e0c1c00	18061216060e1e00	24.46	24.09	2.672%	24.06	1.268%	1.805
DS5b	1e1a0c31e0c1c00	18061a16060e1e00	0.75	0.75	2.670%	0.75	1.654%	0.056
DS5b	1e1a0c31e0c1c00	18061216060e1e00	14.28	14.12	2.766%	14.07	1.169%	1.057
DS5c	1e1a0c31e0c1c00	00060216060e0e00	0.00	0.00	2.567%	0.00	0.787%	0.000
DS5c	1e1a0c31e0c1c00	00060a16060e0e00	0.91	0.89	2.664%	0.91	1.016%	0.067
DS5c	1e1a0c31e0c1c00	00061216060e0e00	10.22	10.15	2.645%	10.03	0.857%	0.757
DS6a	1200000000000800	1002020006046000	1.33	1.31	0.160%	1.31	0.230%	0.099
DS6a	12000c20000c1c00	18061216060c1600	6.93	6.84	0.756%	6.86	0.679%	0.514
DS6a	1202000040c0800	1802020006046000	1.30	1.28	0.284%	1.28	0.275%	0.096
DS6a	12020c0040c1800	1802020006046000	2.37	2.33	0.676%	2.33	0.275%	0.175
DS6a	12080c20000c1c00	18061216060c1600	3.38	3.34	0.931%	3.34	0.677%	0.251
DS6a	12120c3e1c0c1c00	18061216060c1600	0.56	0.54	1.847%	0.56	0.676%	0.041
DS6a	16020c10040c1800	1806020006060000	3.23	3.20	0.883%	3.19	0.416%	0.239
DS6a	160a0c321c0c1c00	1806021006061600	1.98	1.95	2.022%	1.97	0.521%	0.147
DS6a	1e0a0c321c0c1c00	1806020006042000	2.62	2.59	2.275%	2.59	0.260%	0.194
DS6a	1e0a0c321c0c1c00	1806020006046000	1.31	1.29	2.275%	1.29	0.390%	0.097
DS6a	1e0a0c321c0c1c00	1806020006041600	1.30	1.28	2.275%	1.26	0.459%	0.096
DS6a	1e0a0c321c0c1c00	1806021006061600	1.61	1.59	2.275%	1.59	0.521%	0.119
DS6a	1e120c3e1c0c1c00	18061216060c1600	0.95	0.93	2.284%	0.93	0.676%	0.070
DS6a	1e1a0c321c0c1c00	1806020006060600	1.30	1.28	2.457%	1.28	0.416%	0.096
DS6a	1e1a0c321c0c1c00	1806021006046000	3.91	3.88	2.457%	3.87	0.415%	0.291
DS6a	1e1a0c321c0c1c00	1806021006041600	2.92	2.90	2.457%	2.90	0.495%	0.217
DS6a	1e1a0c321c0c1c00	1806021006060000	1.31	1.30	2.455%	1.30	0.436%	0.097
DS6a	1e1a0c3a1c0c1c00	1806020006046000	2.32	2.31	2.553%	2.32	0.390%	0.174
DS6a	1e1a0c3a1c0c1c00	1806021006046000	1.77	1.77	2.552%	1.75	0.415%	0.132
DS6a	1e1a0c3a1c0c1c00	1806021006041600	0.67	0.67	2.553%	0.67	0.494%	0.050
DS6a	1e1a0c3e1c0c1c00	180600000006046000	2.22	2.18	2.631%	2.16	0.360%	0.163
DS6a	1e1a0c3e1c0c1c00	1806020006041600	1.32	1.30	2.630%	1.30	0.458%	0.097
DS6a	1e1a0c3e1c0c1c00	1806021006041600	1.30	1.28	2.630%	1.28	0.494%	0.096
DS6a	1e1a0c3e1c0c1c00	18060210060c1600	4.63	4.58	2.629%	4.55	0.533%	0.342
DS6a	1e1a0c3e1c0c1c00	1806021206041600	2.61	2.56	2.628%	2.57	0.515%	0.192
DS6a	1e1a0c3e1c0c1c00	18060214060c0600	1.70	1.70	2.628%	1.68	0.492%	0.127
DS6a	1e1a0c3e1c0c1c00	18060214060c1600	1.38	1.36	2.627%	1.36	0.576%	0.102
DS6a	1e1a0c3e1c0c1c00	18060214060c1600	23.42	23.19	2.601%	23.12	0.555%	1.736
DS6a	1e1a0c3e1c0c1c00	18061212060c1600	2.93	2.89	2.628%	2.90	0.644%	0.217
DS6a	1e1a0c3e1c0c1c00	18061216060c1600	6.59	6.51	2.628%	6.51	0.690%	0.488
DSTotal	—	—	321.60	318.26	2.354%	238.53	0.987%	21.228

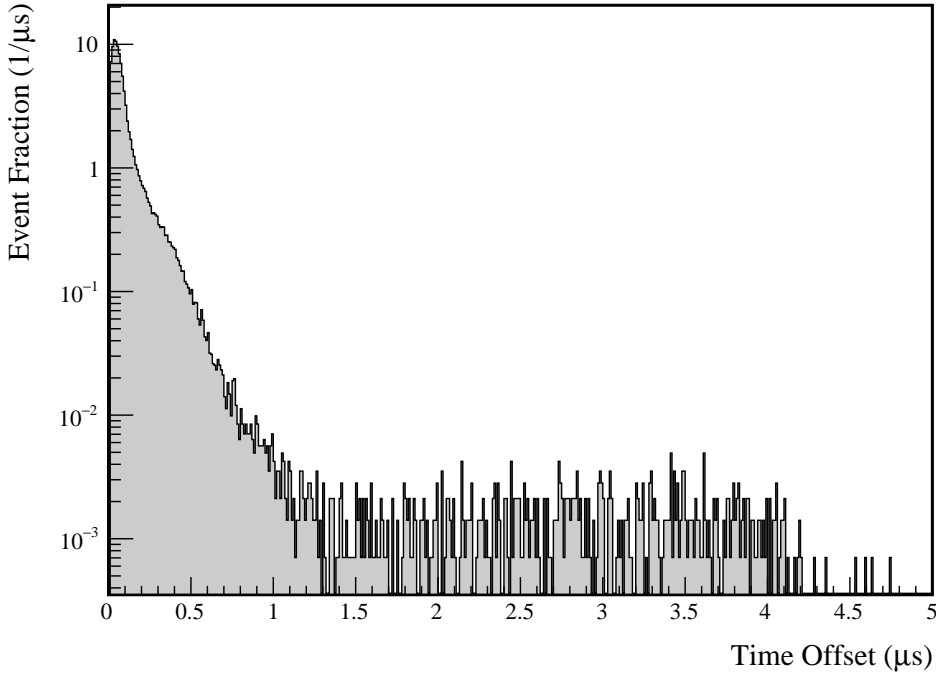


FIG. 7 Distribution of time interval between individual hits within a multi-detector event during a ^{228}Th calibration run. Offsets of greater than $\sim 1.5 \mu\text{s}$ are due to pileup, which is significant due to the high data rate of calibration runs.

155 B. Dead Layer Effects

156 For multi-site event events, each individual hit may be degraded by the deadlayer, so the loss of sensitivity from
157 deadlayers is larger for this search than for searches for single-site events. For this reason, dead layer effects are treated
158 as a loss of detection efficiency instead of a loss of exposure. Dead layers are included in the simulations as a part of
159 post-processing as described in section ?? To account for uncertainty in the thickness of the deadlayer, two separate
160 simulations are run, with and without deadlayers. By comparing the efficiency measurement from each simulation, we
161 measure the size of the dead layer effect. The percent uncertainty in the efficiency loss from dead layers is assumed
162 to be the same as the percent uncertainty in the dead layer thickness. Typical loss of efficiency for multi-site peaks
163 is 25-35%; for the $2\nu\beta\beta$ to the 0_1^+ decay, the losses are 26% for module 1 and 34% for module 2. The uncertainty in
164 the dead layer tends to be one of the dominant uncertainties in measuring the detection efficiency. The effect of dead
165 layers on detection efficiency can be seen in figure 8.
166

168 C. Dead Time Effects

169 Detector deadtimes, which affect only a single detector simultaneously, reduce the detection efficiency for events
170 that occur in all detectors in the module. For this reason, instead of subtracting these deadtimes from the livetime,
171 the deadtimes are incorporated into the detection efficiency. Detector deadtimes are measured individually for each
172 run by counting pulser events and comparing to the number of expected pulser events for each detector. `es_livetime`
173 collects the detector deadtimes that are measured in this way and finds the average detector deadtime for each
174 subdataset. These dead times are then applied to the simulation skimming process as described in section ???. Similar
175 to the dead layers, simulation files are produced with and without deadtimes in order to measure the size of the effect.
176 Uncertainties in the detector deadtimes are measured as the statistical uncertainties from pulser counts. The percent
177 uncertainty in efficiency loss from detector dead times is assumed to be the same as the average percent uncertainty
178 in the detector dead time. Typical loss of efficiency from detector deadtims range from 1-3%. For the $2\nu\beta\beta$ to the 0_1^+

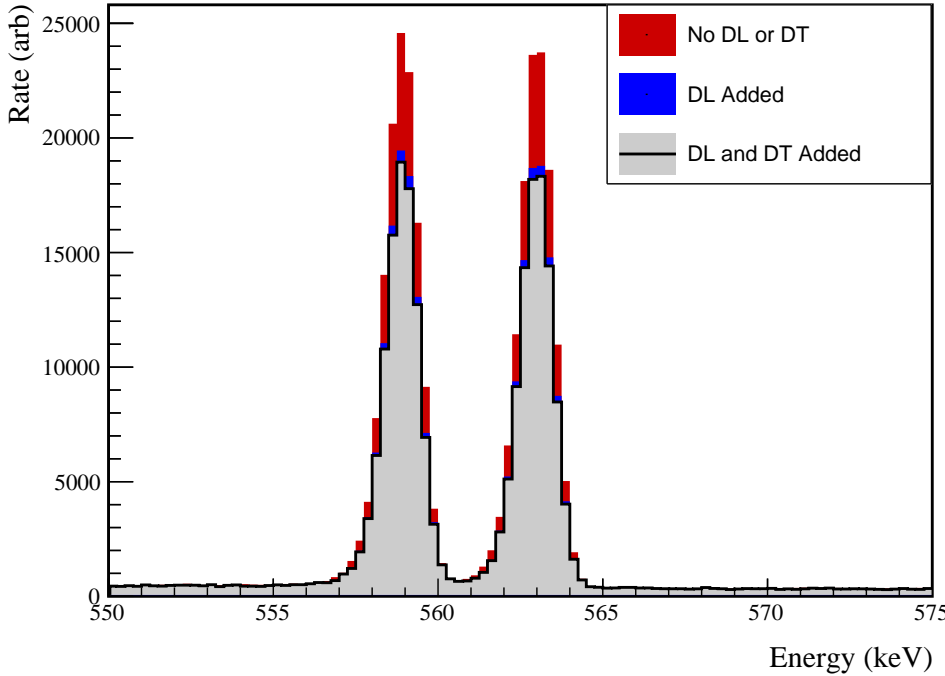


FIG. 8 Effect of dead layers and dead times on peak amplitudes for $2\nu\beta\beta$ to the 0_1^+ peaks in multi-site event events.

179 decay, the losses are 2.5% for module 1 and 1.9% for module 2. The effects of detector deadtimes can be seen in figure 8.
 180

181 D. Additional Effects

182 Other possible sources of systematic uncertainty, which could hypothetically result from inaccuracies in the simulation
 183 geometry, in the detection efficiency must be accounted for. To do so, we use pair production events from
 184 calibration runs as a proxy for $\beta\beta$ E.S. events. In pair production events, an electron-positron pair is produced in the
 185 bulk of a detector, followed promptly by two 511 keV γ s from the annihilation of the positron. Because these events
 186 involve a single pair production site and the prompt emission of gamma rays which may be absorbed in a separate
 187 detector, they make a good proxy for $\beta\beta$ E.S. events. In single-escape peak (SEP) events, one gamma is absorbed
 188 in the same detector as the pair-production, while the other escapes, resulting in a detector hit with energy equal to
 189 the γ energy minus 511 keV. In double-escape peak (DEP) events, both gammas escape the detector, resulting in a
 190 detector hit with energy equal to the γ energy minus 1022 keV. Both both SEP and DEP events present the possibility
 191 for a second 511 keV detector hit. By comparing the rate of multiplicity-1 events in the SEPs and DEPs to the rate
 192 of multiplicity-2 events in which one hit falls into one of these peaks and the other falls into the 511 keV peak, we
 193 can measure a proxy the detection efficiency of our multi-site event signature. By comparing this measurement to
 194 simulation, we can estimate the size of any unknown uncertainties in our simulation-based efficiency estimate.

195 To achieve this, we will use a ^{56}Co calibration source. ^{56}Co presents the advantage of a large number of γ s at
 196 energies high enough to cause pair production, which allows for a comparison of many peaks to our simulation. A
 197 ^{56}Co line source was inserted into the module 1 calibration track on January 15, 2019 and was 168.1 hrs of data were
 198 recorded, until January 22, 2019. Immediately after this, the source was inserted into the module 2 calibration track
 199 and 167.1 hrs of data were recorded until January 29, 2019. The source had a nominal activity of 6 kHz, resulting in a
 200 high enough data rate that the energy threshold for each channel was raised to ~ 400 keV. As discussed in section ??,
 201 3 billion event primaries were simulated for the ^{56}Co source in each module's source track in order to achieve similar
 202 events statistics for both the simulations and data. Simulations were run with and without dead-layers.
 203 8 SEPs and 7 DEPs were selected as proxies for the $\beta\beta$ E.S. signal. A simultaneous fit, as described in appendix ??, of

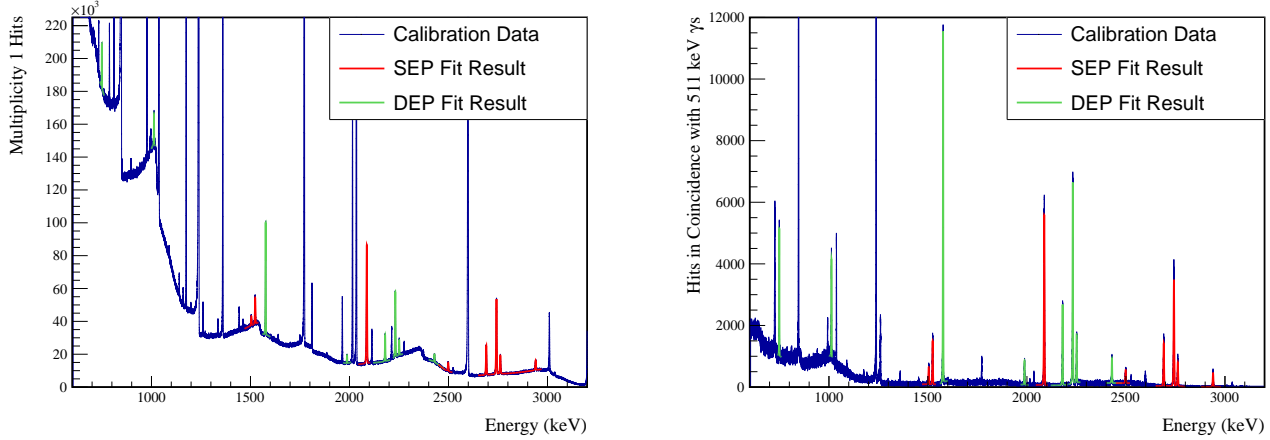


FIG. 9 Spectra of multiplicity 1 ^{56}Co events (left) and multiplicity 2 ^{56}Co events in coincidence with an annihilation gamma. The results of the simultaneous peak fits are drawn in red (SEP fit) and green (DEP fit).

all SEPs as single-detector events and as two-detector events in coincidence with a 511 keV peak event was performed in the calibration data and in the simulations both with and without dead layers. SEPs and DEPs have abnormal peakshapes due to in flight annihilation of the positrons, which results in Doppler broadening of the peak shapes. For this reason, a high energy tail is added to the typical peak shape function. The peak height ratios and uncertainties for peak k are determined as follows:

$$\epsilon_k = \frac{A_{k,m2}}{A_{k,m1}} \quad (4)$$

210

$$\sigma_{stat,k} = \epsilon_k \sqrt{\frac{\Sigma_{A,k,m1;A,k,m1}}{A_{k,m1}^2} - 2\frac{\Sigma_{A,k,m1;A,k,m2}}{A_{k,m1}A_{k,m2}} + \Sigma_{A,k,m2;A,k,m2} A_{k,m2}^2} \quad (5)$$

where $A_{k,m1/2}$ are the fitted amplitudes of peak k with multiplicity 1 and multiplicity 2 respectively, and $\Sigma_{A,k,m1/2;A,k,m1/2}$ is the fitter covariance matrix element for these amplitudes. The same process of simultaneously fitting DEPs is followed to extract the DEP peak-height ratios. The measured data spectra and fit results are shown in figure 9.

Any discrepancy between the simulated and measured data is treated as a systematic error which will be applied to the $\beta\beta$ E.S. measurement. Since some of this discrepancy can be explained by the dead layer uncertainty, the difference between the simulated peak-height ratios with and without the deal layer is multiplied by the percent uncertainty in the dead layer thickness in order to measure the systematic error caused by the dead layer. Finally, a χ^2 value is computed for the comparison between the simulated and measured peak-heights using the statistical and dead-layer uncertainties.

$$\chi^2 = \sum_{k=1}^N \frac{(\epsilon_{k,meas} - \epsilon_{k,sim} - \delta_{DL} \cdot \sigma_{DL,k} - \mu)^2}{\sigma_{stat,dat,k}^2 + \sigma_{stat,sim,k}^2} + \delta_{DL}^2 \quad (6)$$

where δ_{DL} is the error from the deal layer thickness, which is correlated across all peaks, and μ is the mean error that remains. This χ^2 function is minimized, and the systematic error is taken to be

$$\sigma_{sim}^2 = \mu^2 + \sigma_\mu^2 \quad (7)$$

Tables II and III list the peak height ratios and uncertainties for each peak for module 1 and module 2, respectively. The final fractional uncertainties measured are $\sigma_{sim,M1} = 0.0020$ and $\sigma_{sim,M2} = 0.0047$. This uncertainty is applied directly to the detection efficiency measured before applying any other effects such as dead layers, dead times and cuts, without any scaling. This uncertainty is one of the dominant uncertainties on the detection efficiency along with the dead layer uncertainty; while the absolute uncertainty is small, because it is applied to the detection efficiency,



which tends to be $\sim 5\%$, directly rather than to the loss from an individual effect, the fractional uncertain is quite high. In cases where the detection efficiency is very low, such as the 1216 keV peak in module 2 from decays to the 2_2^+ state, this uncertainty can completely overwhelm the detection efficiency. Figure 10 plots the peak height ratios for simulated and measured data for both modules 1 and 2.

TABLE II Table of measured peak height ratios between multiplicity 1 events and multiplicity 2 events containing a 511 keV annihilation γ in module 1 for both simulated and measured ^{56}Co spectra, with uncertainties. A plot of these numbers is shown in figure 10

Peak	$\frac{A_{m2,\text{dat}}}{A_{m1,\text{dat}}}$	$\frac{A_{m2,\text{sim}}}{A_{m1,\text{sim}}}$	$\frac{A_{m2,\text{noDL}}}{A_{m1,\text{noDL}}}$	$\sigma_{\text{dat,stat}}$	$\sigma_{\text{sim,stat}}$	$\sigma_{\text{sim,DL}}$	Residual	σ_{resid}
1504 keV (SEP)	0.098	0.084	0.110	0.004	0.003	0.004	0.014	0.004
1524 keV (SEP)	0.089	0.082	0.109	0.002	0.001	0.005	0.007	0.002
2088 keV (SEP)	0.077	0.073	0.098	0.001	0.001	0.004	0.004	0.001
2499 keV (SEP)	0.081	0.079	0.108	0.003	0.002	0.005	0.002	0.004
2691 keV (SEP)	0.078	0.072	0.099	0.001	0.001	0.005	0.006	0.002
2743 keV (SEP)	0.075	0.073	0.101	0.001	0.001	0.005	0.003	0.001
2762 keV (SEP)	0.070	0.070	0.096	0.001	0.001	0.004	0.000	0.002
2940 keV (SEP)	0.075	0.070	0.100	0.002	0.002	0.005	0.005	0.003
749 keV (DEP)	0.153	0.155	0.225	0.004	0.003	0.012	-0.002	0.005
1013 keV (DEP)	0.166	0.156	0.229	0.005	0.004	0.012	0.010	0.006
1577 keV (DEP)	0.167	0.157	0.224	0.001	0.001	0.011	0.010	0.002
1988 keV (DEP)	0.158	0.155	0.222	0.005	0.005	0.011	0.003	0.007
2180 keV (DEP)	0.163	0.158	0.225	0.002	0.002	0.011	0.005	0.003
2232 keV (DEP)	0.164	0.158	0.225	0.001	0.001	0.012	0.007	0.002
2251 keV (DEP)	0.170	0.166	0.233	0.004	0.003	0.011	0.004	0.005
2429 keV (DEP)	0.165	0.158	0.230	0.005	0.004	0.012	0.007	0.007

TABLE III Table of measured peak height ratios between multiplicity 1 events and multiplicity 2 events containing a 511 keV annihilation γ in module 2 for both simulated and measured ^{56}Co spectra, with uncertainties. A plot of these numbers is shown in figure 10

Peak	$\frac{A_{m2,\text{dat}}}{A_{m1,\text{dat}}}$	$\frac{A_{m2,\text{sim}}}{A_{m1,\text{sim}}}$	$\frac{A_{m2,\text{noDL}}}{A_{m1,\text{noDL}}}$	$\sigma_{\text{dat,stat}}$	$\sigma_{\text{sim,stat}}$	$\sigma_{\text{sim,DL}}$	Residual	σ_{resid}
1504 keV (SEP)	0.077	0.059	0.082	0.004	0.002	0.004	0.018	0.004
1524 keV (SEP)	0.068	0.060	0.081	0.002	0.001	0.004	0.009	0.002
2088 keV (SEP)	0.059	0.054	0.074	0.001	0.000	0.003	0.005	0.001
2499 keV (SEP)	0.062	0.051	0.073	0.002	0.002	0.004	0.011	0.003
2691 keV (SEP)	0.057	0.052	0.074	0.001	0.001	0.004	0.005	0.002
2743 keV (SEP)	0.057	0.053	0.075	0.001	0.001	0.004	0.004	0.001
2762 keV (SEP)	0.055	0.050	0.071	0.002	0.001	0.004	0.005	0.002
2940 keV (SEP)	0.060	0.052	0.072	0.002	0.002	0.003	0.008	0.003
749 keV (DEP)	0.111	0.113	0.155	0.003	0.003	0.007	-0.002	0.004
1013 keV (DEP)	0.118	0.108	0.156	0.003	0.003	0.008	0.009	0.004
1577 keV (DEP)	0.119	0.113	0.161	0.001	0.001	0.008	0.006	0.001
1988 keV (DEP)	0.123	0.112	0.153	0.005	0.003	0.007	0.011	0.006
2180 keV (DEP)	0.119	0.114	0.164	0.002	0.002	0.008	0.005	0.002
2232 keV (DEP)	0.120	0.112	0.160	0.001	0.001	0.008	0.008	0.001
2251 keV (DEP)	0.124	0.120	0.170	0.003	0.003	0.008	0.004	0.004
2429 keV (DEP)	0.125	0.120	0.159	0.005	0.003	0.007	0.005	0.006

V. REGION OF INTEREST SELECTION

Once the multisite events have been collected, we want to search for detector hits with the energies of the γ s emitted in each $\beta\beta$ E.S. decay mode. To do this, a signal region of interest (ROI) must be identified. To estimate the number of background events in the signal ROI, a background ROI must also be selected near the signal ROI. This section will describe the selection of the signal and background ROIs and the calculation of the efficiency and uncertainties on the efficiency due to the ROI selection.

The peakshape function and parameters are described in appendix ???. For each dataset, a simultaneous fit of many peaks is performed to a combined spectrum of all detectors and all calibration runs, ensuring that any variation



240 in gain or energy nonlinearity between detectors is accounted for. From each fit result, a set of parameters de-
241 scribing a single peak shape at the energy of the signal ROI of interest can be extracted, along with a covariance
242 matrix for those parameters. From these fit results, we can compute the optimal ROI, detection efficiency and un-
243 certainty for each data set. An example of a calibration spectrum with the FWHM curve fit to it is shown in figure 11.
245

246 A. Signal ROI Optimization

247 The signal region of interest around each peak is optimized based on the peak shape functions as fit for each data
248 set. The signal region of interest is optimized following the procedure laid out in appendix ?? and maximizing the
249 rate sensitivity with respect to the region of interest upper and lower boundaries, E_{low} and E_{high} respectively.

$$\hat{\Gamma}(E_{low}, E_{high}, \bar{B}) \propto \frac{DP(\bar{B}(E_{high} - E_{low}))}{\epsilon_{ROI}(E_{low}, E_{high})} \quad (8)$$

250 DP is the discovery potential as defined in appendix ??, where a flat background with background index \bar{B} measured
251 from data is assumed. The efficiency is defined by the CDF of the Gaussian and LE tail components

$$\begin{aligned} \epsilon_{ROI}(E_{low}, E_{high}; \mu, \sigma, f_{tail}, \tau) = & \frac{1}{2} \left(\operatorname{erfc}\left(\frac{E_{low} - \mu}{\sqrt{2}\sigma}\right) - \operatorname{erfc}\left(\frac{E_{high} - \mu}{\sqrt{2}\sigma}\right) \right) \\ & + f_{tail}\tau(\operatorname{ExGaus}(E_{high}; \mu, \sigma, \tau) - \operatorname{ExGaus}(E_{low}; \mu, \sigma, \tau)) \end{aligned} \quad (9)$$

252 The optimal ROI is numerically calculated by minimizing $\frac{1}{\hat{\Gamma}(E_{low}, E_{high}, \bar{B})}$ with respect to E_{low} and E_{high} using the
253 minuit minimizer[7].
254

255 B. Background ROI Selection

256 For each peak, a background ROI of width 50 – 100 keV surrounding the peak is selected. The ROI is selected
257 to avoid any known background peaks and exclude them with at least 99.9% efficiency. A 99.9% exclusion region
258 calculated from the peakshape function is selected around the peak and removed from the background ROI.
259

260 C. ROI Detection Efficiency and Uncertainty

261 The ROI detection efficiency is calculated from the CDF defined in equation ?? . The covariance matrix of the peak
262 shape parameters obtained from the fit result is used to calculate the statistical uncertainty of the efficiency. Several
263 additional systematic effects must also be accounted for:

- 264 • **Gain drift:** ^{228}Th energy calibrations are taken once per week, for 90 minutes each. In between these cali-
265 bration runs, the energy calibration parameters undergo small adjustments that result in energy inaccuracies
266 for background runs taken in between. This gain drift results in an increase in the width of the peak, which
267 is accounted for by adding in quadrature σ_{drift} to the value of σ obtained from the fit. This also results in
268 the dominant systematic uncertainty on the peak width, $\delta_{fwhm,drift}$. The gain drift also results in a small
269 systematic error in the measured energy of the peak $\delta_{\mu,drift}$. A detailed description of the measurement of each
270 of this systematic effect is contained in referece [8].
- 271 • **Energy nonlinearity:** While the energy response for HPGe detectors is ostensibly linear, several factors result
272 in small nonlinearities. Local nonlinearities that are correlated over small energy scales of arise from the response
273 of the Gretina digitizers. While these nonlinearities are corrected for, a nonlinearity of ~ 0.1 keV with a period
274 of ~ 300 keV remains. Global nonlinearities result from systematic uncertainties in the energy estimation.
275 One source of global nonlinearity arises from uncertainty in the start time of the waveform, which is energy
276 dependant. Another is a small quadratic term resulting from charge recombination. Because calibrations are
277 performed on peaks with energies ranging from 238 keV to 2614 keV, energy shifts due to global nonlinearities



are very small in this range and local energy nonlinearities dominate. At smaller and larger energies, the shifts can be as large as ~ 0.5 keV in some detectors. Energy nonlinearities result in an increase in σ as a result of the combining of peaks with different shifts; however, since the energy calibrations include all detectors, this shift is already included in the fit result, so no action is required. Energy nonlinearities also have a significant affect on the uncertainty in the measured peak energy, $\delta_{\mu,NL}$, which is a dominant uncertainty. A detailed description of the measurement of each of this systematic effect is contained in reference [8].

• **Detector Crosstalk:** Because we are searching for peaks in coincidence events, the possibility for a distortion in the energy measurement due to crosstalk between the involved events exists. This effect is measured in section ?? to be small enough that no energy correction or peakshape correction is required. However, this effect does contribute to small uncertainties in the peak position, $\delta_{\mu,xtalk}$ and peak width, $\delta_{fwhm,xtalk}$.

Once these uncertainties have been measured, they must be propagated into the detection efficiency. The statistical and systematic uncertainties on μ and the FWHM are added in quadrature to obtain δ_μ and δ_{fwhm} . The uncertainty on the FWHM is used to calculate a width scale uncertainty, δ_α , which is simply the fractional uncertainty on the FWHM. To compute the uncertainty on the efficiency, the efficiency is computed after modifying the peakshape parameters by one-sigma in either direction. For the uncertainty from the width, we take:

$$\begin{aligned} \sigma_{\epsilon_{ROI,fwhm}} = & \frac{1}{2} (\epsilon_{ROI}(E_{low}, E_{high}; \mu, \sigma(1 + \delta_\alpha), f_{LE}, \tau(1 + \delta_\alpha)) \\ & + \epsilon_{ROI}(E_{low}, E_{high}; \mu, \sigma(1 - \delta_\alpha), f_{LE}, \tau(1 - \delta_\alpha))) \end{aligned} \quad (10)$$

Because the ROI is optimized to around μ , shifts in the peak in either direction will cause a reduction in efficiency; for this reason, we must perform a second order propagation of uncertainties. The result is a slight degradation in the efficiency, so that

$$\epsilon_{ROI} = \frac{\epsilon_{ROI}(E_{low}, E_{high}; \mu + \delta_\mu, \sigma, f_{LE}, \tau) + \epsilon_{ROI}(E_{low}, E_{high}; \mu - \delta_\mu, \sigma, f_{LE}, \tau)}{2} \quad (11)$$

and

$$\sigma_{\epsilon_{ROI,\mu}} = \epsilon_{ROI}(E_{low}, E_{high}; \mu) - \epsilon_{ROI} \quad (12)$$

These uncertainties are taken to be uncorrelated and added in quadrature to obtain the final uncertainty on the ROI efficiency. Table XXVI contains a full summary of all of the energy uncertainties, the ROIs, and the ROI efficiencies and uncertainties.

D. Detector Crosstalk

Detector crosstalk is caused when a true signal in one detector channel induces a small signal in another channel. This is not a large enough event to trigger events in a separate channel, meaning that it does not effect β events. However, it could produce an energy estimation error in multi-detector event events since coincident pulses could induce signals that interfere either constructively or destructively, shifting the measured energy. In practice, this could produce both a shift and additional uncertainty in both the measured energy of the peak and in the width of the peak. To check for this effect, we can look at multi-detector event events in ^{228}Th calibration data. In particular, we will compare the centroid and FWHM for several peaks in both single-detector event events and multi-detector event events.

5 peaks were selected from the ^{208}Tl γ cascade, at 277, 583, 763, 860 and 2614 keV, and one additional peak was selected from the ^{212}Bi cascade, at 785 keV. The combined calibration spectra from dataset 6 were used to perform this analysis. These peaks were fit individually, and the centroid and FWHM were computed for multiplicity 1 and multiplicity 2 events. Figure 12 shows the results of these measurements. While a very small reduction in peak centroid and increase in peak width are observed, the shifts are small compared to the existing uncertainties in these parameters. As a result, we will ignore this shift and instead compute an uncertainty in each parameter caused by crosstalk. We will treat the systematic error as uncorrelated between the peaks and compute the necessary error needed to make the combined statistical and systematic errors large enough to make the χ^2 value computed by comparing these peaks equal to 1:

$$\chi^2 = \sum_{k=0}^N \frac{(\text{cen}_{k,m1} - \text{cen}_{k,m2})^2}{\sigma_{\text{cen},k,m1}^2 + \sigma_{\text{cen},k,m2}^2 + \delta_{\mu,xtalk}^2} \quad (13)$$



TABLE IV Table of energy estimation uncertainties, regions of interest, and efficiencies

DS	E_{peak} (keV)	σ_{fit} (keV)	σ_{drift} (keV)	σ (keV)	$f_{t,fit}$ (keV)	τ_{fit} (keV)	$\delta_{\mu,fit}$ (keV)	$\delta_{\mu,NL}$ (keV)	$\delta_{\mu,drift}$ (keV)	$\delta_{\mu,peak}$ (keV)	δ_u (keV)	FWHM (keV)	$\delta_{fwhm,drift}$ (keV)	$\delta_{fwhm,fit}$ (keV)	$\delta_{fwhm,xtalk}$ (keV)	δ_{FWHM} (keV)	δ_α	$E_{ROI,1}$ (keV)	$E_{ROI,2}$ (keV)	ϵ_{ROI}	$\sigma_{\epsilon_{ROI}}$	
DS1	559.101	0.460	0.063	0.464	0.230	0.515	0.001	0.104	0.002	0.012	0.005	0.105	1.152	0.001	0.039	0.011	0.040	0.035	558.199	559.847	0.871	0.015
DS2	559.101	0.461	0.055	0.464	0.249	0.515	0.002	0.067	0.004	0.012	0.005	0.068	1.158	0.001	0.107	0.011	0.108	0.093	558.186	559.845	0.874	0.031
DS3	559.101	0.470	0.066	0.474	0.224	0.505	0.001	0.026	0.024	0.012	0.005	0.038	1.174	0.001	0.073	0.011	0.074	0.063	558.187	559.863	0.879	0.021
DS4	559.101	0.455	0.077	0.461	0.108	0.445	0.002	0.076	0.010	0.012	0.005	0.078	1.111	0.001	0.106	0.011	0.107	0.096	558.283	559.856	0.888	0.032
DS5a	559.101	0.560	0.085	0.567	0.106	0.855	0.002	0.079	0.005	0.012	0.005	0.080	1.367	0.002	0.055	0.011	0.056	0.041	558.098	560.022	0.875	0.014
DS5b	559.101	0.469	0.074	0.475	0.158	0.491	0.001	0.020	0.011	0.012	0.005	0.026	1.157	0.001	0.125	0.011	0.125	0.108	558.229	559.872	0.885	0.036
DS5c	559.101	0.460	0.085	0.468	0.174	0.489	0.001	0.037	0.030	0.012	0.005	0.050	1.145	0.001	0.162	0.011	0.162	0.142	558.231	559.860	0.883	0.046
DS6a	559.101	0.456	0.044	0.458	0.191	0.463	0.001	0.069	0.025	0.012	0.005	0.075	1.123	0.000	0.041	0.011	0.042	0.038	558.241	559.841	0.881	0.014
DS1	563.178	0.461	0.064	0.466	0.230	0.518	0.001	0.104	0.002	0.012	0.005	0.105	1.156	0.001	0.039	0.011	0.040	0.035	562.273	563.927	0.871	0.015
DS2	563.178	0.463	0.055	0.466	0.249	0.517	0.002	0.067	0.004	0.012	0.005	0.068	1.162	0.001	0.107	0.011	0.108	0.093	562.259	563.924	0.874	0.030
DS3	563.178	0.471	0.066	0.476	0.224	0.508	0.001	0.026	0.024	0.012	0.005	0.038	1.179	0.001	0.073	0.011	0.074	0.063	562.261	563.943	0.879	0.021
DS4	563.178	0.457	0.077	0.463	0.108	0.447	0.002	0.076	0.010	0.012	0.005	0.078	1.115	0.001	0.106	0.011	0.107	0.096	562.357	563.935	0.888	0.032
DS5a	563.178	0.562	0.086	0.569	0.106	0.858	0.002	0.079	0.006	0.012	0.005	0.080	1.372	0.002	0.055	0.011	0.056	0.041	562.172	564.103	0.875	0.014
DS5b	563.178	0.471	0.074	0.477	0.158	0.494	0.001	0.020	0.011	0.012	0.005	0.026	1.162	0.001	0.125	0.011	0.125	0.108	562.303	563.952	0.885	0.035
DS5c	563.178	0.462	0.086	0.470	0.174	0.492	0.001	0.037	0.030	0.012	0.005	0.050	1.49	0.001	0.162	0.011	0.162	0.141	562.305	563.939	0.883	0.046
DS6a	563.178	0.457	0.044	0.459	0.191	0.465	0.001	0.069	0.026	0.012	0.005	0.075	1.127	0.000	0.041	0.011	0.042	0.038	562.315	563.921	0.881	0.013



320

$$\chi^2 = \sum_{k=0}^N \frac{(\text{FWHM}_{k,m1} - \text{FWHM}_{k,m2})^2}{\sigma_{fwhm,k,m1}^2 + \sigma_{fwhm,k,m2}^2 + \delta_{fwhm,xtalk}^2} \quad (14)$$

321 Both systematic errors are numerically computed using a Brent minimization algorithm. The results are $\delta_{\mu,xtalk} =$
322 0.012 keV and $\delta_{fwhm,xtalk} = 0.011$ keV, both of which are subdominant uncertainties.

323 **VI. BACKGROUND CUTS**

324 By making use of known properties of background events, data cleaning cuts can be designed to selectively reduce
325 backgrounds while minimizing sacrifice of excited state events. Because of the multi-detector event nature of the
326 event selection, many of these background cuts are designed that make use of observables from the detector hits in
327 coincidence with candidate hits.

328 **A. Enriched Source Detector Cut**

329 Since the $\beta\beta$ E.S. events must originate in ^{76}Ge , events are far likelier to originate in enriched Germanium detectors
330 than those with natural Germanium isotopic abundances. There are 29.8 kg of enriched detectors, with $88.1 \pm 0.7\%$
331 abundance of ^{76}Ge and 14.4 kg of natural detectors, with $7.83 \pm 0.07\%$ abundance of ^{76}Ge . This means that $95.8 \pm 0.1\%$
332 of $\beta\beta$ E.S. events will originate in enriched detectors. If we assume that background events will hit all detector mass
333 at the same rate, then we would expect only 67% of hits from background events involving two detectors to be in
334 coincidence with a hit in an enriched detector. This means that a significant gain in sensitivity can be achieved by
335 cutting hits that are not in coincidence with an enriched detector hit. While the detection efficiency of this cut is
336 expected to be close to 95.8%, the actual efficiency is measured from simulations, and tends to be greater, since a
337 greater proportion of enriched detectors are active than of natural detectors.

338 **B. Coincident and Sum Energy Cuts**

339 The greatest source of background events is expected to be γ -rays from a handful of known primordial and cosmogenic
340 isotopes. Because γ photons are monoenergetic, these backgrounds will often present a clear detection signature
341 that can be targeted. γ photons will often Compton scatter from one detector into another, depositing their entire
342 energy between the two. For this reason, events whose total energy is equal to the energy of a known γ can be cut.
343 β -decays will often result in a cascade of multiple γ s, at least one of which may be fully absorbed in a single detector.
344 These events can be cut by searching for a coincident detector with energy equal to that of a known γ . Finally,
345 whereas the $\beta\beta$ decay spectrum approaches zero amplitude at low energies and at $Q_{\beta\beta}$, the Compton continuum of
346 γ s has finite amplitude at low energies. This means that sensitivity can be gained by setting low- and high-energy
347 thresholds on hits in coincidence with a candidate event. These combined backgrounds can be reduced by cutting
348 events with either sum energies or coincident hit energies that fall in a set of energy ranges. For $\beta\beta$ E.S. modes with
349 multiple γ s, the expected energy ranges will vary differ in natural and enriched detectors, since natural detectors will
350 mostly include hits from one of the γ s, while enriched events will include $\beta\beta$ hits, γ hits, and pileup events including
351 both of these, allowing a much wider energy range. For this reason, a separate set of coincident cut energy ranges are
352 found for natural and enriched detectors.

353 The energy ranges that are cut can be determined by comparing the background model simulation to simulations of
354 each $\beta\beta$ E.S. decay mode. An algorithm was written that simultaneously selects a set of both sum and coincident
355 energy ranges to cut that optimizes discovery potential, as described in appendix ???. The algorithm begins by identifying
356 events in the $\beta\beta$ E.S. simulation that include at least one hit consisting of the full absorption of a γ photon and
357 events in the background model simulation that include at least one hit in the background region of interest. These
358 events are then sorted into energy bins for each coincident hit and for the sum energy of the event (a single event will
359 be in multiple bins). For each bin, the algorithm checks the change in discovery potential if the bin was toggled to be
360 either cut or readded. Following equation ???, the discovery potential will be improved for bin k if:

$$\text{DP}'(s \cdot N_{BG}) \frac{s \cdot n_{k,BG}}{\text{DP}(s \cdot N_{BG})} < \frac{n_{k,ES}}{N_{ES}} \quad (15)$$



where N_{ES} and N_{BG} are the total number of events remaining in the simulated $\beta\beta$ E.S. and background spectra, respectively, s is a scaling to estimate the number of background events in the data from the number in the simulation, and $n_{k,ES}$ and $N_{k,BG}$ are the number of simulated $\beta\beta$ E.S. and background events contained in the bin. A χ value is computed representing the normal quadrile of the probability that cutting or readding the bin will improve the discovery potential. This is done by assuming that the uncertainty on the number of events in the bin is Gaussian distributed, with standard deviations $\sqrt{n_{k,ES}}$ and $\sqrt{n_{k,BG}}$, respectively. In this case, we get:

$$\chi_k = \frac{\frac{n_{k,ES}}{N_{ES}} - DP'(s \cdot N_{BG}) \frac{s \cdot n_{k,BG}}{DP(s \cdot N_{BG})}}{\sqrt{(DP'(s \cdot N_{BG}) \frac{s}{DP(s \cdot N_{BG})})^2 n_{k,BG} + \frac{n_{k,ES}}{N_{ES}}}} \quad (16)$$

All events in the bin with highest probability of improving the discovery potential are then either cut or readded, and must be cut or readded to all other bins that they fall into. Note that a readded event will only be readded if it is not cut by any other bin. This process is repeated until toggling any bin will have $\chi_k < 0$, meaning there is a $< 50\%$ chance of improving the discovery potential. At this point, the bins are then combined in order to determine the ranges of energies to be cut in sum energy and coincident energies.

Because of limited statistics in the simulations, this cut will be biased to cut events with a downward fluctuation in $\beta\beta$ E.S. amplitude and accept bins with an upward fluctuation in $\beta\beta$ E.S. amplitude, and vice-versa for the background model. In order to minimize this bias and ensure that energy ranges are selected based on real backgrounds rather than statistical fluctuations, a penalty is applied to the probability calculations if a new range would be added. If a cutting or readding a bin would increase the number of energy ranges, a penalty of 3 is added to the χ value, and if it would reduce the number of ranges, a penalty of -3 is added. This corresponds to requiring a 99.8% chance that adding a new energy range will represent an improvement before we conclude that it is not a statistical fluctuation. This is inspired by the Akaike Information Criterion (AIC), which adds a penalty of 1 to a likelihood for each parameter added to a model. In this case, adding an energy range adds two parameters to our cut, so the equivalent penalty is 1.5 per parameter, which is a larger penalty than AIC.

To further control limited simulation statistics, a variety of bin widths is used to determine the optimal energy ranges. This is necessary because with a narrow binning, bins do not have enough statistics to overcome the penalty described above, but wider bins produce very imprecise energy ranges. The algorithm starts by optimizing the cut ranges with a bin width of 6.4 keV starting from a prior of cutting no energy ranges. Once this optimization is complete, the bin width is split in half and the algorithm re-optimizes the energy ranges, using the previous ranges as a prior. This halving of bin width is repeated until a final bin width of 0.2 keV is reached. The results of this cut optimization procedure are shown in figures 14 and 15.

The application of the sum and coincident energy cuts will introduce systematic error to the efficiency measurement. For the $2\nu\beta\beta$ decay modes, the coincidence events will have a broad energy spectrum, so the systematic error will be dominated by errors in that spectrum or in the energy estimation. Since the efficiency is calculated by integrating over portions of the coincidence spectrum, an upper limit on the systematic error can be found using the KS statistic of a comparison between the simulated spectrum and the true spectrum. As discussed in section ??, we can compare the decay0 simulated spectrum to the true spectrum using the Iachello simulated spectrum. To account for energy nonlinearity, each energy is shifted to represent the effects of digitizer nonlinearity and energy drift. Digitizer nonlinearity originates from the fact that some digitizer energy bins are slightly wider than others and has an approximately sawtooth dependency on energy with a period of ~ 600 keV. A correction is applied that reduces the size of this nonlinearity to ~ 0.1 keV in magnitude and smooths it out significantly, as shown in figure 16. Digitizer nonlinearity is corrected by shifting each energy according to a sawtooth function with rms 0.1 keV and period 600 keV:

$$\Delta(E) = \sqrt{3} \cdot (0.1 \text{ keV}) \left(\text{rem}\left(\frac{E - 150 \text{ keV}}{600 \text{ keV}}\right) \right) \quad (17)$$

where rem is the remainder function as defined in the C++ standard library. An additional shift that is randomly sampled from a Gaussian distribution with standard deviation $0.00015 \cdot E$ is applied to simulate the effect of gain drift, based on the drift observed during DS5. After applying both of these corrections to the decay0 spectrum, a KS test is performed against the Iachello spectrum, and a KS statistic of 0.08% is observed, as shown in figure 17. This statistic is used as an upper limit on the uncertainty from the energy range cuts for $2\nu\beta\beta$ modes. For $0\nu\beta\beta$, the energy ranges selected by this cut tend to surround peaks corresponding to the $Q_{\beta\beta}$ s of the decay modes. In this case, since we are no longer integrating over a $\beta\beta$ -spectrum, the uncertainty in the efficiency will depend on shifts in the peak, similar to the ROI-efficiency. Since the energy regions selected keep at least 99.9%



411 of these peaks in all cases, we can set an upper limit on the uncertainty by checking the ROI efficiency uncertainty
 412 around the 2039 keV $Q_{\beta\beta}$, assuming an ROI tuned to select 99.9% of the peak. The uncertainty observed in this case
 413 is 0.325%, which is applied to the energy range cuts for $0\nu\beta\beta$ modes. For both $0\nu\beta\beta$ and $2\nu\beta\beta$ modes, this efficiency
 414 uncertainty is sub-dominant, so these upper limits will suffice.

415

416 C. Muon Veto Cut

417 Cosmic ray muons have the potential to produce partial showers in the MAJORANA DEMONSTRATOR that can
 418 produce multi-site event events and can activate short-lived isotopes that in turn may decay, producing delayed
 419 multi-site event events. Background events caused by muons can be cut using the muon veto system described in
 420 [9]. Any Germanium detector events for 20 ms before and 1 s after a tagged muon event cut. This cut will remove
 421 $> 99.9\%$ of events induced by the muon shower, based on simulations shown. In reality, the cut efficiency is slightly
 422 lower due to periods of time where the muon veto system clock became desynchronized with the Germanium detector
 423 clock. The impact of this cut is to reduce the total livetime in each module by < 40 s per day.
 424

425 VII. FINAL EFFICIENCY MEASUREMENTS

426 The final efficiency measurement combining all of the effects described in this chapter for each $\beta\beta$ E.S. mode
 427 is measured directly from the simulations. The efficiency used is the average of the simulated efficiency for each
 428 subdataset, weighted by the exposure of that subdataset. Because each module is an independent measurement,
 429 separate efficiencies are measured for modules 1 and 2. Because of correlations causing the probability of certain
 430 effects causing sacrifice of a $\beta\beta$ E.S. event to be conditional on other effects, the combined efficiency will differ from
 431 simply being the product of the individual efficiencies. This means that the combined efficiency ϵ_{comb} for each effect
 432 k is:

$$\epsilon_{comb} = \prod_{k=0}^N P(\text{event is cut} | \text{cuts } 0 \dots k-1 \text{ are applied}) \quad (18)$$

433 In spite of this, we will assume that the sources of error are uncorrelated and the fractional uncertainty is independent
 434 of what other effects have been applied. This implies that the uncertainty on the combined efficiency, $\sigma_{\epsilon,comb}$ can be
 435 expressed as:

$$\sigma_{\epsilon,comb} = \epsilon_{comb} \sqrt{\sum_{k=0}^N N \left(\frac{\sigma_{\epsilon,k}}{\epsilon_k} \right)^2} \quad (19)$$

436 The values ϵ_k represent the probability of cutting an event assuming all other cuts are applied. Table V shows the
 437 efficiency for each effect described in this chapter and uncertainty on each efficiency, and the combined efficiency
 438 and uncertainty. Similar tables for each other $\beta\beta$ E.S. peak are shown in appendix A. In all cases the dominant

Source	Module 1 efficiency	Module 2 efficiency
M. S. Event Signature	$5.2 \pm 0.2\%$	$2.8 \pm 0.5\%$
Region of Interest	$87.9 \pm 1.4\%$	$87.9 \pm 1.4\%$
Dead Layer	$74.5 \pm 4.3\%$	$65.7 \pm 6.0\%$
Detector Dead Times	$97.5 \pm 1.2\%$	$98.1 \pm 0.9\%$
Enriched Source Detector Cut	$98.7 \pm < 0.1\%$	$95.7 \pm < 0.1\%$
Coincident Energy Cut	$93.5 \pm < 0.1\%$	$93.1 \pm < 0.1\%$
Sum Energy Cut	$63.4 \pm < 0.1\%$	$59.3 \pm < 0.1\%$
Final Efficiency	$2.29 \pm 0.17\%$	$0.97 \pm 0.19\%$

TABLE V Table of detection efficiencies and uncertainties for $2\nu\beta\beta$ of ^{76}Ge to the 0_1^+ state of ^{76}Se . Note that the efficiencies
 439 are the combined efficiency for the 559 and 563 keV peaks.

440

441 uncertainties come from either the dead layer thickness or the simulation uncertainty. Figure 19 shows the effect of
 442 each cut as it is applied sequentially to the $2\nu\beta\beta$ to 0_1^+ peaks.
 443



444 VIII. DOUBLE BETA DECAY TO EXCITED STATES RESULTS

445 Now that we have found and characterized a specific detection signature for each decay mode, we can apply this
446 search to data. This result will look at open runs from datasets 1 through 6a that were designated silver or gold in
447 run quality. The duty cycle and changes that define each data set are shown in figure 20. These were taken from
448 January 12, 2016 to April 18, 2018, and contains a total of 13.4 kg y of isotopic exposure for module 1 and 7.9 kg y
449 for module 2. Approximately half the data in these datasets is blinded, and is not included in this analysis. The
450 MAJORANA DEMONSTRATOR uses a statistical blinding scheme in which 3/4 of runs are blinded administratively (i.e.
451 through file access) in cycles of 31 hrs of unblinded runs followed by 93 hrs of blinded runs. The data is unblinded
452 in a staged fashion, where first single-site events, not including any interesting physics regions are unblinded (i.e. no
453 background ROI, $0\nu\beta\beta$ to the ground state ROI, low energy or multisite data). This data is used for a variety of
454 data validation checks prior to unblinding of any other data. The remaining data are separately unblinded after a
455 collaboration review for individual analyses and users. For this analysis, the multi-site data has been left blinded.

456
458 In the open multi-site data, 5558 multi-detector events were observed. A histogram of the event multiplicities is
459 shown in figure 21, and a spectrum of all multiplicity 2 event energies is shown in figure 22.

462 IX. VALIDATION

463 In addition to the basic run selection and data cleaning validation checks that are run on all multiplicity 1 data, we
464 will perform some additional checks on high multiplicity data. As previously, this section will describe these checks
465 applied to the $2\nu\beta\beta$ to the 0_1^+ state of ^{76}Se . Similar checks are performed on other decay modes in appendix A.

466 A. Data Rate

467 Any spikes in the rate of multisite events would potentially indicate problems with run selection or data cleaning.
468 Significant variation in the data rate is expected due to changes in which detectors are active. For this reason, the
469 rate of multisite events with respect to the effective exposure, which is the exposure times the detection efficiency of
470 $\beta\beta$ E.S. events is used instead. This quantity is interesting because the rate of observed $\beta\beta$ E.S. events should be
471 constant with respect to it. The changes in detection efficiency from one subdataset to another for both backgrounds
472 and $\beta\beta$ E.S. are highly correlated and driven by which detectors are enabled. For this reason, we can reasonably expect
473 that the backgrounds should also have a nearly constant rate with respect to effective exposure, although differences
474 between background source positions and the distribution of ^{76}Ge in the detectors imply that some difference should be
475 expected. Figure 23 indeed shows a slow reduction in the overall background rate over time. One possible explanation
476 for this is that a significant quantity of ^{68}Ge exists in natural HPGe detectors as a result of cosmogenic activation,
477 and has a half-life of 271 days, which is observable on the timescale of the MAJORANA DEMONSTRATOR's operation.
478 ^{68}Ga is a β^+ emitter which is a part of the ^{68}Ge decay chain, which produces two 511 keV γ s, resulting in many
479 multi-site events.

481 B. Background Cut Evaluation

482 A second important check to ensure that the cuts applied to each $\beta\beta$ E.S. mode is to compare each cut efficiency to
483 the expected background cut efficiency. Since the background model used for this analysis uses preliminary results,
484 disagreement between the expected and measured cut efficiencies could indicate a difference between the background
485 model and the measured backgrounds rather than a problem with the application of cuts. However, any major
486 discrepancies could indicate a bug in the analysis. To perform this comparison, the cut efficiencies are measured both
487 in terms of the total number of events cut, ϵ_{total} and the number of events that are uniquely cut, ϵ_{unique} (i.e., not cut
488 by any of the others). Table VI lists each cut for the $\beta\beta$ E.S. decay to the 0_1^+ state and the expected and measured
489 cut efficiencies. The expected background cut efficiencies, $\langle\epsilon\rangle$ represent the fraction of events cut, averaged over all
490 datasets, weighted by exposure. The measured background cut efficiencies, $\hat{\epsilon}$ represent the measured fraction of events
491 cut. Statistical uncertainties in the expected efficiencies are negligible compared to the uncertainties in the measured
492 efficiencies, and are not included. The sacrifice is the number of events uniquely sacrificed by the cut. ΔDP is the
493 expected improvement in discovery potential, as defined in appendix ?? as a result in the cut. Figure 24 shows the



494 effects of data cuts on multiplicity 2 events. Figure 25 shows the effects of cuts on events in the ROI in both measured
 495 and simulated data.

496 X. RESULTS

497 A. Statistical Methods

498 Neyman confidence intervals are computed for each peak in each $\beta\beta$ E.S. decay mode, and each module. For a
 499 given peak k , the expected number of signal counts is

$$500 \langle s_k \rangle = \ln 2 \frac{N_A}{m_{76}} \epsilon_k \frac{M_{iso} T_{live}}{T_{1/2}} \quad (20)$$

500 where M_{iso} is the total isotopic mass and T_{live} is the livetime ($M_{iso} T_{live}$ is the exposure and is calculated in section ??
 501 to be 13.356 ± 0.021 for module 1 and 7.872 ± 0.13 for module 2. ϵ_k is the total detection efficiency of the decay mode
 502 using peak k , and is calculated in chapter ??, and can be found in appendix A. $m_{76} = 0.0759214$ kg is the molar
 503 mass of ^{76}Ge , and $N_A = 6.02214076 \times 10^{23}$ is Avagadro's number. Fun fact: an Avagadro's number of avocados has
 504 approximately the volume of Mars. We will define the single count half-life to be

$$505 T_k^* = \ln 2 \frac{N_A}{m_{76}} \epsilon_k M_{iso} T_{live} \quad (21)$$

505 which is the decay half-life that would produce on average one count in signal ROI k .

506 Because of the nearly background free nature of this search, a likelihood construction is used that assumes Poisson
 507 statistics for the number of counts in the signal and background ROIs.

$$508 \mathcal{L}(T_{1/2}, T_k^*, b_k | n_k, m_k, \langle T_k^* \rangle, \sigma_{T^*,k}, \tau) = \frac{\mu_k^{n_k} e^{-\mu_k}}{n_k!} \cdot \frac{(b_k \tau)^{m_k} e^{-b_k/\tau}}{m_k!} \cdot \frac{1}{\sigma_{T^*,k} \sqrt{2\pi}} e^{-\frac{(T_k^* - \langle T_k^* \rangle)^2}{2\sigma_{T^*,k}^2}} \\ 509 \mu_k = s_k + b_k = \frac{T_k^*}{T_{1/2}} + b_k \quad (22)$$

510 $T_{1/2}$ represents the decay mode half-life and is the parameter of interest. T_k^* and b_k are nuisance parameters representing
 511 the measured single count halflife and expected backgrounds in the ES ROI, respectively. μ_k is the total expected number of counts, combining background and signal, in the ES ROI. n_k is the measured number of events
 512 in the ES ROI and is expected to be drawn from a Poisson distribution with mean μ_k . m_k is the measured number of events in the BG ROI and is expected to be drawn from a Poisson distribution with mean b_k/τ , where τ is the ratio
 513 between the number of expected background counts in the BG ROI to the number in the ES ROI. Note that since
 514 these events are multi-site event, it is possible for multiple hits in the event to fall into one of the ROIs; however, we
 515 will choose a single hit to represent the whole event. In this case, any hit that falls into the ES ROI takes precedence
 516 over any hit that falls into the BG ROI, and if multiple hits fall into the ES ROI, one is chosen at random. τ is
 517 usually determined based on the background simulation; however, in cases where the simulation statistics are limited
 518 after applying all cuts, a flat background is assumed and the ratio of the ES ROI width to the BG ROI width is used.
 519 $\langle T_k^* \rangle$ represents the expected value of T_k^* based on previous measurements of exposure and detection efficiency, which
 520 is assumed to have Gaussian uncertainty:

$$521 \sigma_{T^*,k} = \langle T_k^* \rangle \sqrt{\left(\frac{\sigma_{\epsilon,k}}{\epsilon_k}\right)^2 + \left(\frac{\sigma_{exposure}}{M_{iso} T_{live}}\right)^2} \quad (23)$$

521 The implementation of equation 22 is performed by the `TRolke` class in ROOT [10]. This likelihood function is used
 522 to compute a likelihood ratio

$$523 \text{LR}(T_{1/2}) = \frac{\sup_{T_k^*, b_k} (\mathcal{L}(T_{1/2}, T_k^*, b_k | n_k, m_k, \langle T_k^* \rangle, \sigma_{T^*,k}, \tau))}{\sup_{T_{1/2}, T_k^*, b_k} (\mathcal{L}(T_{1/2}, T_k^*, b_k | n_k, m_k, \langle T_k^* \rangle, \sigma_{T^*,k}, \tau))} \quad (24)$$

524 The `TRolke` class analytically computes the supremum over T_k^* and b_k , returning the log-likelihood difference. $T_{1/2}$ is
 525 restricted to positive values. Since the likelihood ratio is expected to be χ^2 -distributed, to construct a 90% confidence interval, we seek the values of $T_{1/2}$ corresponding to a log-likelihood ratio value of 2.7. In cases where the lower limit



Cut Name	Cut Description	$\langle \epsilon_{total} \rangle$	$\hat{\epsilon}_{total}$	$\langle \epsilon_{unique} \rangle$	$\hat{\epsilon}_{unique}$	Sacrifice	ΔDP
Enriched Source Detector Cut	Any other detector: <code>iStar</code>	M1: 23.2 % M2: 42.7 %	27.2 ^{+3.8} _{-3.5} % 62.8 ^{+7.0} _{-7.6} %	2.2 % 4.4 %	2.0 ^{+1.5} _{-0.9} % 4.7 ^{+4.4} _{-2.3} %	0.7 % 2.1 %	7%
Coincident Energy Cut	No other detector: <code>((energy<40.6) (energy>402.6 && energy<409.6) (energy>506.8 && energy<512.4) (energy>608.6 && energy<610.2) (energy>170.6 && energy<175.6) (energy>125.6 && isbn) ((energy<83.) (energy>228.2 && energy<350.6) (energy>75.2 && energy<16.8) (energy>566.6 && energy<613.4) (energy>737.4) && iStar)</code>	M1: 29.6 % M2: 37.5 %	33.3 ^{+4.0} _{-3.8} % 48.8 ± 7.5 %	4.4 % 4.2 %	4.8 ^{+2.1} _{-1.5} % 2.3 ^{+3.6} _{-1.4} %	3.9 % 3.5 %	7%
Sum Energy Cut	<code>Note: (sumE<870.) (sumE>870.6 && sumE<877.6) (sumE>878.6 && sumE<891.) (sumE>891.2 && sumE<913.6) (sumE>960.8 && sumE<972.) (sumE>1066.8 && sumE<1072.6) (sumE>1170.8 && sumE<1174.6) (sumE>1330.8 && sumE<1335.6) (sumE>1484.2 && sumE<1461.6) (sumE>1761.8 && sumE<1765.6) (sumE>1794.4)</code>	M1: 75.0 % M2: 75.6 %	74.8 ^{+3.4} _{-3.7} % 74.4 ^{+6.0} _{-7.2} %	44.5 % 33.0 %	41.5 ^{+4.1} _{-4.0} % 25.6 ^{+7.2} _{-6.0} %	31.8 % 32.1 %	20%
Combined Cuts		M1: 84.5 % M2: 89.5 %	84.4 ^{+2.8} _{-3.2} % 95.3 ^{+2.3} _{-4.4} %	—	—	44.9 % 53.1 %	27%

TABLE VI Table of detection efficiencies and uncertainties for $2\nu\beta\beta$ of ^{76}Ge to the 0_1^+ state of ^{76}Se .



526 is found to be < 0 , a lower limit on the half-life is reported.

527 After constructing confidence intervals for each peak and module individually, a combined confidence interval is
528 constructed for each $\beta\beta$ E.S. decay mode. A combined log-likelihood over all peak/module combinations k is defined
529 by

$$\mathcal{L}(T_{1/2}) = \sum_{k=0}^N \sup_{T_k^*, b_k} (\log(\mathcal{L}(T_{1/2}, T_k^*, b_k | n_k, m_k, \langle T_k^* \rangle, \sigma_{T^*, k}, \tau))) \quad (25)$$

530 This construction relies on the fact that the T_k^* and b_k values across each peak can be independantly maximized,
531 enabling the continued use of the TRolke implementation. A combined likelihood ratio is constructed and used to
532 compute a confidence interval as above. Table VII contains the limits constructed for each decay mode, peak and
533 module. For all modes, a lower half-life limit is set.

534 Note that each decay mode is analyzed independantly. The problem with this approach is that all decay modes
535 have the 559 keV peak in common, meaning that the results will be correlated. For this result, since all modes only
536 have a lower limit on half-life set, this approach is not problematic since for any individual mode, we would take the
537 supremum over all other half-lives, which would be at or near infinity, resulting in the same sets of equations used
538 here. However, if the $\beta\beta$ E.S. to the 0_1^+ mode is discovered, it will become necessary to perform a full combined
539 analysis.

540 The detection sensitivity is computed by constructing a toy Monte Carlo for each decay mode, assuming that each
541 $T_{1/2}$ is infinite. For each sample i , a random n_i and m_i is drawn from a Poisson distribution with mean n_k and m_k .
542 The confidence interval for a measurement with these values is computed. The median sensitivity is extracted by
543 taking the median lower half-life limit over all samples. For the results in table VII, 100001 samples were used.

544

545 B. Limits and Sensitivities

546 The limits and sensitivities for each peak and module individually, and the combination for each mode, are shown
547 in table VII. Figure 26 shows the event spectrum after all cuts have been applied with both ROIs highlighed.

548 REFERENCES

- 549 [1] J. Kotila and F. Iachello. Phase-space factors for double- β decay. *Phys. Rev. C*, 85:034316, Mar 2012.
- 550 [2] O. A. Ponkratenko, V. I. Tretyak, and Yu. G. Zdesenko. Event generator decay4 for simulating double-beta processes and
551 decays of radioactive nuclei. *Physics of Atomic Nuclei*, 63(7):1282–1287, Jul 2000.
- 552 [3] Balraj Singh. Nuclear data sheets update for a = 76. *Nuclear Data Sheets*, 74(1):63 – 164, 1995.
- 553 [4] Robley D. Evans. *The Atomic Nucleus*, chapter 6, page 240. International series in pure and applied physics. McGraw-Hill,
554 New York, 1955.
- 555 [5] Pavol Vojtyla. Fast computer simulations of background of low-level ge γ -spectrometers induced by ^{210}pb ^{210}bi in shielding
556 lead. *Nuclear Instruments and Methods in Physics Research Section B: Beam Interactions with Materials and Atoms*,
557 117(1):189 – 198, 1996.
- 558 [6] A Reine, T Caldwell, C Cuesta, I Guinn, and J Myslik. Run selection and data cleaning of ds5 (m1 and m2) (internal).
559 Technical Report 2017-020, University of North Carolina at Chapel Hill, May 2018.
- 560 [7] F. James. MINUIT Function Minimization and Error Analysis: Reference Manual Version 94.1. Technical Report CERN-
561 D506, CERN CN Division, Geneva, 1994.
- 562 [8] P. Chu, J. Detwiler, and I. Guinn. Energy systematic of MAJORANA DEMONSTRATOR. Technical Report 2017-021, Los
563 Alamos National Laboratory, Oct 2017.
- 564 [9] C Wiseman. Muon veto analysis for the MAJORANA DEMONSTRATOR (internal). Technical report, University of South
565 Carolina, 2016.
- 566 [10] Wolfgang A. Rolke, Angel M. López, and Jan Conrad. Limits and confidence intervals in the presence of nuisance
567 parameters. *Nuclear Instruments and Methods in Physics Research Section A: Accelerators, Spectrometers, Detectors
568 and Associated Equipment*, 551(2):493 – 503, 2005.

569 Appendix A: Detailed Results for All Decay Modes

570 The main document concerned itself primarily with the $2\nu\beta\beta$ of ^{76}Ge to the 0_1^+ excited state. However, results
571 are presented for all decay modes and energy peaks. This appendix will present figures and tables detailing the
572 simulations, cuts, efficiencies and results for each decay mode and peak.



Decay Mode	Peak	Module	n_{ROI}	m_{BG}	Expected ROI BGs	$T^* (\times 10^{23} \text{y})$	$T_{1/2} (\times 10^{23} \text{y})$ 90% Limit	$T_{1/2} (\times 10^{23} \text{y})$ 90% Sensitivity
$0_{g.s.}^+ \xrightarrow{2\nu\beta\beta} 0_1^+$	559 keV	M1	2	23	0.88	8.41 ± 0.62	> 1.9	> 3.2
		M2	0	2	0.09	2.10 ± 0.41	> 1.5	> 1.5
		M1	0	23	0.97	8.42 ± 0.62	> 6.2	> 3.2
	563 keV	M2	0	2	0.08	2.08 ± 0.40	> 1.5	> 1.5
		Combined					> 6.8	> 7.0
$0_{g.s.}^+ \xrightarrow{2\nu\beta\beta} 2_1^+$	559 keV	M1	0	16	0.68	10.43 ± 1.10	> 7.6	> 7.6
		M2	0	1	0.04	2.66 ± 0.98	> 1.8	> 1.8
		Combined					> 9.6	> 5.3
	657 keV	M1	2	38	1.46	7.24 ± 0.97	> 1.8	> 2.9
		M2	0	5	0.22	1.89 ± 0.97	> 1.1	> 1.1
		M1	1	20	0.69	5.49 ± 0.77	> 1.8	> 4.0
$0_{g.s.}^+ \xrightarrow{2\nu\beta\beta} 2_2^+$	1216 keV	M2	0	3	0.10	1.50 ± 0.84	> 0.8	> 0.8
		M1	0	29	0.79	3.14 ± 0.95	> 2.2	> 1.0
		M2	0	4	0.14	0.77 ± 1.07	> 1.5	> 1.5
	Combined	Combined					> 5.6	> 5.3
$0_{g.s.}^+ \xrightarrow{0\nu\beta\beta} 0_1^+$	559 keV	M1	0	2	0.09	11.47 ± 0.99	> 8.4	> 8.4
		M2	0	0	0.00	2.92 ± 0.59	> 2.1	> 2.1
		M1	0	2	0.09	11.32 ± 0.98	> 8.3	> 8.3
	563 keV	M2	0	0	0.00	2.86 ± 0.58	> 2.1	> 2.1
		Combined					> 21.1	> 21.1
$0_{g.s.}^+ \xrightarrow{0\nu\beta\beta} 2_1^+$	559 keV	M1	0	0	0.00	12.04 ± 1.35	> 8.8	> 8.8
		M2	0	0	0.00	3.01 ± 1.10	> 2.0	> 2.0
		Combined					> 11.0	> 11.0
	657 keV	M1	0	2	0.08	7.16 ± 1.01	> 5.2	> 5.2
		M2	0	0	0.00	1.81 ± 0.93	> 1.0	> 1.0
		M1	0	7	0.27	7.00 ± 1.04	> 5.1	> 5.1
$0_{g.s.}^+ \xrightarrow{0\nu\beta\beta} 2_2^+$	1216 keV	M2	0	1	0.02	1.76 ± 1.01	> 0.8	> 0.9
		M1	0	0	0.00	3.23 ± 0.92	> 2.3	> 2.3
		M2	0	0	0.00	0.81 ± 1.04	> 0.3	> 0.3
	Combined	Combined					> 16.0	> 16.0

TABLE VII Results for all decay modes.

573 **Appendix B: $2\nu\beta\beta$ to 0_1^+**

575 Note that both the 559 and 563 keV peaks will be shown together since they use the same sets of cuts.

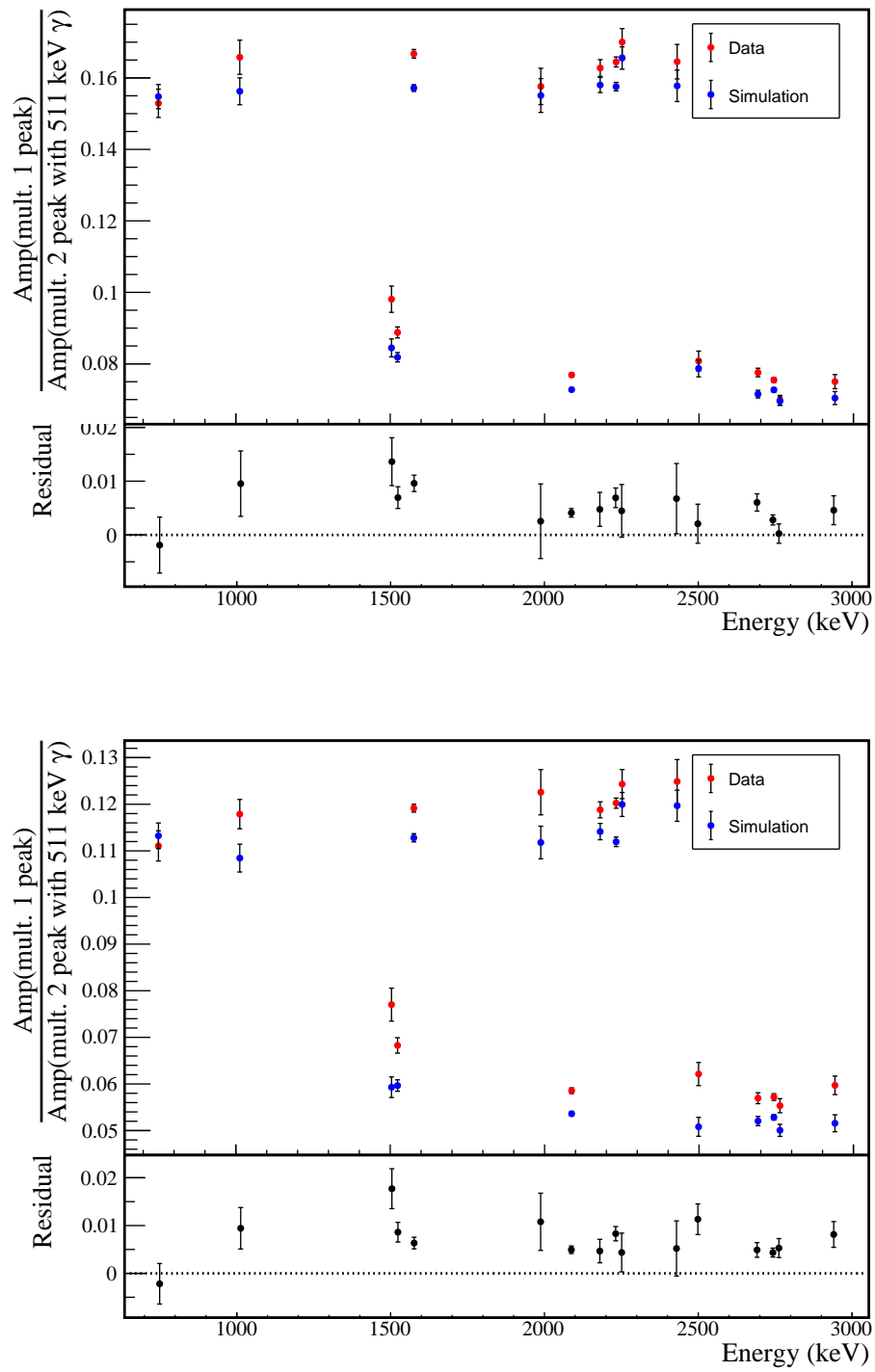


FIG. 10 Measurement of peak height ratios between multiplicity 1 events and multiplicity 2 events containing a 511 keV annihilation γ for both simulated and measured ^{56}Co spectra. Module 1 is shown on top, and Module 2 below. Only statistical error bars are drawn. These ratios are listed in tables II and III.

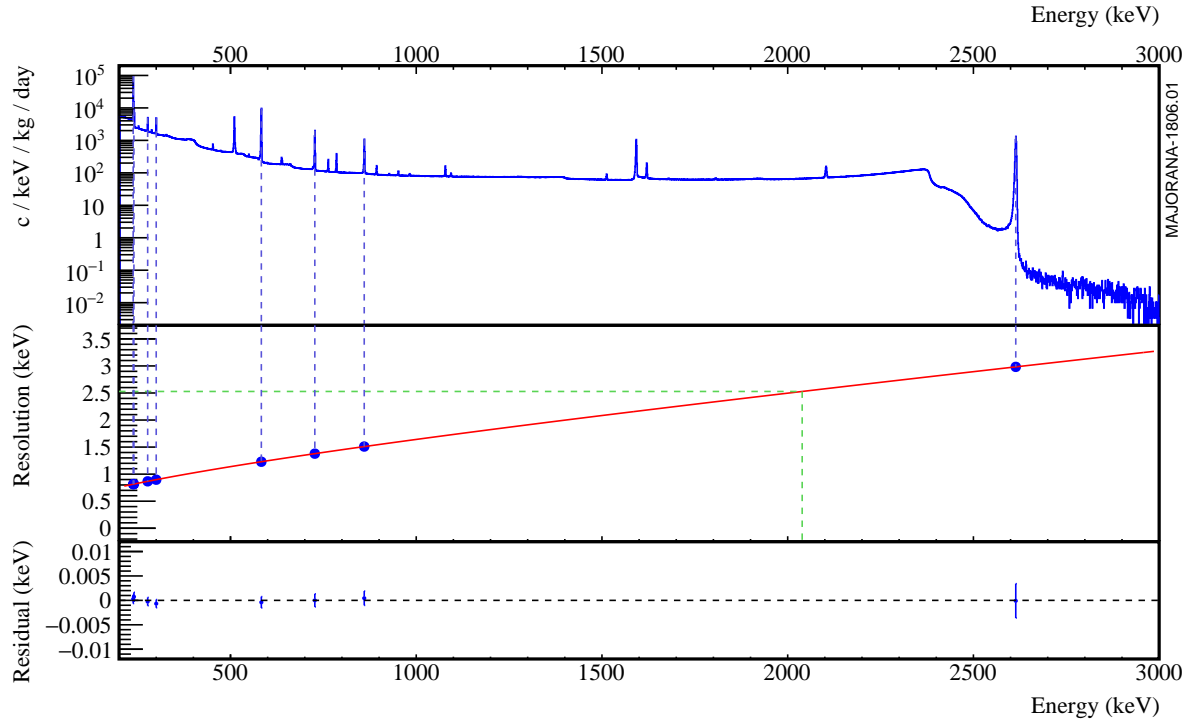


FIG. 11 A ^{228}Th calibration run with the FWHM fit curve and individual uncertainties at several peaks. This curve is used to compute the FWHM for a peak at a given energy. The statistical uncertainty is extracted from the fit result. An additional uncertainty is added to account for the uncertainties in the individual peaks; this is used to measure the uncertainty from energy nonlinearity.

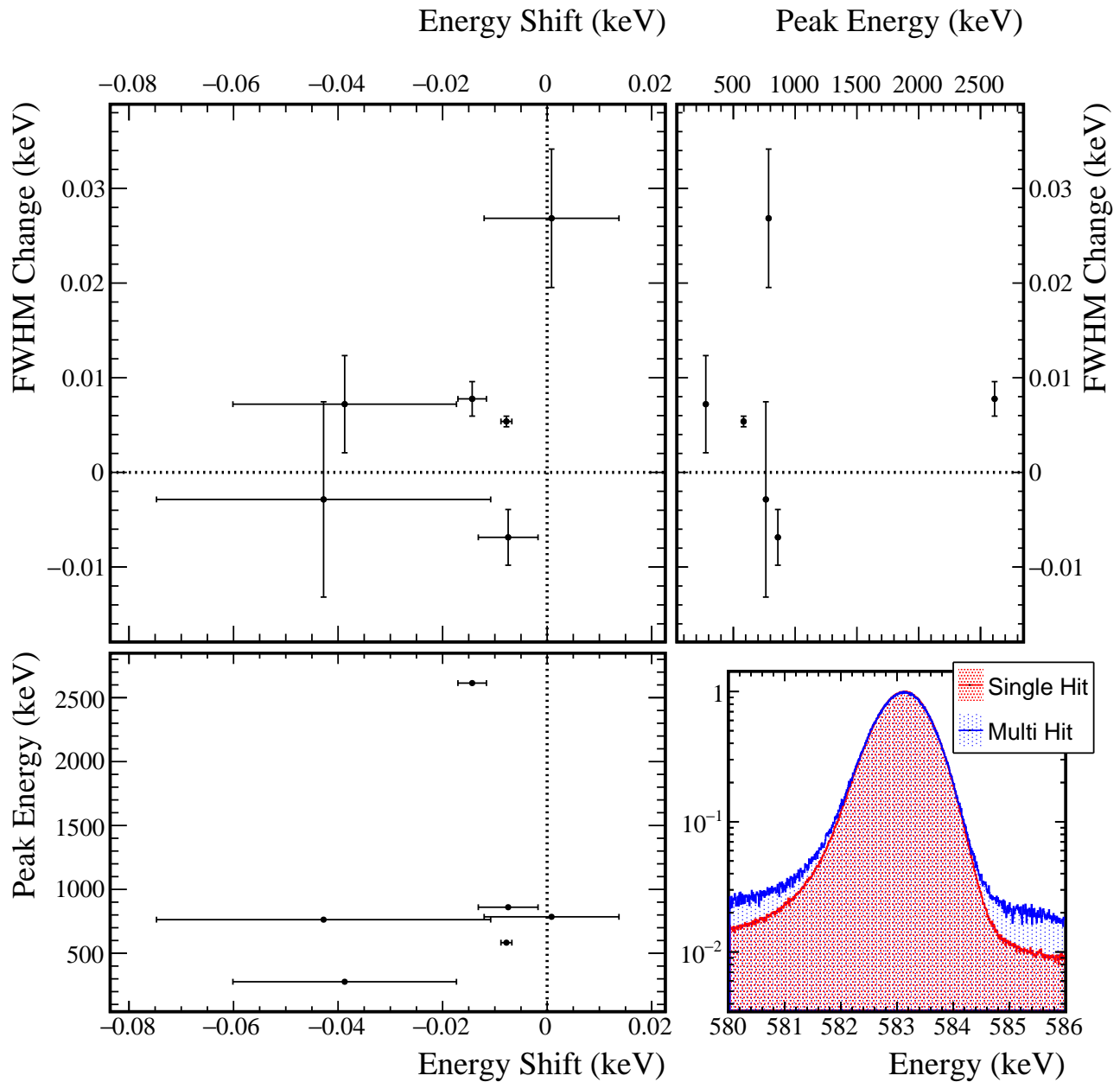


FIG. 12 Difference of the measured centroid and FWHM of several ^{228}Th calibration peaks. Error bars represent the fit errors. Notice on the bottom right, that any difference is not visible to the naked eye.



FIG. 13 Diagram showing each detector in each module, arranged by which string and position they are in. Enriched detectors are colored green and natural detectors are colored blue. 95% of ^{76}Ge is contained in the enriched detectors.

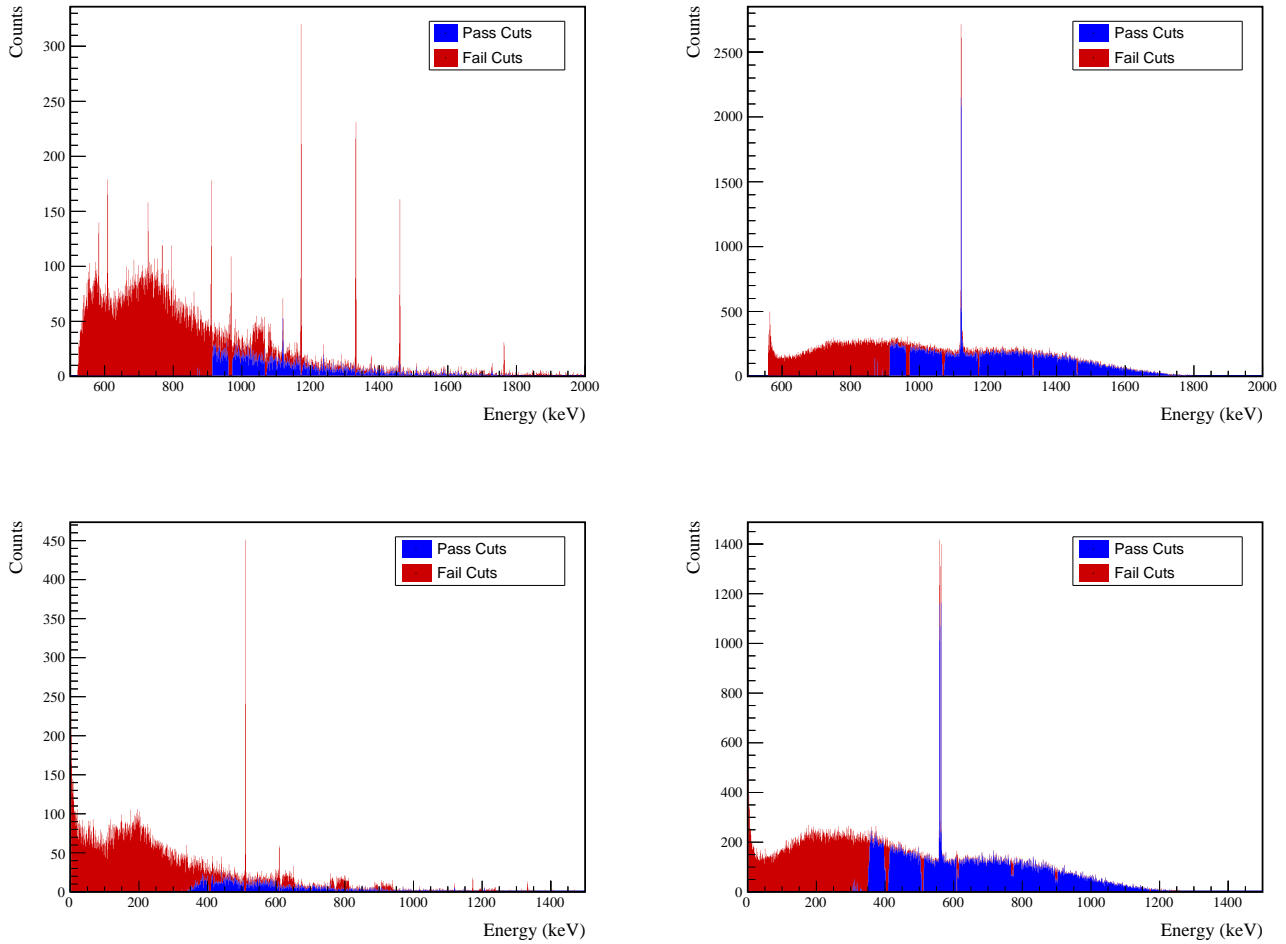


FIG. 14 Top: Sum energy spectra of simulated ES (left) and BG (right) events. The events in red are cut by the sum- or coincident-energy cut. Note that the region around many peaks is cut out. This is the intended effect of the sum energy cut. Bottom: Energy spectrum of events in coincidence with events in the ROI from simulations (left) and measured data (right). Events in red are cut by the sum- or coincident-energy cut. Once again, regions around prominent peaks are cut out as intended.

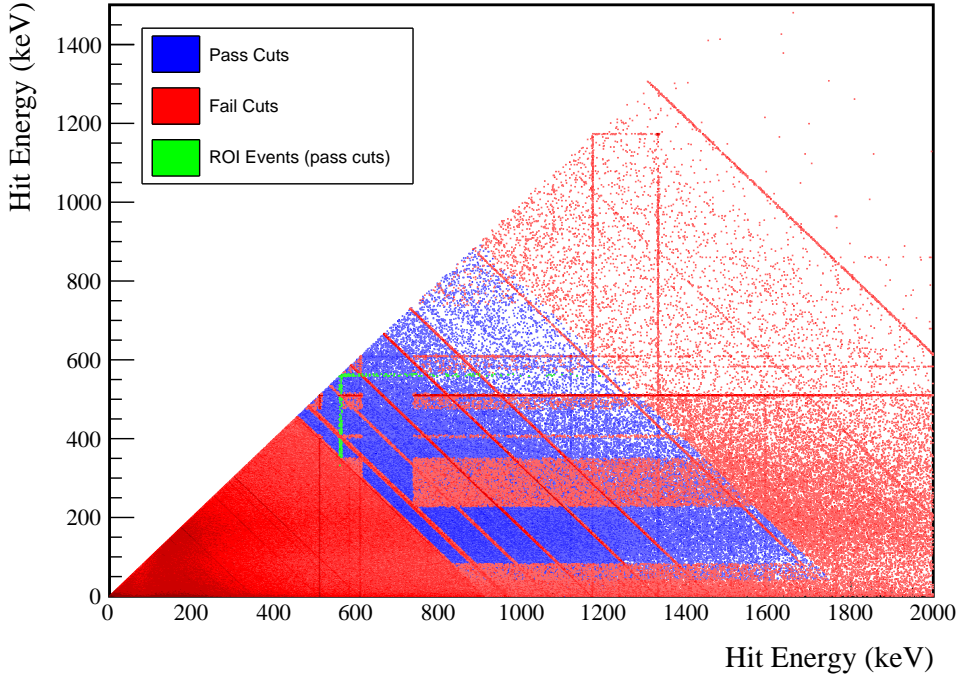


FIG. 15 2D energy spectrum of simulated BG events. Blue bins have at least one hit that passes both the sum- or coincident-energy cuts. For red bins, both hits have failed at least one of these cuts. Green bins have at least one hit in the BG or ES ROI that passes these cuts.

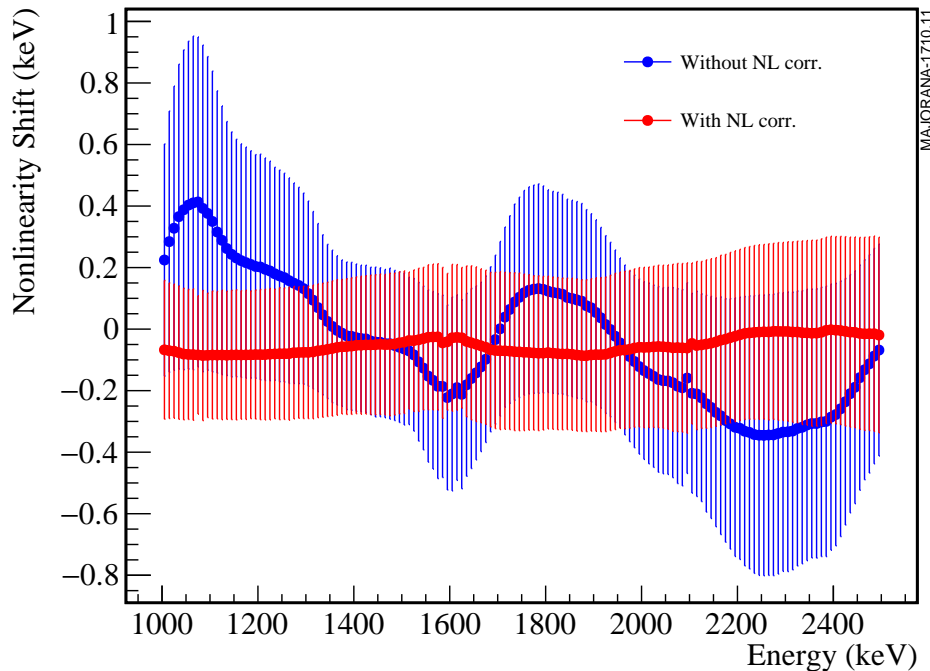


FIG. 16 Digitizer nonlinearity before (red) and after (blue) begin corrected. This nonlinearity is measured by comparing the energy measured in the high gain channel to that of the low gain channel.

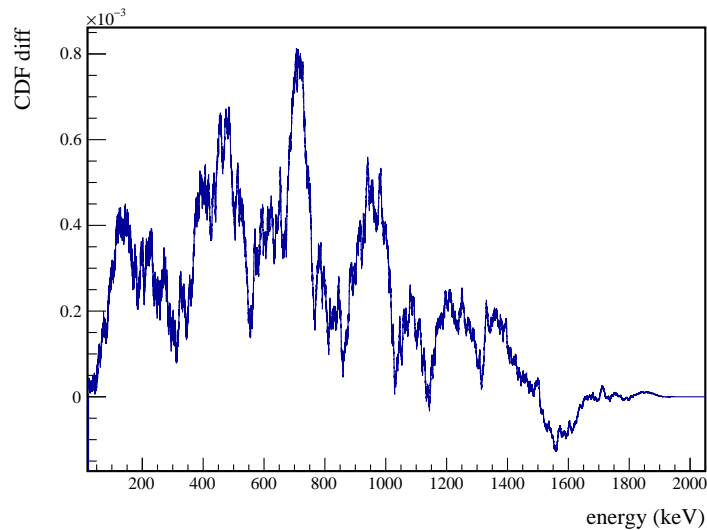


FIG. 17 KS test comparing the simulated decay0 $2\nu\beta\beta$ ground state decay with energy nonlinearities applied to the simulated spectrum using the Iachello phase space factors.

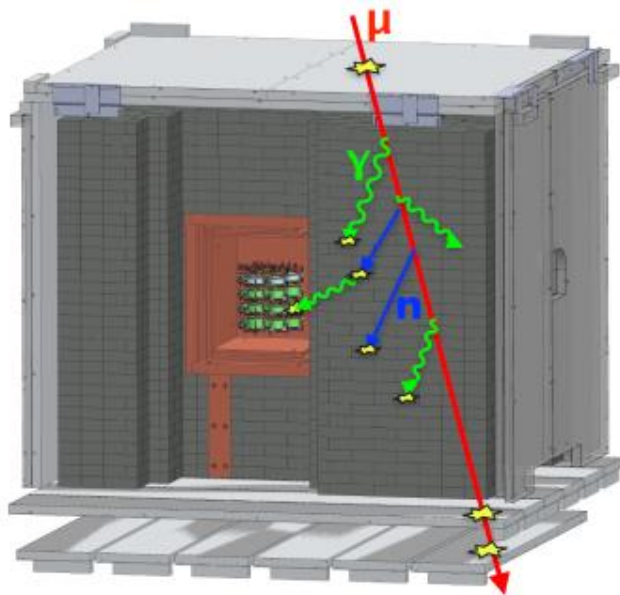


FIG. 18 A cartoon of a particle shower created by a muon event. The particles produced in such a shower can hit multiple detectors, producing multi-detector events.

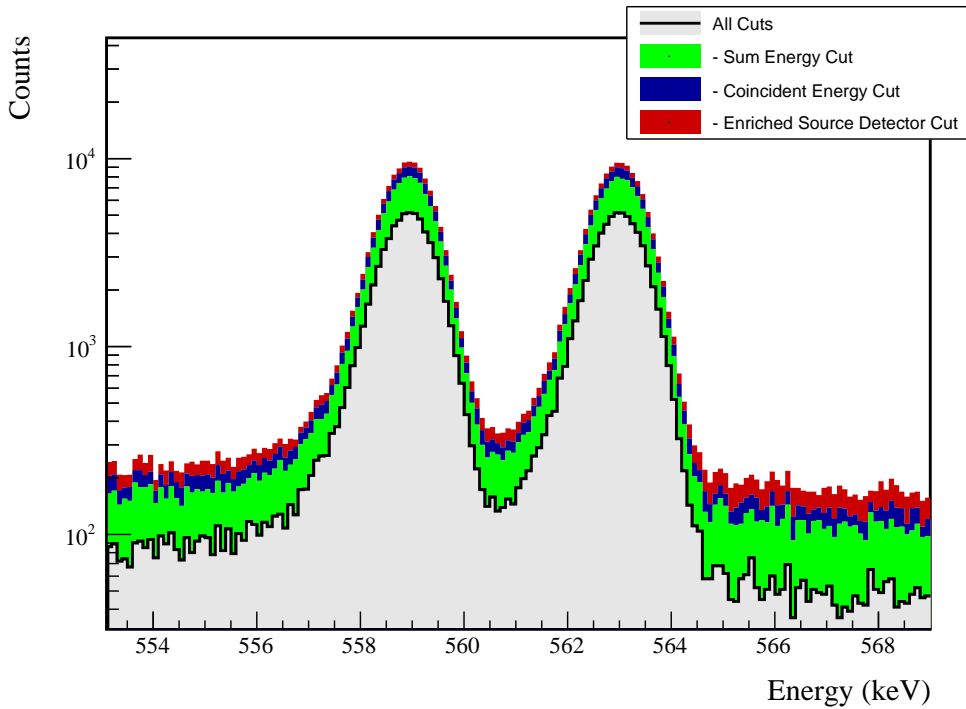


FIG. 19 The 559 and 563 keV peaks from the $2\nu\beta\beta$ decay to the 0_1^+ decay mode, with the effect of all cuts applied sequentially to simulated ES events. The cuts are applied from top to bottom (i.e. red, blue, then green). Many events will be cut by more than one of these; in that case it will be colored by whichever cut is applied first.

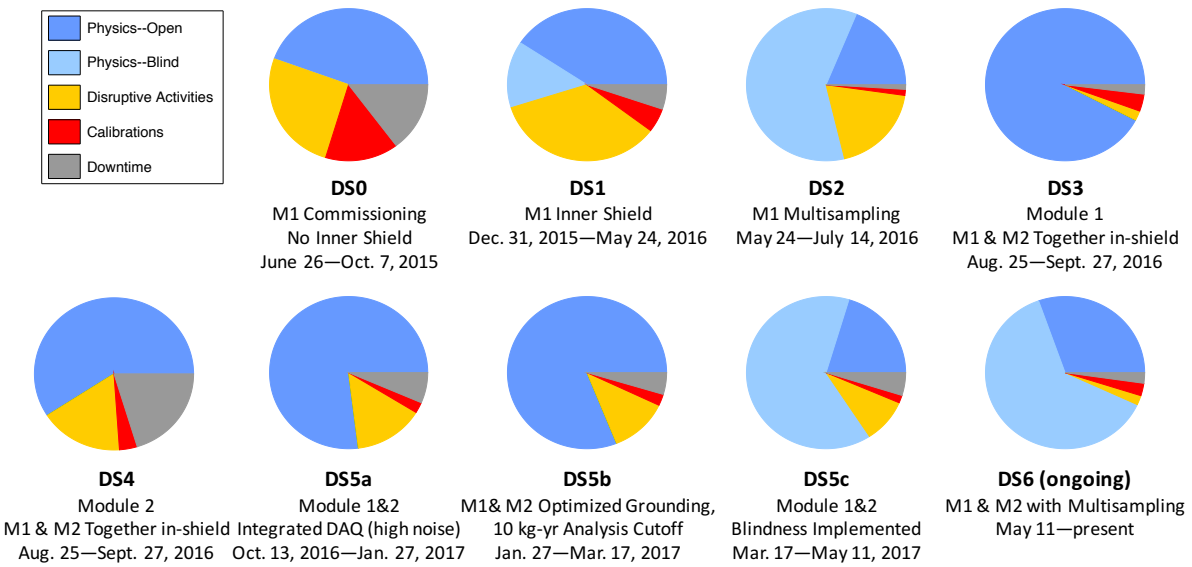


FIG. 20 The duty cycles for each major dataset, and a brief discription of the major changes in configuration that define each data set.

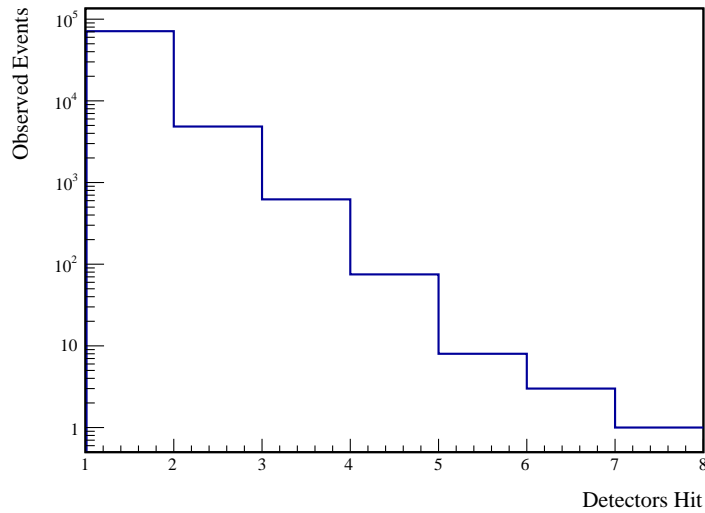


FIG. 21 The measured multiplicities for events in datasets 1-6a. For multiplicity 1 events, only events with energy between 40 keV and 4 MeV were considered.

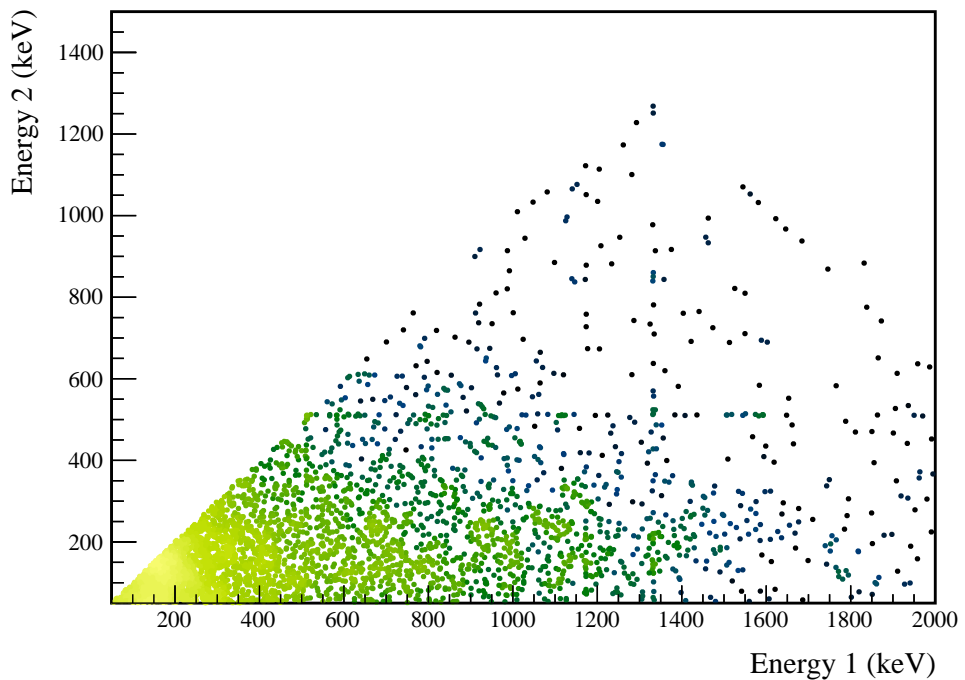


FIG. 22 Measured energy spectrum of multiplicity 2 events in datasets 1-6a.

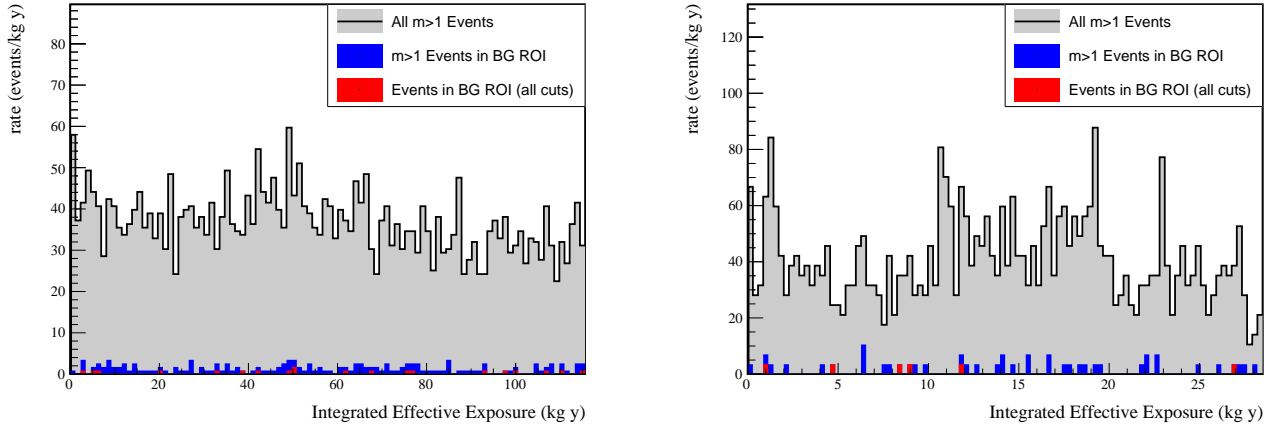


FIG. 23 Event rate with respect to effective exposure, or the detection efficiency of the $2\nu\beta\beta$ decay to the 0_1^+ excited state times the exposure. Integrated exposure is the total effective exposure prior to an event. The background rate is expected to be mostly flat. Left is module 1, right is module 2.

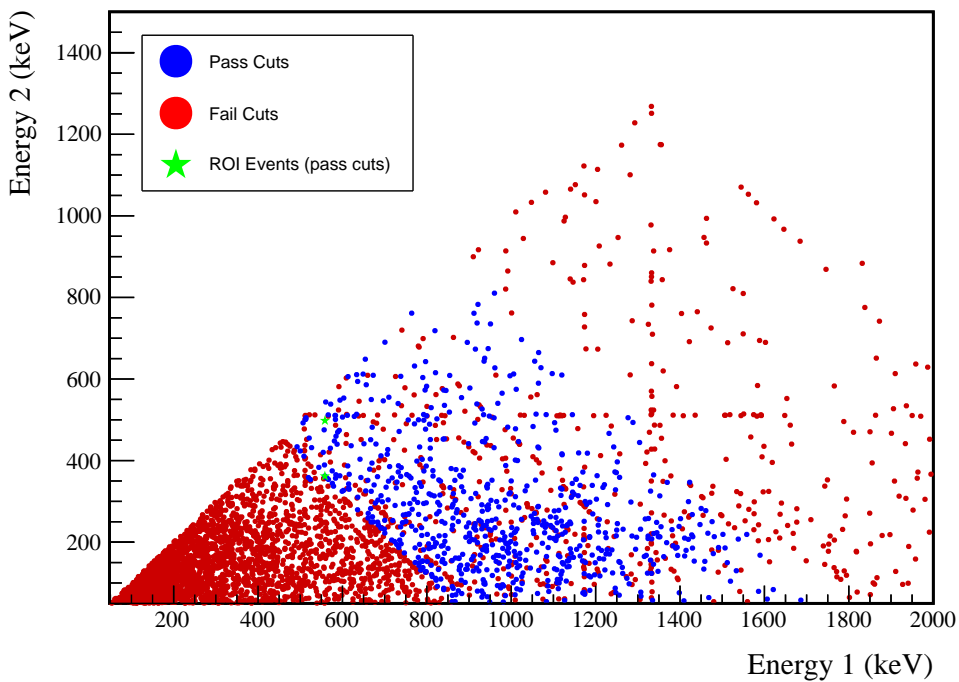


FIG. 24 Energy spectrum of multiplicity 2 events. Red events are events that are cut. For blue events, at least one of the hits passes all cuts; however, the other hit may fail. For green events, one of the hits must both pass all cuts and place the event in the BG or ES ROI. Note that the green events include any events of multiplicity > 1; for higher multiplicity events, instead of showing the energy in the second detector, the sum of the energy in all other detectors is shown.

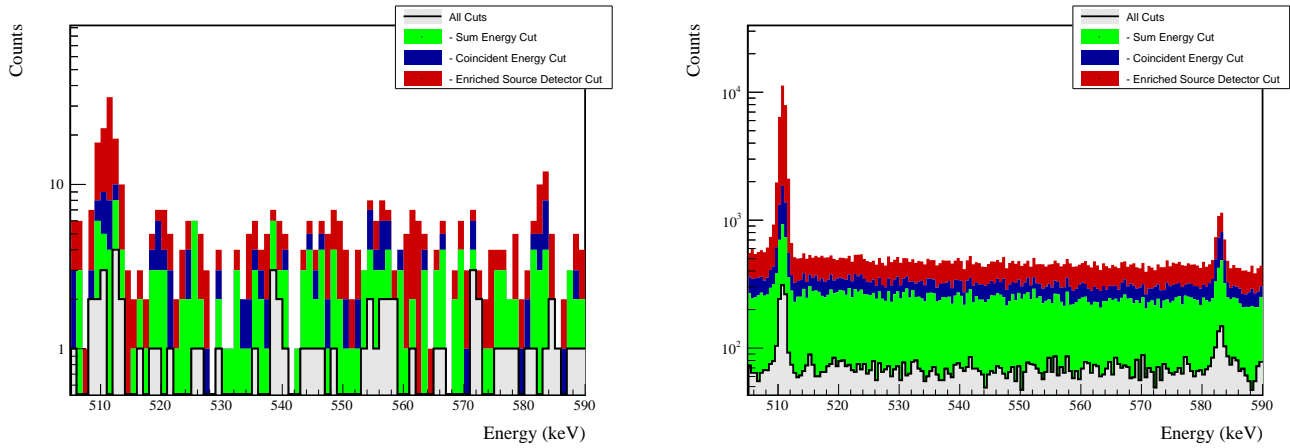


FIG. 25 Effect of cuts on all events in the BG and ES ROIs. Events are applied in sequence from top to bottom, meaning that if an event is cut by multiple cuts, it will be colored based on the first cut that applied. Both measured (left) and simulated (right) event spectra are shown for comparison.

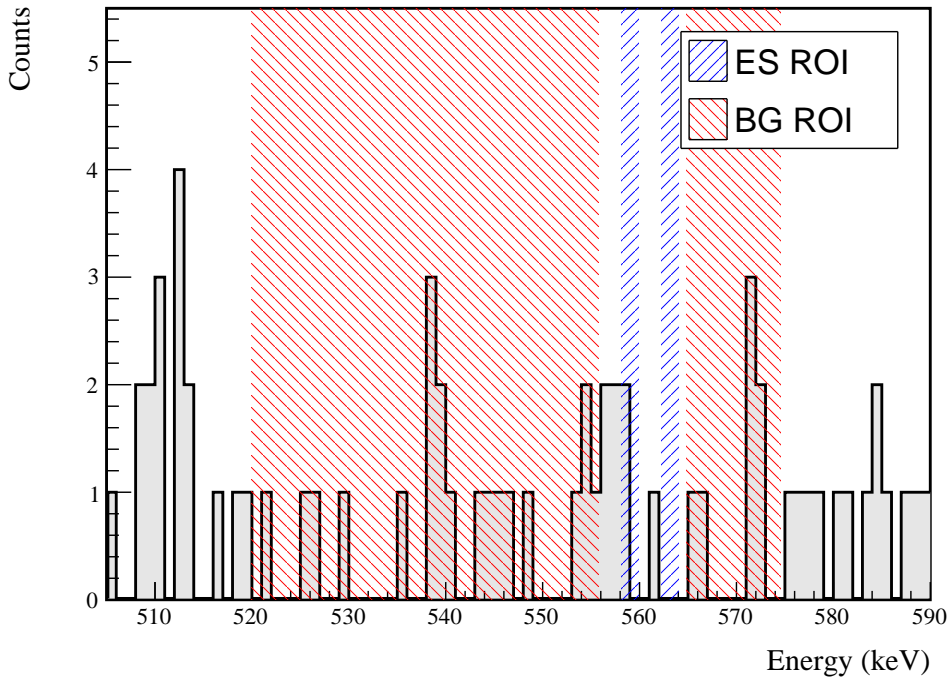


FIG. 26 Events that pass all cuts for the $2\nu\beta\beta$ to 0_1^+ decay mode. The ES and BG ROIs are highlighted. Note that these ROIs undergo small variations from dataset to dataset, and the ROIs drawn here are averaged over all datasets. The energies shown in this spectrum are the energies of the hit that places the event in the ROI. A single event will only be placed once into an ROI; however, as drawn here, if multiple hits in a single event fall into an ROI, they will all be drawn.

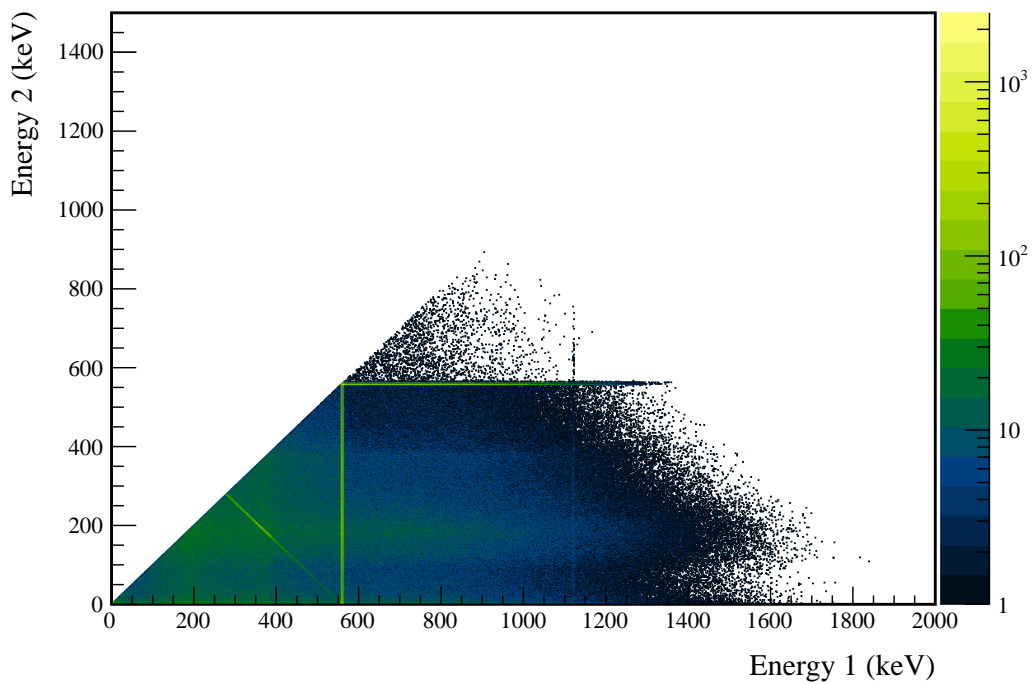


FIG. 27 Simulated multiplicity 2 energy spectrum of the $2\nu\beta\beta$ to 0_1^+ decay mode

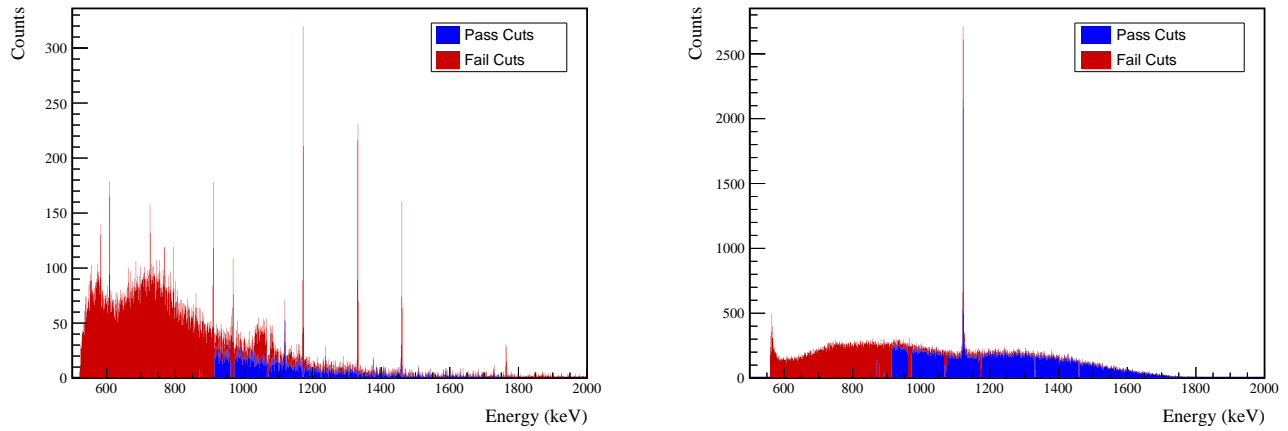


FIG. 28 Effect of 559 and 563 keV peaks cuts on sum energy spectra in BG (left) and ES (right) simulations.

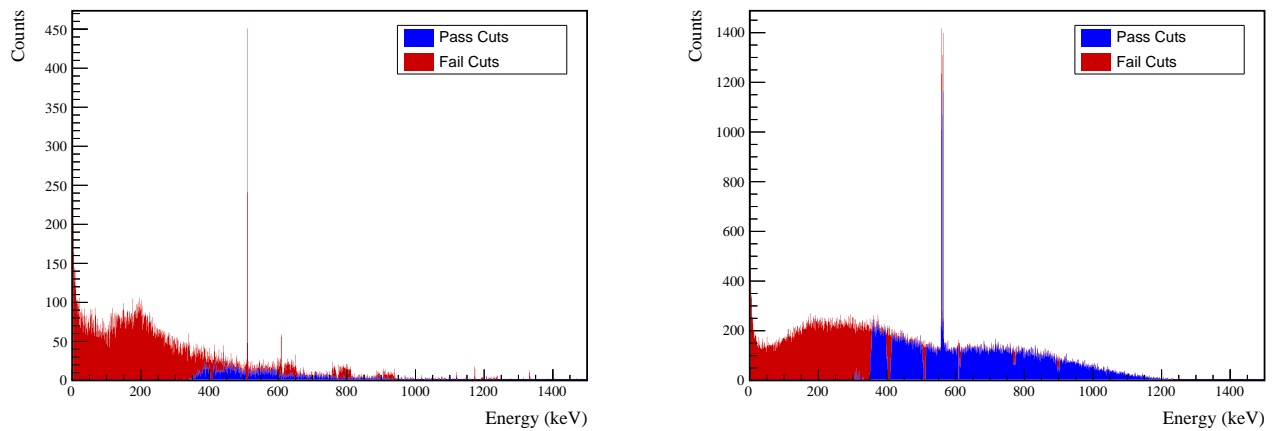


FIG. 29 Effect of 559 and 563 keV peaks cuts on coincident energy spectra in BG (left) and ES (right) simulations.



TABLE VIII Table of energy estimation uncertainties for the 559 and 563 keV peaks.

DS	E_{peak} (keV)	σ_{fit} (keV)	σ_{drift} (keV)	σ (keV)	$f_{t,fit}$ (keV)	$f_{t,fit}$ (keV)	τ_{fit} (keV)	$\delta_{\mu,fit}$ (keV)	$\delta_{\mu,NL}$ (keV)	$\delta_{\mu,drift}$ (keV)	$\delta_{\mu,peak}$ (keV)	δ_u (keV)	FWHM (keV)	$\delta_{fwhm,drift}$ (keV)	$\delta_{fwhm,fit}$ (keV)	$\delta_{fwhm,xtalk}$ (keV)	δ_{FWHM} (keV)	δ_α	$E_{ROI,1}$ (keV)	$E_{ROI,2}$ (keV)	ϵ_{ROI}	$\sigma_{\epsilon_{ROI}}$
DS1	559.101	0.460	0.063	0.464	0.230	0.515	0.001	0.104	0.002	0.012	0.005	0.105	1.152	0.001	0.039	0.011	0.040	0.035	558.199	559.847	0.871	0.015
DS2	559.101	0.461	0.055	0.464	0.249	0.515	0.002	0.067	0.004	0.012	0.005	0.068	1.158	0.001	0.107	0.011	0.108	0.093	558.186	559.845	0.874	0.031
DS3	559.101	0.470	0.066	0.474	0.224	0.505	0.001	0.026	0.024	0.012	0.005	0.038	1.174	0.001	0.073	0.011	0.074	0.063	558.187	559.863	0.879	0.021
DS4	559.101	0.455	0.077	0.461	0.108	0.445	0.002	0.076	0.010	0.012	0.005	0.078	1.111	0.001	0.106	0.011	0.107	0.096	558.283	559.856	0.888	0.032
DS5a	559.101	0.560	0.085	0.567	0.106	0.855	0.002	0.079	0.005	0.012	0.005	0.080	1.367	0.002	0.055	0.011	0.056	0.041	558.098	560.022	0.875	0.014
DS5b	559.101	0.469	0.074	0.475	0.158	0.491	0.001	0.020	0.011	0.012	0.005	0.026	1.157	0.001	0.125	0.011	0.125	0.108	558.229	559.872	0.885	0.036
DS5c	559.101	0.460	0.085	0.468	0.174	0.489	0.001	0.037	0.030	0.012	0.005	0.050	1.145	0.001	0.162	0.011	0.162	0.142	558.231	559.860	0.883	0.046
DS6a	559.101	0.456	0.044	0.458	0.191	0.463	0.001	0.069	0.025	0.012	0.005	0.075	1.123	0.000	0.041	0.011	0.042	0.038	558.241	559.841	0.881	0.014
DS1	563.178	0.461	0.064	0.466	0.230	0.518	0.001	0.104	0.002	0.012	0.005	0.105	1.156	0.001	0.039	0.011	0.040	0.035	562.273	563.927	0.871	0.015
DS2	563.178	0.463	0.055	0.466	0.249	0.517	0.002	0.067	0.004	0.012	0.005	0.068	1.162	0.001	0.107	0.011	0.108	0.093	562.259	563.924	0.874	0.030
DS3	563.178	0.471	0.066	0.476	0.224	0.508	0.001	0.026	0.024	0.012	0.005	0.038	1.179	0.001	0.073	0.011	0.074	0.063	562.261	563.943	0.879	0.021
DS4	563.178	0.457	0.077	0.463	0.108	0.447	0.002	0.076	0.010	0.012	0.005	0.078	1.115	0.001	0.106	0.011	0.107	0.096	562.357	563.935	0.888	0.032
DS5a	563.178	0.562	0.086	0.569	0.106	0.858	0.002	0.079	0.006	0.012	0.005	0.080	1.372	0.002	0.055	0.011	0.056	0.041	562.172	564.103	0.875	0.014
DS5b	563.178	0.471	0.074	0.477	0.158	0.494	0.001	0.020	0.011	0.012	0.005	0.026	1.162	0.001	0.125	0.011	0.125	0.108	562.303	563.952	0.885	0.035
DS5c	563.178	0.462	0.086	0.470	0.174	0.492	0.001	0.037	0.030	0.012	0.005	0.050	1.449	0.001	0.162	0.011	0.162	0.141	562.305	563.939	0.883	0.046
DS6a	563.178	0.457	0.044	0.459	0.191	0.465	0.001	0.069	0.026	0.012	0.005	0.075	1.127	0.000	0.041	0.011	0.042	0.038	562.315	563.921	0.881	0.013



Cut Name	Cut Description	$\langle \epsilon_{total} \rangle$	$\hat{\epsilon}_{total}$	$\langle \epsilon_{unique} \rangle$	$\hat{\epsilon}_{unique}$	Sacrifice	ΔDP
Enriched Source Detector Cut	Any other detector: isBar	M1: 23.2 % M2: 42.7 %	27.2 ^{+3.8} _{-3.5} % 62.8 ^{+7.0} _{-7.6} %	2.2 % 4.4 %	2.0 ^{+1.5} _{-0.9} % 4.7 ^{+4.4} _{-2.3} %	0.7 % 2.1 %	7%
Coincident Energy Cut	No other detector: ((energy<40.6) (energy>402.6 && energy>409.6) (energy>2506.8 && energy<512.4) (energy>402.6 && && energy<410.2) (energy>170.6 && energy<1175.) (energy>1235.) && isBar) ((energy<83.) (energy>228.2 && energy<356.6) (energy>75.2 && energy<516.8) (energy>866.6 && energy<13.4) (energy>737.4) && (energy<613.4) (energy>737.4) &&) Note: (sumE<870.) (sumE>870.6 && sumE<877.6) (sumE>878. && sumE<891.) (sumE>891.2 && sumE<913.8) (sumE>960.8 && sumE<972.) (sumE>1066.8 && sumE<1072.6) (sumE>1170.8 && sumE<1174.6) (sumE>1330.8 && sumE<1333.6) (sumE>1458.2 && sumE<1461.6) (sumE>1751.8 && sumE<1765.6) (sumE>1794.4)	M1: 29.6 % M2: 37.5 %	33.3 ^{+4.0} _{-3.8} % 48.8 ^{+7.5} _{-7.5} %	4.4 % 4.2 %	4.8 ^{+2.1} _{-1.5} % 2.3 ^{+3.6} _{-1.4} %	3.9 % 3.5 %	7%
Sum Energy Cut		M1: 75.0 % M2: 75.6 %	74.8 ^{+3.4} _{-3.7} % 74.4 ^{+3.0} _{-7.2} %	44.5 % 33.0 %	41.5 ^{+4.1} _{-4.0} % 25.6 ^{+7.2} _{-6.0} %	31.8 % 32.1 %	20%
Combined Cuts		M1: 84.5 % M2: 89.5 %	84.4 ^{+2.8} _{-3.2} % 95.3 ^{+2.3} _{-4.4} %	— —	44.9 % 53.1 %	27%	

TABLE IX Table of cut descriptions and efficiencies for simulated backgrounds and measured data for the 559 and 563 keV peaks.

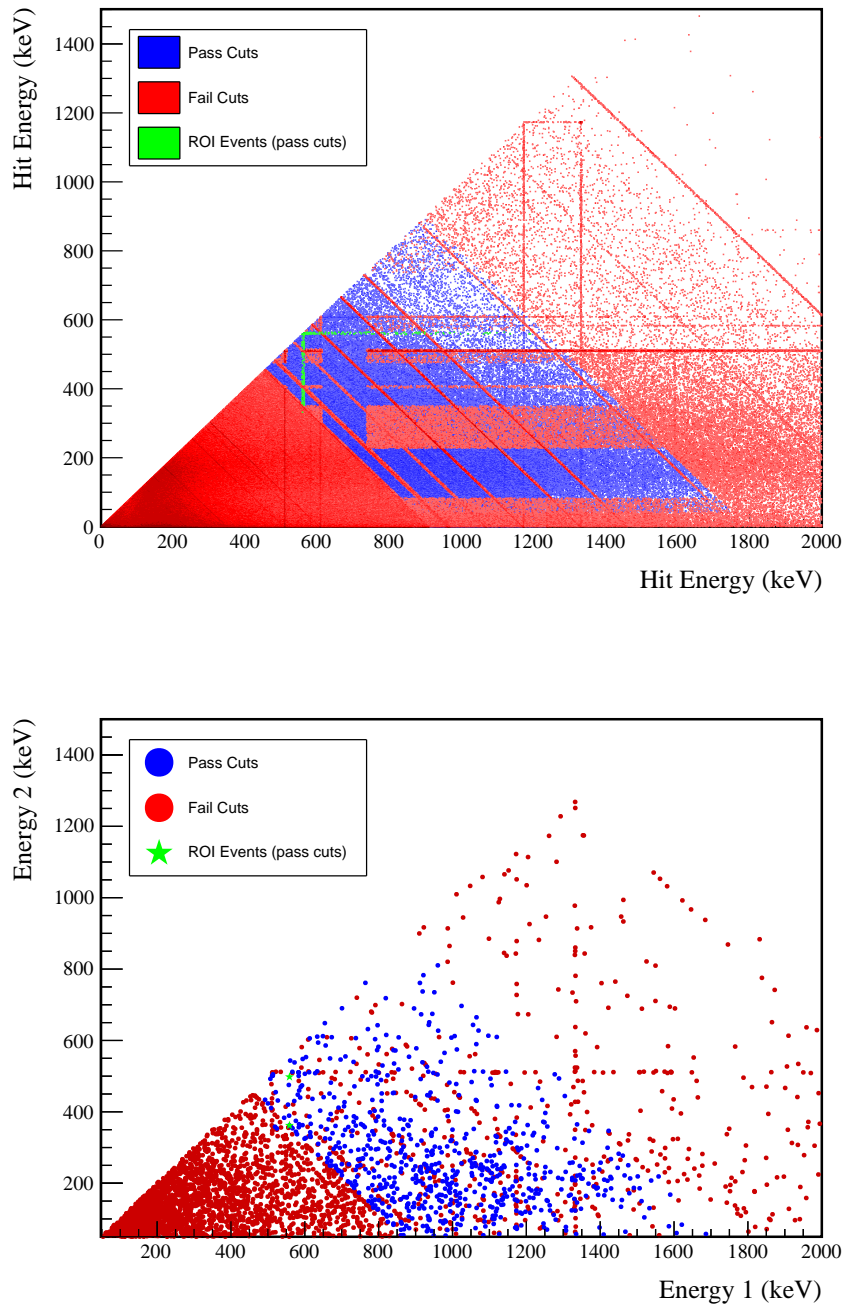
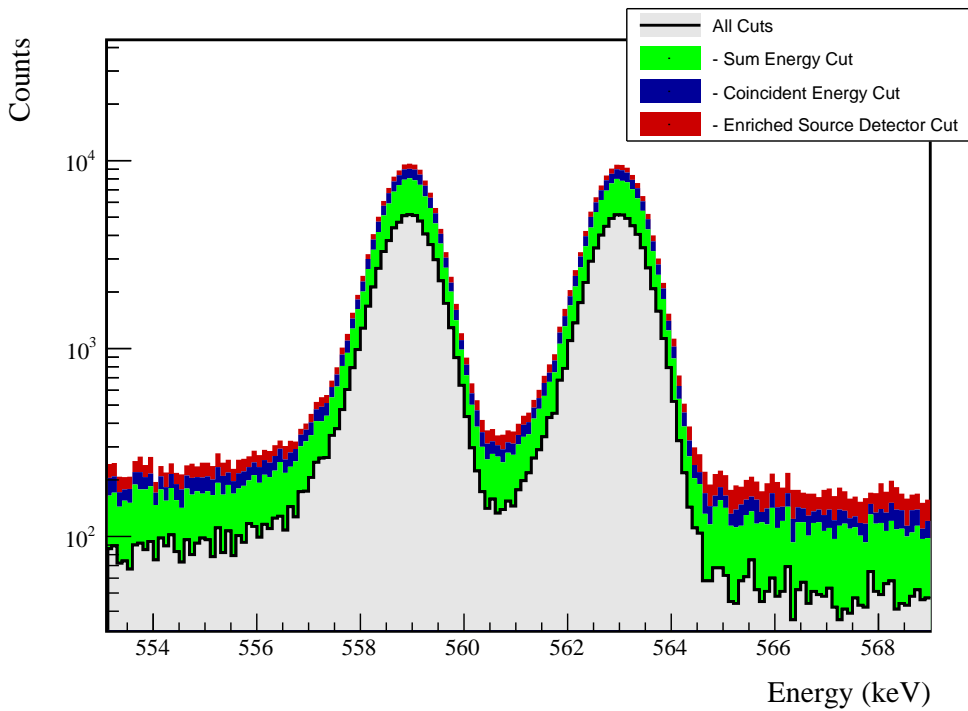


FIG. 30 Simulated (left) and measured (right) multiplicity 2 energy spectrum with sum and coincident energy cuts included for the 559 and 563 keV peaks.

FIG. 31 Effect of all cuts applied sequentially on ROI for 559 and 563 keV peaks of $2\nu\beta\beta$ to 0_1^+

Source	Module 1 efficiency	Module 2 efficiency
M. S. Event Signature	$5.2 \pm 0.2\%$	$2.8 \pm 0.5\%$
Region of Interest	$87.9 \pm 1.4\%$	$87.9 \pm 1.4\%$
Dead Layer	$74.5 \pm 4.3\%$	$65.7 \pm 6.0\%$
Detector Dead Times	$97.5 \pm 1.2\%$	$98.1 \pm 0.9\%$
Enriched Source Detector Cut	$98.7 \pm <0.1\%$	$95.7 \pm <0.1\%$
Coincident Energy Cut	$93.5 \pm <0.1\%$	$93.1 \pm <0.1\%$
Sum Energy Cut	$63.4 \pm <0.1\%$	$59.3 \pm <0.1\%$
Final Efficiency	$2.29 \pm 0.17\%$	$0.97 \pm 0.19\%$

FIG. 32 Table of detection efficiencies for the 559 and 563 keV peaks.

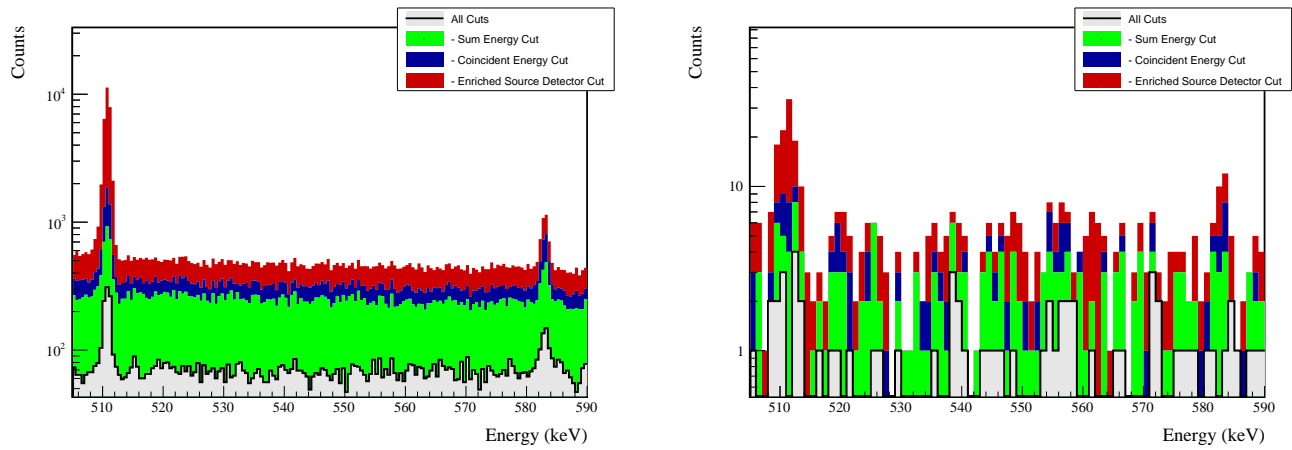
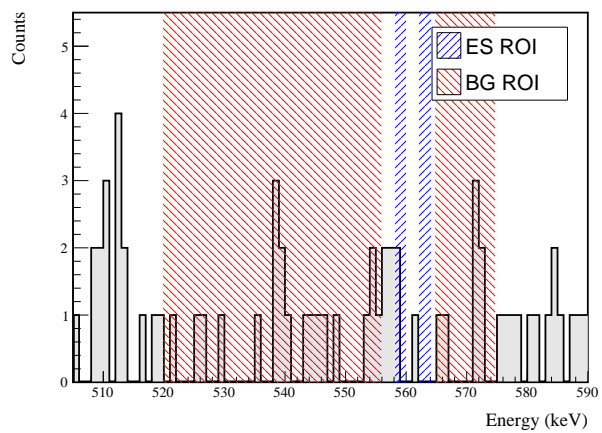


FIG. 33 Effect of all cuts applied to sequentially simulated (left) and measured (right) background data.

FIG. 34 All events after cuts in background (red) and signal (blue) ROIs for 559 and 563 keV peaks of $2\nu\beta\beta$ to 0_1^+

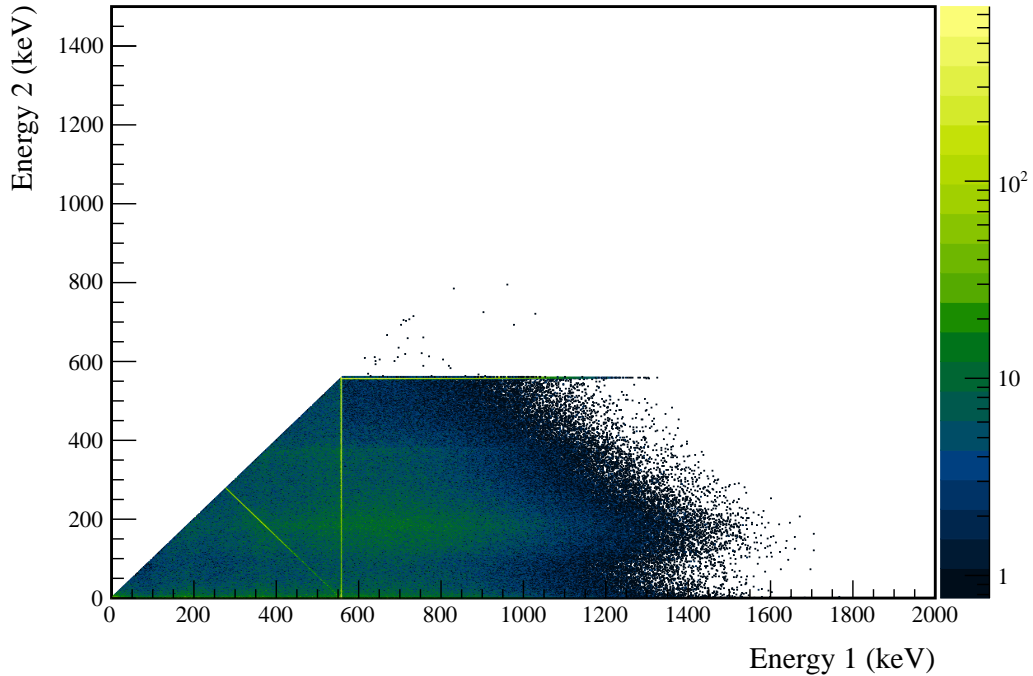
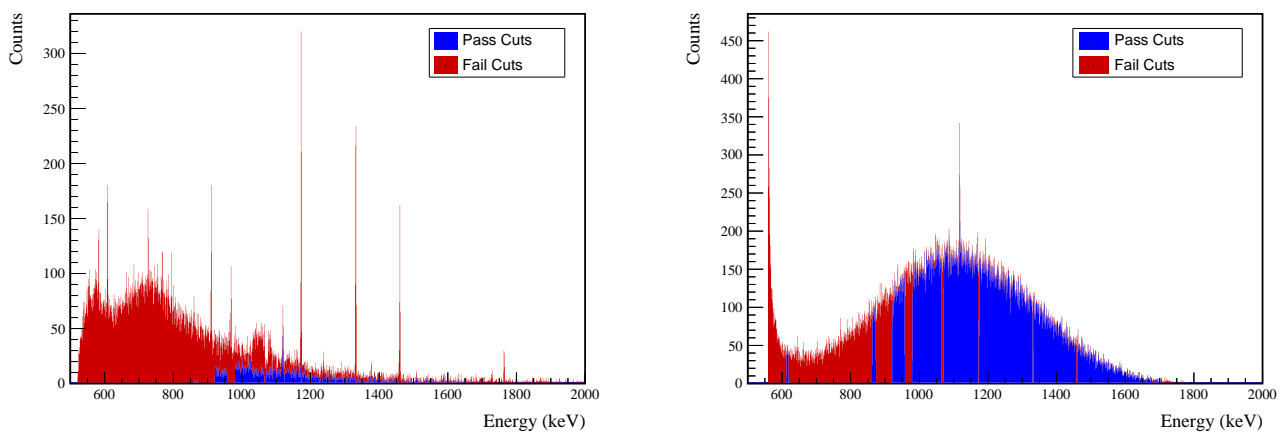
576 **Appendix C: $2\nu\beta\beta$ to 2_1^+** FIG. 35 Simulated multiplicity 2 energy spectrum of the $2\nu\beta\beta$ to 2_1^+ decay mode

FIG. 36 Effect of 559 keV peak cuts on sum energy spectra in BG (left) and ES (right) simulations.



TABLE X Table of energy estimation uncertainties for the 559 keV peak.

DS	E_{peak} (keV)	σ_{drift} (keV)	σ_{fit} (keV)	f_{fit} (keV)	σ (keV)	τ_{fit} (keV)	$f_{t,fit}$ (keV)	$\delta_{\mu,NL}$ (keV)	$\delta_{\mu,drift}$ (keV)	$\delta_{\mu,talk}$ (keV)	$\delta_{\mu,peak}$ (keV)	δ_u (keV)	FWHM	$\delta_{fwhm,fit}$ (keV)	$\delta_{fwhm,drift}$ (keV)	$\delta_{fwhm,talk}$ (keV)	$\delta_{fwhm,HM}$ (keV)	δ_α	$E_{ROI,1}$ (keV)	$E_{ROI,2}$ (keV)	ϵ_{ROI}	$\sigma_{e_{ROI}}$
DS1	559.101	0.460	0.063	0.464	0.230	0.515	0.001	0.104	0.002	0.012	0.005	0.105	1.152	0.001	0.039	0.011	0.040	0.035	558.183	559.860	0.877	0.015
DS2	559.101	0.461	0.055	0.464	0.249	0.515	0.002	0.067	0.004	0.012	0.005	0.068	1.158	0.001	0.107	0.011	0.108	0.093	558.169	559.858	0.880	0.030
DS3	559.101	0.470	0.066	0.474	0.224	0.505	0.001	0.026	0.024	0.012	0.005	0.038	1.174	0.001	0.073	0.011	0.074	0.063	558.170	559.876	0.885	0.020
DS4	559.101	0.455	0.077	0.461	0.108	0.445	0.002	0.076	0.010	0.012	0.005	0.078	1.111	0.001	0.106	0.011	0.107	0.096	558.269	559.869	0.893	0.031
DS5a	559.101	0.560	0.085	0.567	0.106	0.885	0.002	0.079	0.005	0.012	0.005	0.080	1.367	0.002	0.055	0.011	0.056	0.041	558.081	560.038	0.881	0.014
DS5b	559.101	0.469	0.074	0.475	0.158	0.491	0.001	0.020	0.011	0.012	0.005	0.026	1.157	0.001	0.125	0.011	0.125	0.108	558.214	559.886	0.891	0.035
DS5c	559.101	0.460	0.085	0.468	0.174	0.489	0.001	0.037	0.030	0.012	0.005	0.050	1.145	0.001	0.162	0.011	0.162	0.142	558.216	559.873	0.888	0.045
DS6a	559.101	0.456	0.044	0.458	0.191	0.463	0.001	0.069	0.025	0.012	0.005	0.075	1.123	0.000	0.041	0.011	0.042	0.038	558.226	559.854	0.886	0.013



Cut Name	Cut Description	$\langle \epsilon_{total} \rangle$	$\hat{\epsilon}_{total}$	$\langle \epsilon_{unique} \rangle$	$\hat{\epsilon}_{unique}$	Sacrifice	ΔDP
Enriched Source		M1: 23.2 %	26.5 ^{+3.8} _{-3.5} %	4.5 %	4.1 ^{+2.0} _{-1.3} %	1.7 %	18%
Detector Cut	Any other detector: isEarr	M2: 42.7 %	62.8 ^{+7.0} _{-7.6} %	8.7 %	11.6 ^{+5.8} _{-4.9} %	4.1 %	
Multiplicity 2 Cut	m==2	M1: 15.4 %	16.3 ^{+3.3} _{-2.8} %	0.7 %	0.0 ^{+0.7} _{-0.0} %	0.0 %	2%
		M2: 11.7 %	16.3 ^{+6.4} _{-4.9} %	0.7 %	0.0 ^{+2.3} _{-0.0} %	0.0 %	
Coincident Energy Cut	No other detector: ((energy<53.8) (energy>59.4 && energy<93.8) (energy>144.4 && energy<362.4) (energy>398.6 && energy<421.) (energy>506.2 && energy<512.2) (energy>1116.4 && energy<1124.2) (energy>1147.8)) && isEarr (energy>1147.8) && isEarr)	M1: 59.2 %	55.8 ± 4.1 %	3.8 %	4.8 ^{+2.1} _{-1.5} %	0.3 %	12%
		M2: 44.9 %	30.2 ^{+7.4} _{-6.5} %	3.5 %	0.0 ^{+2.3} _{-0.0} %	0.3 %	
Sum Energy Cut	Note: (sumE<612.8) (sumE>862.6) (sumE>873.4 && sumE<862.6) (sumE>1064.8 && sumE<1070.8) (sumE>1171.6 && sumE<1174.6) (sumE>1333.6) (sumE>1457. (sumE>1706.4) (sumE>1706.4) (sumE>1684.8) (sumE>1706.4) && sumE<1462.4) (sumE>1675.2 && sumE<1684.8) (sumE>1706.4) && sumE<1462.4)	M1: 74.9 %	74.8 ^{+3.4} _{-3.7} %	6.3 %	5.4 ^{+2.2} _{-1.6} %	1.2 %	17%
		M2: 75.6 %	76.7 ^{+2.8} _{-7.0} %	4.3 %	2.3 ^{+3.6} _{-1.4} %	1.2 %	
Combined Cuts		M1: 89.9 %	89.1 ^{+2.3} _{-2.8} %	—	—	30.9 %	79%
		M2: 93.0 %	97.7 ^{+1.4} _{-3.6} %	—	—	34.0 %	

TABLE XI Table of cut descriptions and efficiencies for simulated backgrounds and measured data for the 559 keV peak.

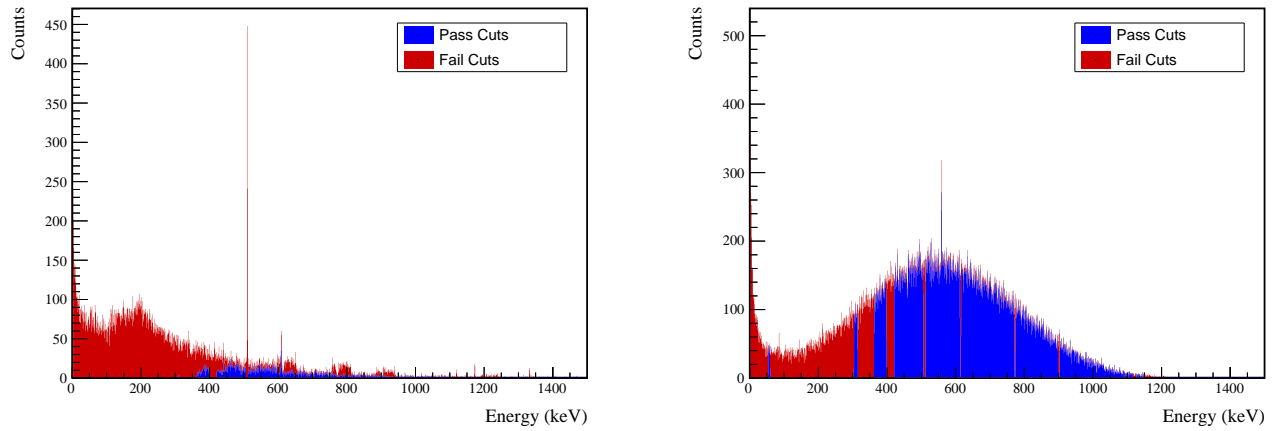


FIG. 37 Effect of 559 keV peak cuts on coincident energy spectra in BG (left) and ES (right) simulations.

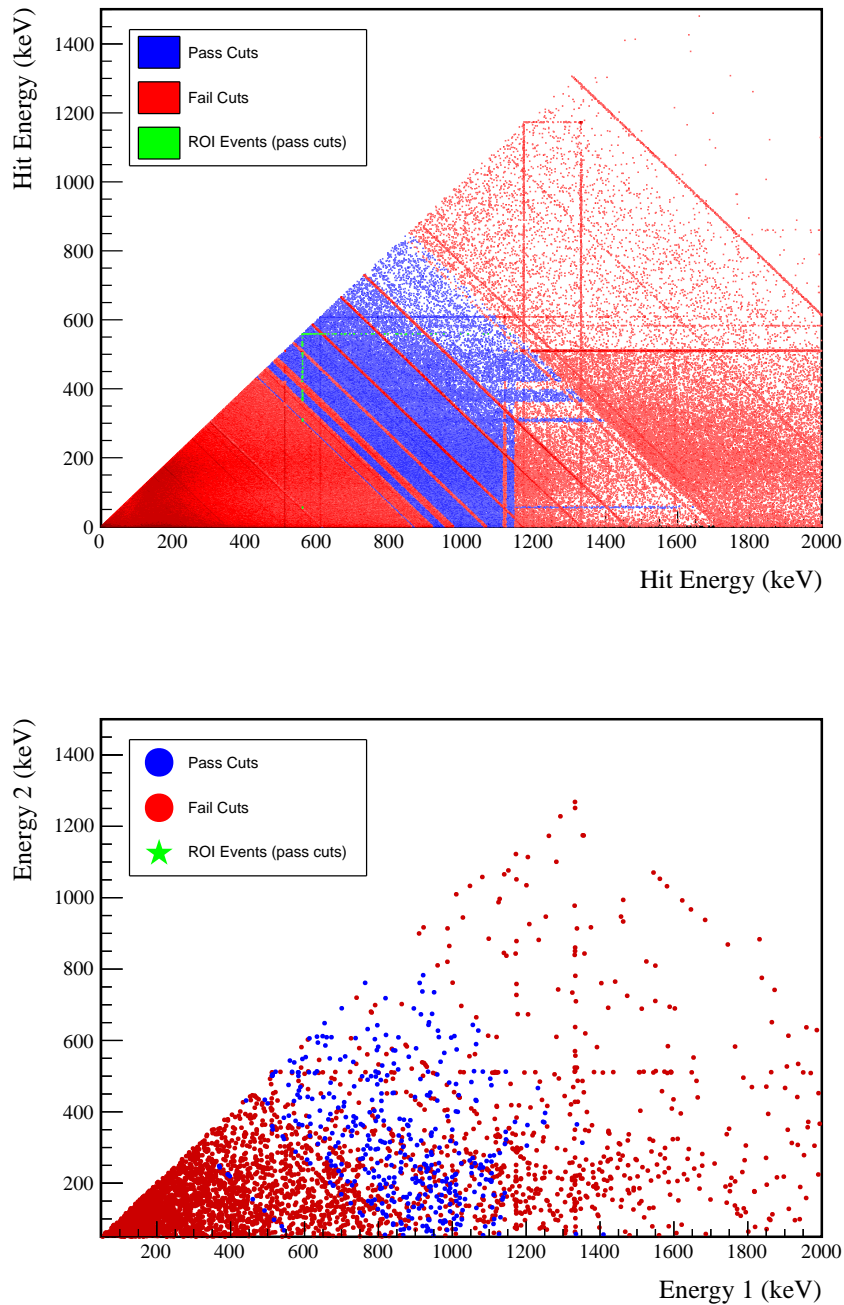
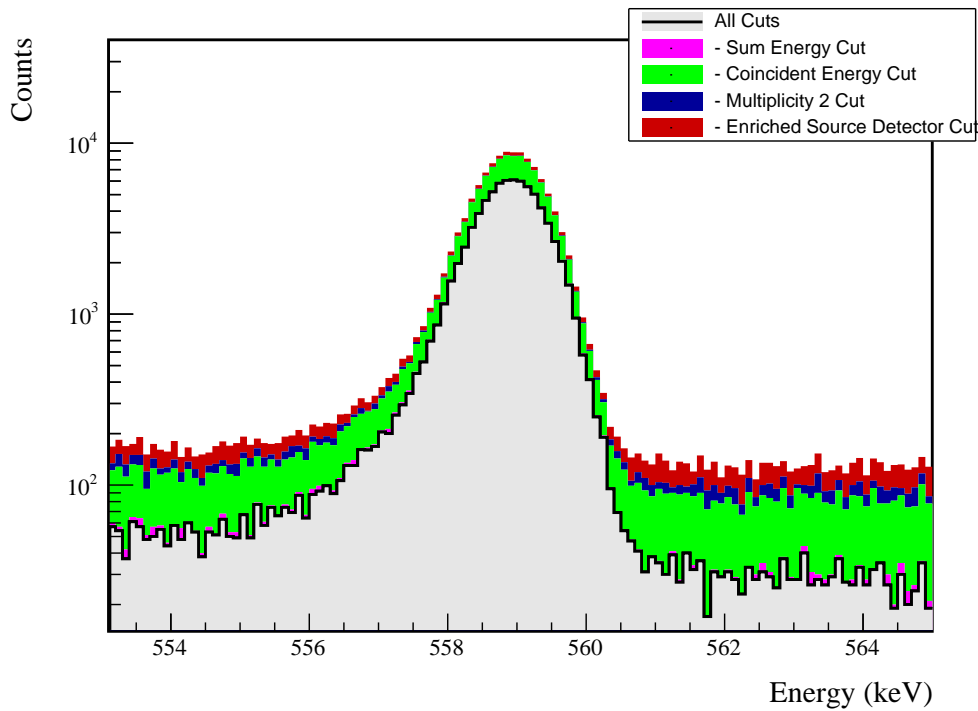


FIG. 38 Simulated (left) and measured (right) multiplicity 2 energy spectrum with sum and coincident energy cuts included for the 559 keV peak.

FIG. 39 Effect of all cuts applied sequentially on ROI for 559 keV peak of $2\nu\beta\beta$ to 2_1^+

Source	Module 1 efficiency	Module 2 efficiency
M. S. Event Signature	$2.7 \pm 0.2\%$	$1.3 \pm 0.5\%$
Region of Interest	$88.4 \pm 2.0\%$	$88.4 \pm 2.0\%$
Dead Layer	$71.4 \pm 4.9\%$	$62.8 \pm 6.5\%$
Detector Dead Times	$97.5 \pm 1.2\%$	$98.0 \pm 0.9\%$
Enriched Source Detector Cut	$97.5 \pm <0.1\%$	$94.2 \pm <0.1\%$
Multiplicity 2 Cut	$100.0 \pm <0.1\%$	$99.9 \pm <0.1\%$
Coincident Energy Cut	$99.6 \pm <0.1\%$	$99.6 \pm <0.1\%$
Sum Energy Cut	$98.3 \pm <0.1\%$	$98.2 \pm <0.1\%$
Final Efficiency	$1.42 \pm 0.15\%$	$0.61 \pm 0.23\%$

FIG. 40 Table of detection efficiencies for the 559 keV peak.

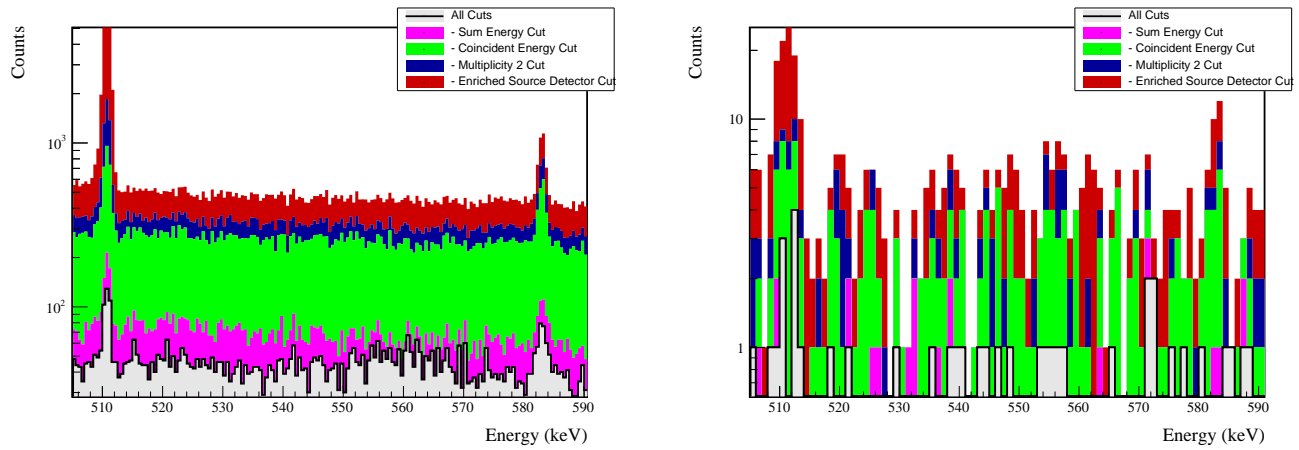
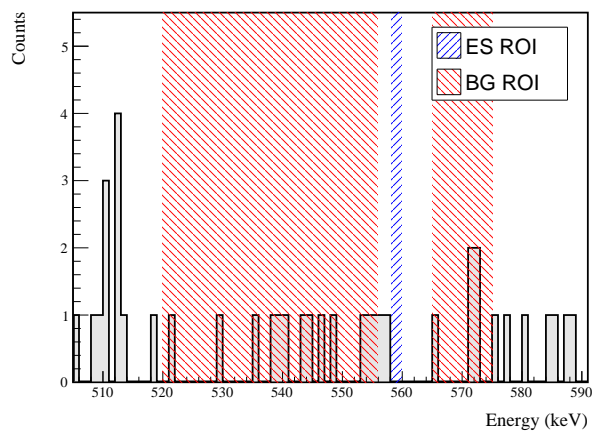


FIG. 41 Effect of all cuts applied to sequentially simulated (left) and measured (right) background data.

FIG. 42 All events after cuts in background (red) and signal (blue) ROIs for 559 keV peak of $2\nu\beta\beta$ to 2_1^+

577 **Appendix D: $2\nu\beta\beta$ to 2_2^+**

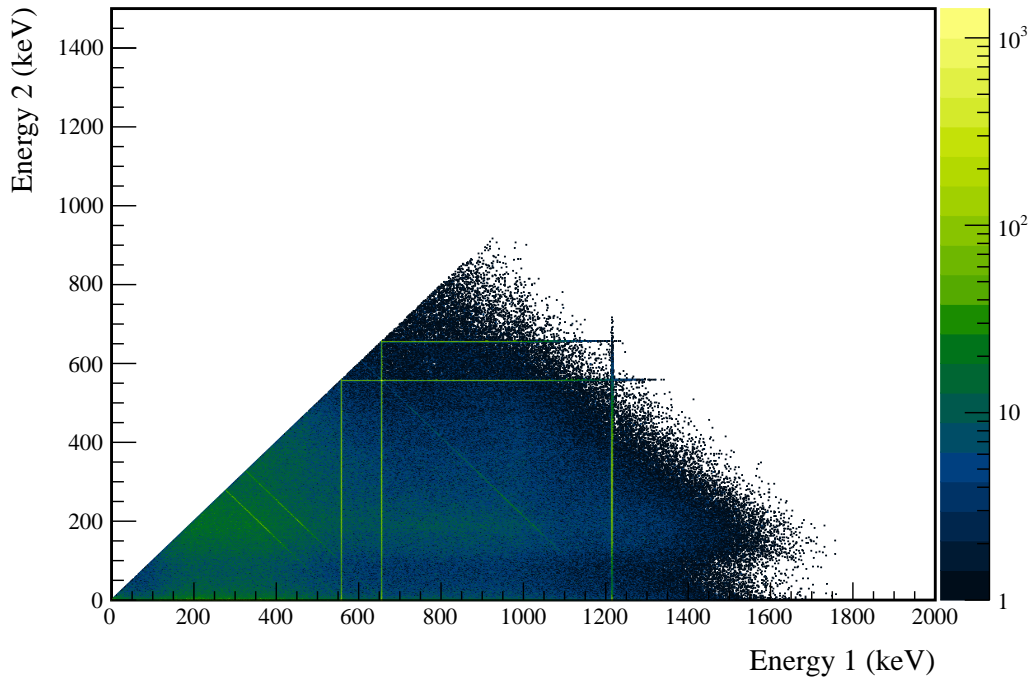


FIG. 43 Simulated multiplicity 2 energy spectrum of the $2\nu\beta\beta$ to 2_2^+ decay mode

578 **1. 559 keV peak**

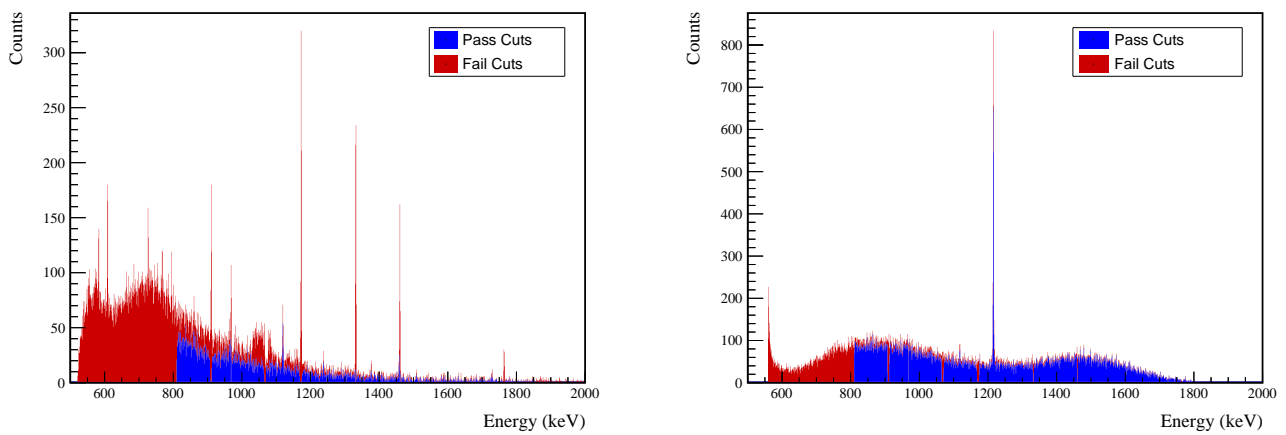


FIG. 44 Effect of 559 keV peak cuts on sum energy spectra in BG (left) and ES (right) simulations.



TABLE XII Table of energy estimation uncertainties for the 559 keV peak.

DS	E_{peak} (keV)	σ_{fit} (keV)	σ_{drift} (keV)	$f_{t,fit}$	σ (keV)	$\tau_{f,it}$ (keV)	$\delta_{\mu,f,it}$ (keV)	$\delta_{\mu,NL}$ (keV)	$\delta_{\mu,drift}$ (keV)	$\delta_{\mu,atalk}$ (keV)	$\delta_{\mu,peak}$ (keV)	δ_u (keV)	FWHM	$\delta_{fwhm,fit}$ (keV)	$\delta_{fwhm,drift}$ (keV)	$\delta_{fwhm,atalk}$ (keV)	$\delta_{fwhm,HM}$ (keV)	δ_α	$E_{ROI,1}$ (keV)	$E_{ROI,2}$ (keV)	ϵ_{ROI}	$\sigma_{e_{ROI}}$
DS1	559.101	0.460	0.063	0.464	0.230	0.515	0.001	0.104	0.002	0.012	0.005	0.105	1.152	0.001	0.039	0.011	0.040	0.035	558.218	559.832	0.864	0.016
DS2	559.101	0.461	0.055	0.464	0.249	0.515	0.002	0.067	0.004	0.012	0.005	0.068	1.158	0.001	0.107	0.011	0.108	0.093	558.206	559.830	0.867	0.032
DS3	559.101	0.470	0.066	0.474	0.224	0.505	0.001	0.026	0.024	0.012	0.005	0.038	1.174	0.001	0.073	0.011	0.074	0.063	558.206	559.847	0.872	0.021
DS4	559.101	0.455	0.077	0.461	0.108	0.445	0.002	0.076	0.010	0.012	0.005	0.078	1.111	0.001	0.106	0.011	0.107	0.096	558.299	559.841	0.881	0.033
DS5a	559.101	0.560	0.085	0.567	0.106	0.885	0.002	0.079	0.005	0.012	0.005	0.080	1.367	0.002	0.055	0.011	0.056	0.041	558.119	560.004	0.868	0.015
DS5b	559.101	0.469	0.074	0.475	0.158	0.491	0.001	0.020	0.011	0.012	0.005	0.026	1.157	0.001	0.125	0.011	0.125	0.108	558.247	559.857	0.878	0.037
DS5c	559.101	0.460	0.085	0.468	0.174	0.489	0.001	0.037	0.030	0.012	0.005	0.050	1.145	0.001	0.162	0.011	0.162	0.142	558.249	559.844	0.876	0.048
DS6a	559.101	0.456	0.044	0.458	0.191	0.463	0.001	0.069	0.025	0.012	0.005	0.075	1.123	0.000	0.041	0.011	0.042	0.038	558.259	559.826	0.874	0.014



Cut Name	Cut Description	$\langle \epsilon_{total} \rangle$	$\hat{\epsilon}_{total}$	$\langle \epsilon_{unique} \rangle$	$\hat{\epsilon}_{unique}$	Sacrifice	ΔDP
Enriched Source Detector Cut	Any other detector: isBar	M1: 23.2 %	26.5 ^{+3.8} _{-3.5} %	6.1 %	6.1 ^{+2.3} _{-1.7} %	1.7 %	1.7 %
Coincident Energy Cut	No other detector: (((energy<41.) (energy>349.6 && energy<352.8) (energy>306.8 && energy<312.2) (energy>305.4 && energy<312.6) (energy>307.4) && isBar) ((energy<42.) (energy>120.2 && energy>235.8) (energy>807.8 && energy<14.2) (energy>856.2) && 1.8bar) Note: ((sumE<10.2) (sumE>907.2 && sumE<912.4) (sumE>968. && sumE<969.2) (sumE>1064.8 && sumE<1070.) (sumE>1168.6 && sumE<1174.6) (sumE>1330.4 && sumE<1333.4) (sumE>1455.4 && sumE<1461.8) (sumE>1761.8 && sumE<1766.) (sumE>1906.)	M1: 42.7 %	62.8 ^{+7.0} _{-7.6} %	11.8 %	18.6 ^{+6.6} _{-5.2} %	5.2 %	10%
Sum Energy Cut		M1: 28.8 %	34.0 ^{+4.0} _{-3.8} %	5.3 %	5.4 ^{+2.2} _{-1.6} %	4.7 %	3%
Combined Cuts		M2: 35.6 %	48.8 ^{+7.5} _{-7.5} %	5.0 %	7.0 ^{+3.0} _{-3.0} %	4.3 %	
		M1: 61.1 %	59.9 ^{+4.1} _{-4.0} %	34.7 %	31.3 ^{+3.9} _{-3.7} %	16.3 %	
		M2: 61.8 %	53.5 ^{+7.4} _{-7.6} %	25.8 %	16.3 ^{+6.4} _{-4.9} %	16.8 %	18%
		M1: 74.4 %	74.1 ^{+3.4} _{-3.8} %	—	28.6 %	30%	
		M2: 82.2 %	88.4 ^{+4.0} _{-5.8} %	—	37.3 %	30%	

TABLE XIII Table of cut descriptions and efficiencies for simulated backgrounds and measured data for the 559 keV peak.

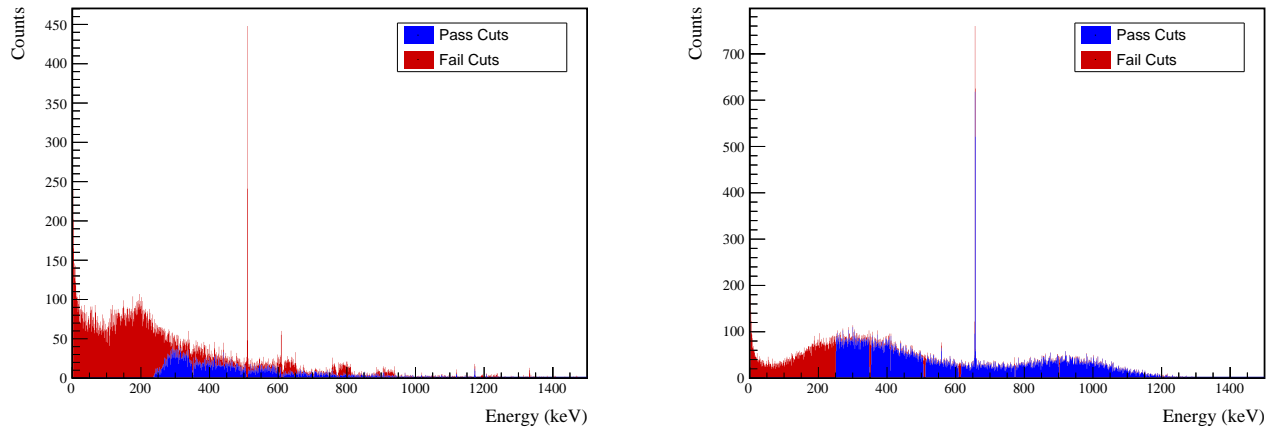


FIG. 45 Effect of 559 keV peak cuts on coincident energy spectra in BG (left) and ES (right) simulations.

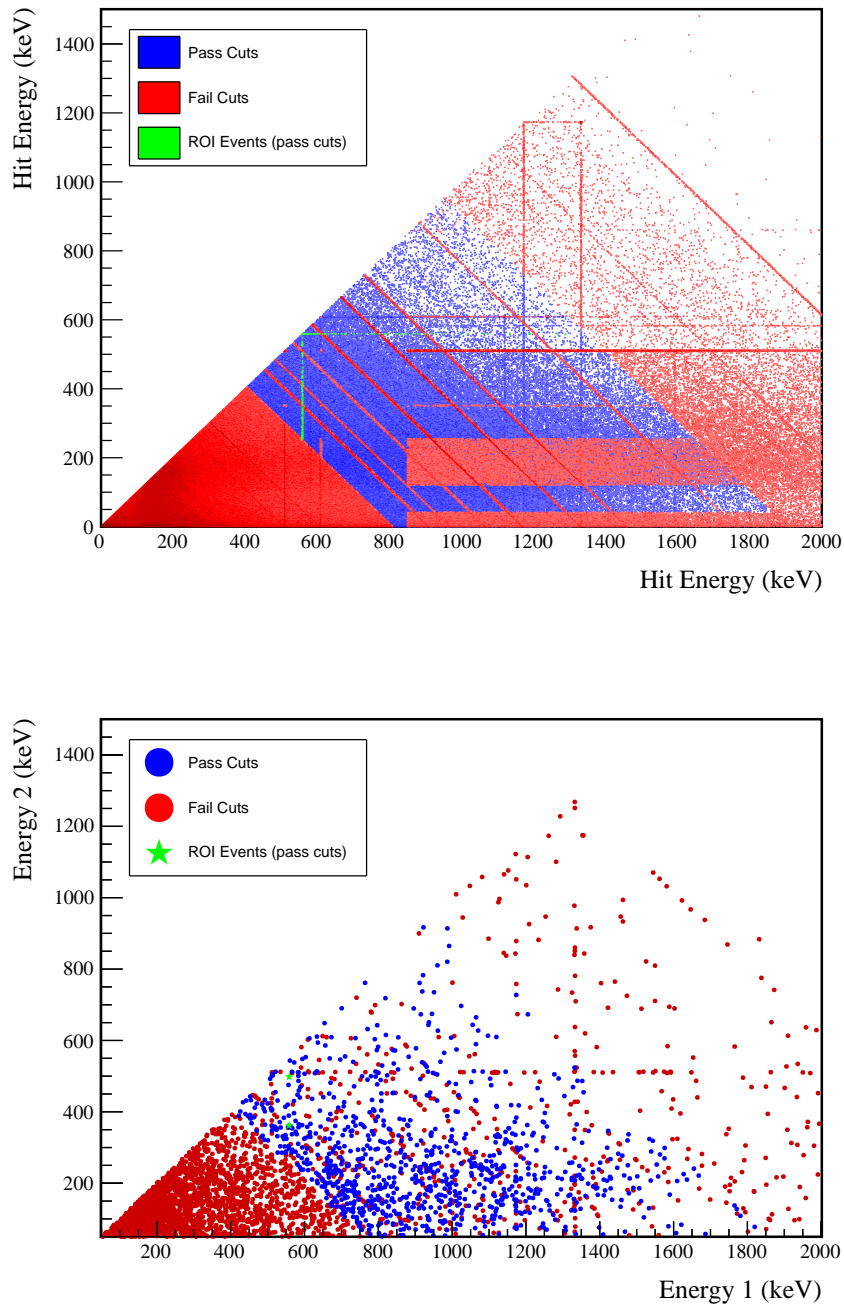
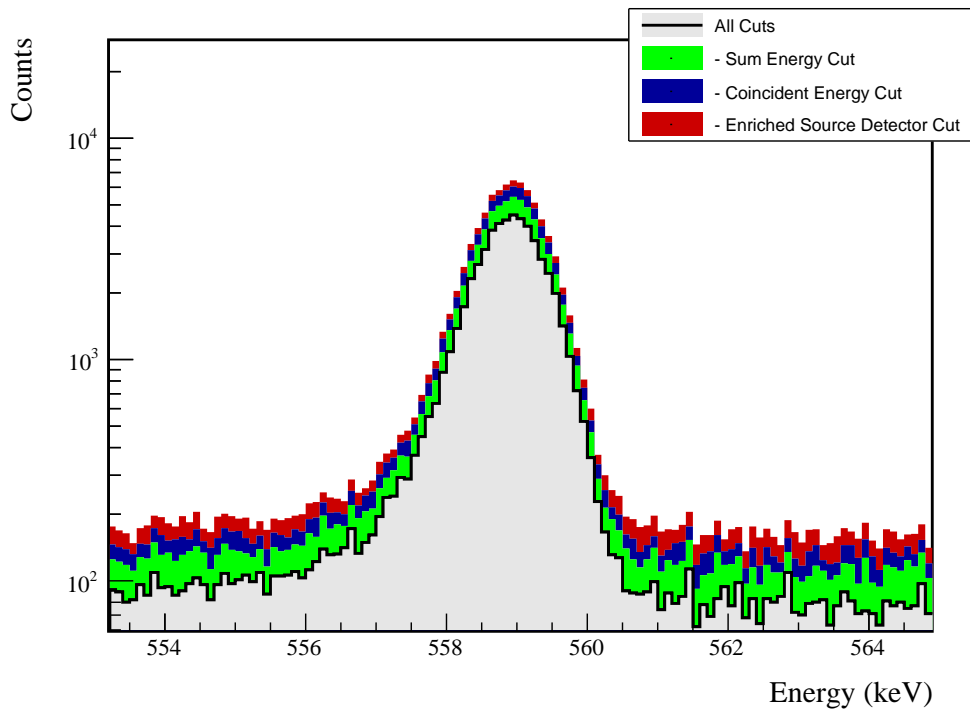


FIG. 46 Simulated (left) and measured (right) multiplicity 2 energy spectrum with sum and coincident energy cuts included for the 559 keV peak.

FIG. 47 Effect of all cuts applied sequentially on ROI for 559 keV peak of $2\nu\beta\beta$ to 2_2^+

Source	Module 1 efficiency	Module 2 efficiency
M. S. Event Signature	$1.7 \pm 0.2\%$	$0.9 \pm 0.5\%$
Region of Interest	$87.1 \pm 2.1\%$	$87.1 \pm 2.1\%$
Dead Layer	$75.3 \pm 4.2\%$	$67.3 \pm 5.7\%$
Detector Dead Times	$97.6 \pm 1.1\%$	$98.2 \pm 0.9\%$
Enriched Source Detector Cut	$97.6 \pm <0.1\%$	$92.3 \pm <0.1\%$
Coincident Energy Cut	$93.9 \pm <0.1\%$	$93.6 \pm <0.1\%$
Sum Energy Cut	$81.4 \pm <0.1\%$	$78.9 \pm <0.1\%$
Final Efficiency	$0.99 \pm 0.13\%$	$0.44 \pm 0.22\%$

FIG. 48 Table of detection efficiencies for the 559 keV peak.

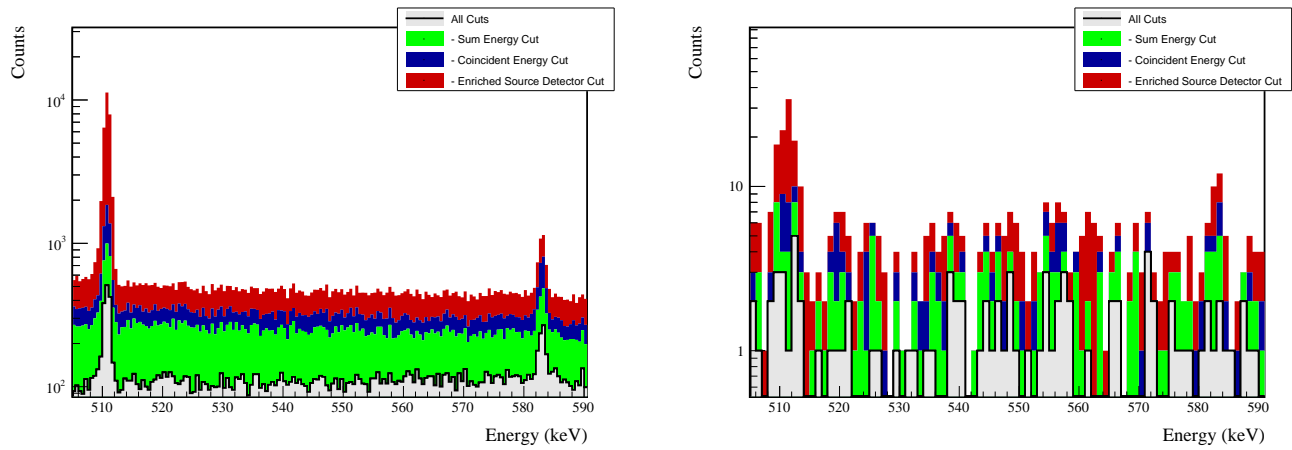
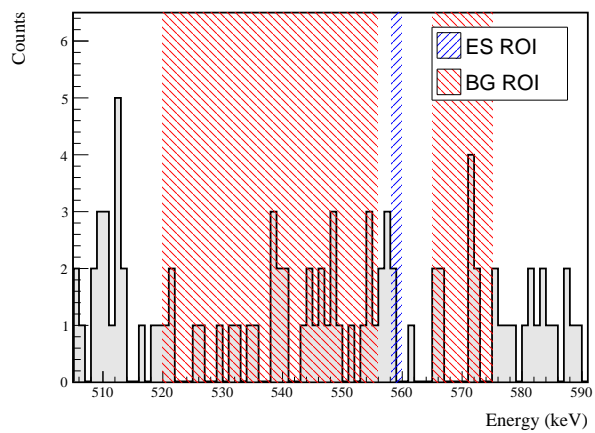


FIG. 49 Effect of all cuts applied to sequentially simulated (left) and measured (right) background data.

FIG. 50 All events after cuts in background (red) and signal (blue) ROIs for 559 keV peak of $2\nu\beta\beta$ to 2_2^+



579 2. 657 keV peak

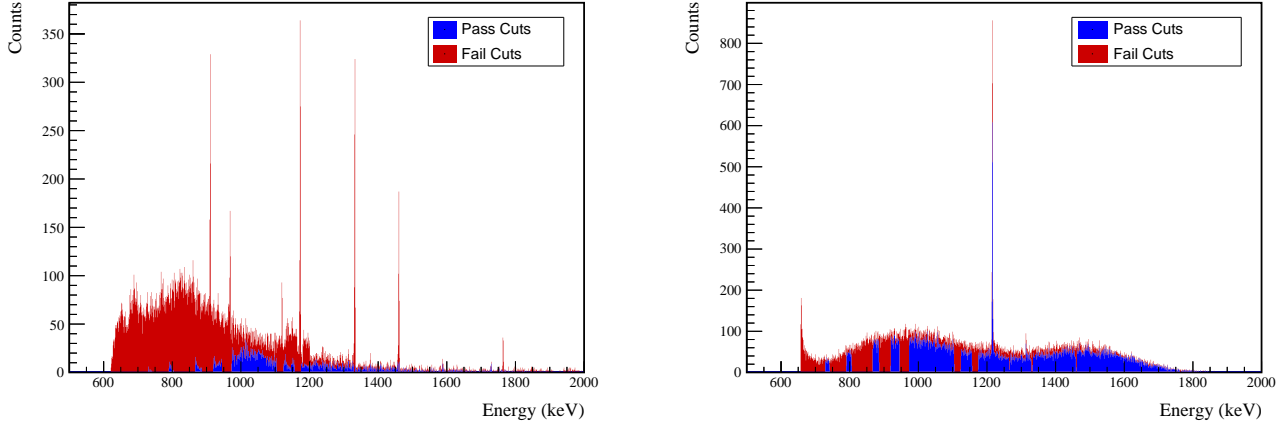


FIG. 51 Effect of 657 keV peak cuts on sum energy spectra in BG (left) and ES (right) simulations.

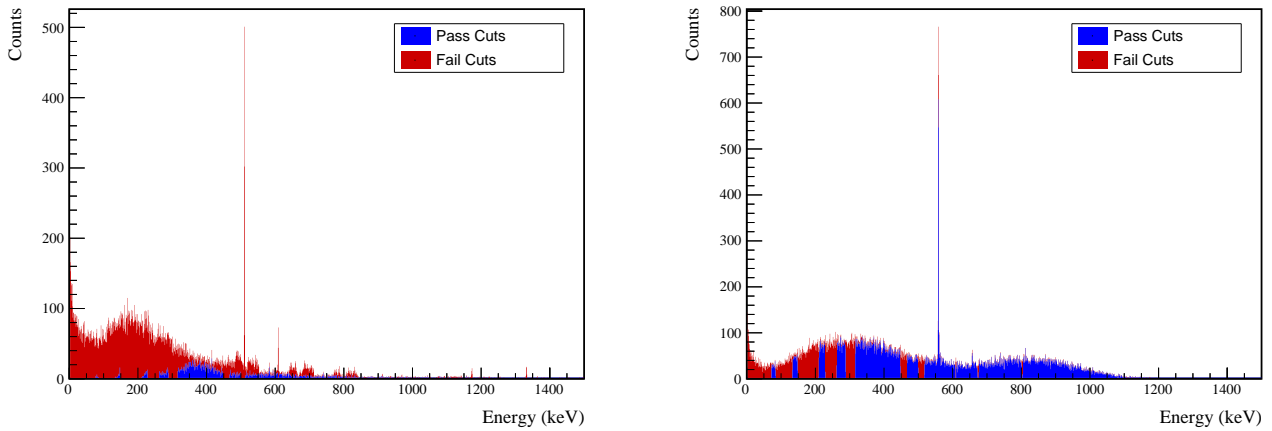


FIG. 52 Effect of 657 keV peak cuts on coincident energy spectra in BG (left) and ES (right) simulations.



TABLE XIV Table of energy estimation uncertainties for the 657 keV peak.

DS	E_{peak} (keV)	σ_{fit} (keV)	σ_{drift} (keV)	$f_{t,fit}$	σ (keV)	$\tau_{f,it}$ (keV)	$\delta_{\mu,f,it}$ (keV)	$\delta_{\mu,NL}$ (keV)	$\delta_{\mu,drift}$ (keV)	$\delta_{\mu,xtalk}$ (keV)	δ_u (keV)	FWHM	$\delta_{fwhm,fit}$ (keV)	$\delta_{fwhm,drift}$ (keV)	$\delta_{fwhm,xtalk}$ (keV)	δ_{FWHM} (keV)	δ_α	$E_{ROI,1}$ (keV)	$E_{ROI,2}$ (keV)	ϵ_{ROI}	$\sigma_{e_{ROI}}$	
DS1	657.041	0.500	0.074	0.505	0.230	0.579	0.002	0.104	0.003	0.012	0.005	0.105	1.256	0.001	0.039	0.011	0.040	0.032	656.051	657.858	0.873	0.013
DS2	657.041	0.502	0.064	0.506	0.249	0.580	0.002	0.067	0.005	0.012	0.005	0.068	1.263	0.001	0.107	0.011	0.108	0.085	656.035	657.856	0.875	0.028
DS3	657.041	0.510	0.078	0.516	0.224	0.568	0.002	0.026	0.026	0.012	0.005	0.040	1.278	0.001	0.073	0.011	0.074	0.058	656.039	657.874	0.879	0.019
DS4	657.041	0.493	0.090	0.501	0.108	0.490	0.002	0.076	0.076	0.012	0.005	0.078	1.207	0.001	0.106	0.011	0.107	0.088	656.147	657.865	0.890	0.029
DS5a	657.041	0.606	0.100	0.614	0.106	0.924	0.002	0.079	0.006	0.012	0.005	0.080	1.481	0.002	0.055	0.011	0.056	0.038	655.948	658.045	0.878	0.013
DS5b	657.041	0.509	0.087	0.517	0.158	0.562	0.001	0.020	0.013	0.012	0.005	0.027	1.259	0.001	0.125	0.011	0.125	0.100	656.086	657.884	0.886	0.032
DS5c	657.041	0.500	0.100	0.510	0.174	0.555	0.002	0.037	0.035	0.012	0.005	0.053	1.247	0.001	0.162	0.011	0.162	0.130	656.087	657.872	0.883	0.042
DS6a	657.041	0.495	0.051	0.497	0.191	0.524	0.001	0.069	0.030	0.012	0.005	0.076	1.221	0.001	0.041	0.011	0.042	0.035	656.099	657.850	0.882	0.012



Cut Name	Cut Description	$\langle \epsilon_{total} \rangle$	$\hat{\epsilon}_{total}$	$\langle \epsilon_{unique} \rangle$	$\hat{\epsilon}_{unique}$	Sacrifice	ΔIDP
Enriched Source Detector Cut	Any other detector: $i \neq \text{Bar}$	M1: 23.9 % M2: 43.7 %	25.2 ^{+3.9} _{-3.5} % 60.4 ^{+6.8} _{-7.2} %	7.2 % 13.5 %	7.4 ^{+2.6} _{-2.0} % 14.6 ^{+5.8} _{-4.4} %	1.7 % 5.5 %	21 %
Coincident Energy Cut	No other detector: (((energy>71.8) (energy>94.4 && energy<135.4) (energy>148.4 && energy<209.3) (energy>228.4 && energy<262.) (energy>285.4 && energy<316.2) (energy>447.4 && energy<467.2) (energy>499.6 && energy<512.8) (energy>607.6 && energy<610.4) (energy>1165.8 && energy<1175.6) (energy>157.6)) && isBar) ((energy>55.2) (energy>563.6 && energy<516.4) (energy>820.)) && 1.5*Bar)	M1: 54.0 % M2: 47.6 %	51.9 ± 4.3 % 37.5 ^{+7.2} _{-6.7} %	16.7 % 13.1 %	17.0 ^{+3.5} _{-3.0} % 10.4 ^{+5.2} _{-3.6} %	13.6 % 8.0 %	17 %
Sum Energy Cut	Not: (sumE>729.) (sumE>741.8 && sumE>700.4) (sumE>805.4 && sumE>867.) (sumE>865.6 && sumE>919.6) (sumE>945. && sumE>973.2) (sumE>1104.4 && sumE<1123.8) (sumE>1156.4 && sumE>1174.8) (sumE>1328.8 && sumE<1333.6) (sumE>1458.8 && sumE>1461.8) (sumE>1762.4 && sumE<1766.) (sumE>1897.4)	M1: 60.9 % M2: 60.3 %	57.0 ^{+4.2} _{-4.3} % 64.6 ^{+6.5} _{-7.1} %	14.3 % 9.7 %	15.6 ^{+3.4} _{-2.9} % 8.3 ^{+4.9} _{-3.2} %	1.4 % 1.4 %	29 %
Combined Cuts		M1: 86.5 % M2: 89.9 %	85.2 ^{+2.8} _{-3.3} % 93.8 ^{+2.7} _{-4.5} %	—	—	42.0 % 45.2 %	34 %

TABLE XV Table of cut descriptions and efficiencies for simulated backgrounds and measured data for the 657 keV peak.

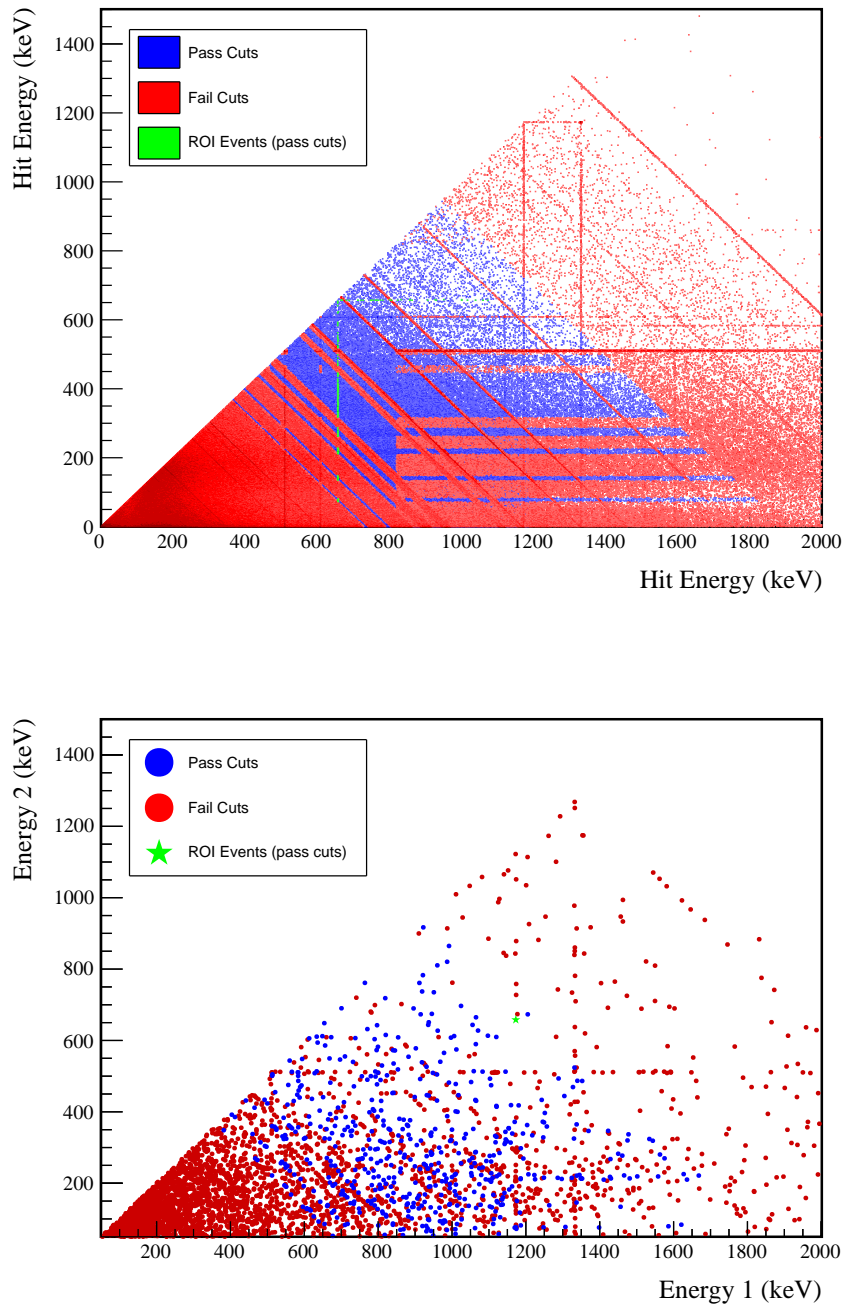
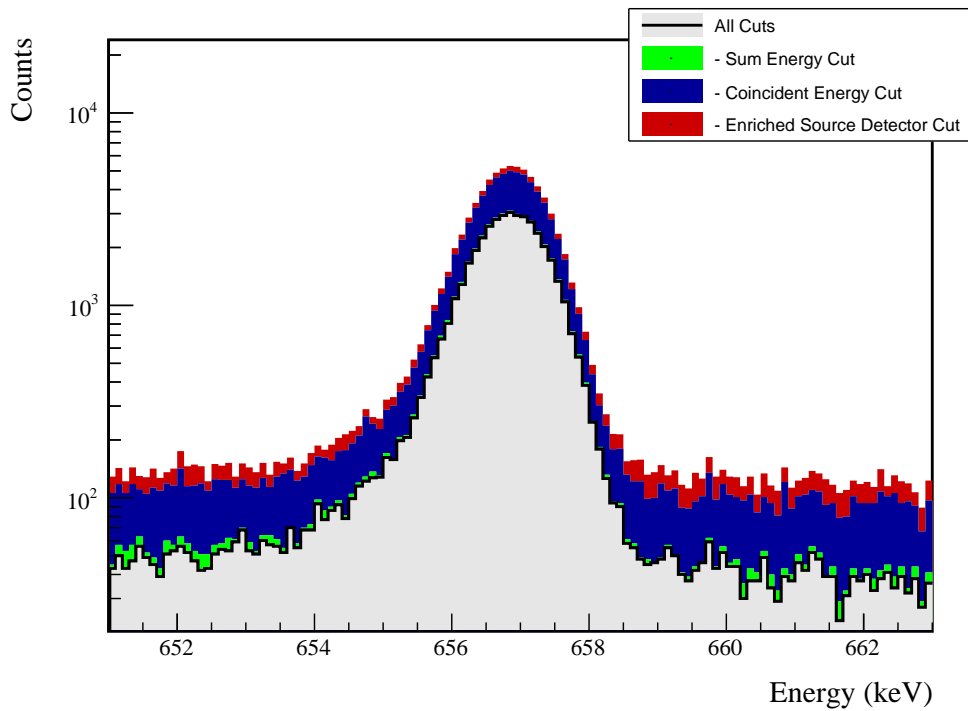


FIG. 53 Simulated (left) and measured (right) multiplicity 2 energy spectrum with sum and coincident energy cuts included for the 657 keV peak.

FIG. 54 Effect of all cuts applied sequentially on ROI for 657 keV peak of $2\nu\beta\beta$ to 2_2^+

Source	Module 1 efficiency	Module 2 efficiency
M. S. Event Signature	$1.6 \pm 0.2\%$	$0.9 \pm 0.5\%$
Region of Interest	$88.0 \pm 1.8\%$	$88.0 \pm 1.8\%$
Dead Layer	$75.6 \pm 4.1\%$	$66.9 \pm 5.8\%$
Detector Dead Times	$97.8 \pm 1.0\%$	$98.2 \pm 0.8\%$
Enriched Source Detector Cut	$97.1 \pm <0.1\%$	$90.8 \pm <0.1\%$
Coincident Energy Cut	$81.1 \pm <0.1\%$	$87.2 \pm <0.1\%$
Sum Energy Cut	$97.6 \pm <0.1\%$	$97.6 \pm <0.1\%$
Final Efficiency	$0.75 \pm 0.10\%$	$0.35 \pm 0.19\%$

FIG. 55 Table of detection efficiencies for the 657 keV peak.

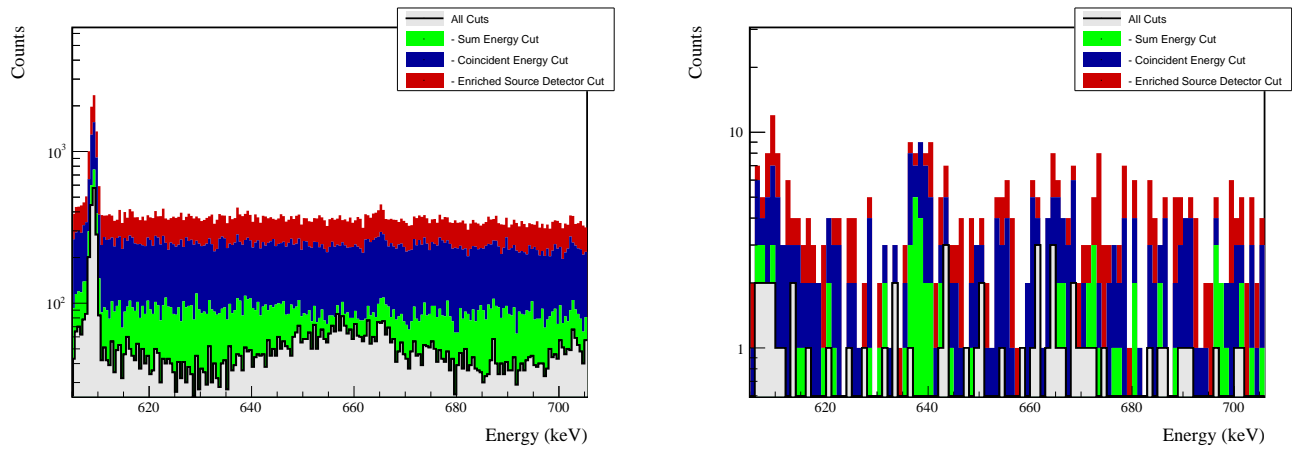
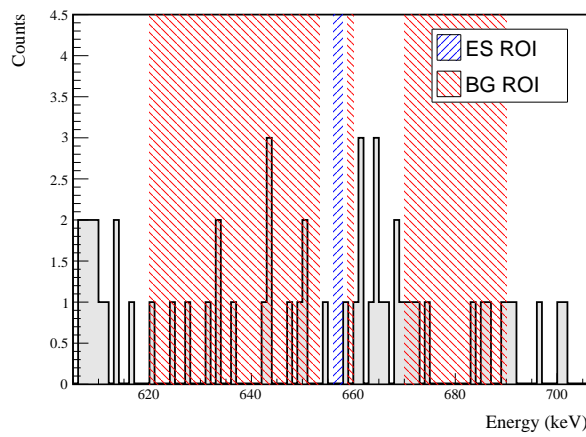


FIG. 56 Effect of all cuts applied to sequentially simulated (left) and measured (right) background data.

FIG. 57 All events after cuts in background (red) and signal (blue) ROIs for 657 keV peak of $2\nu\beta\beta$ to 2_2^+



580 3. 1216 keV peak

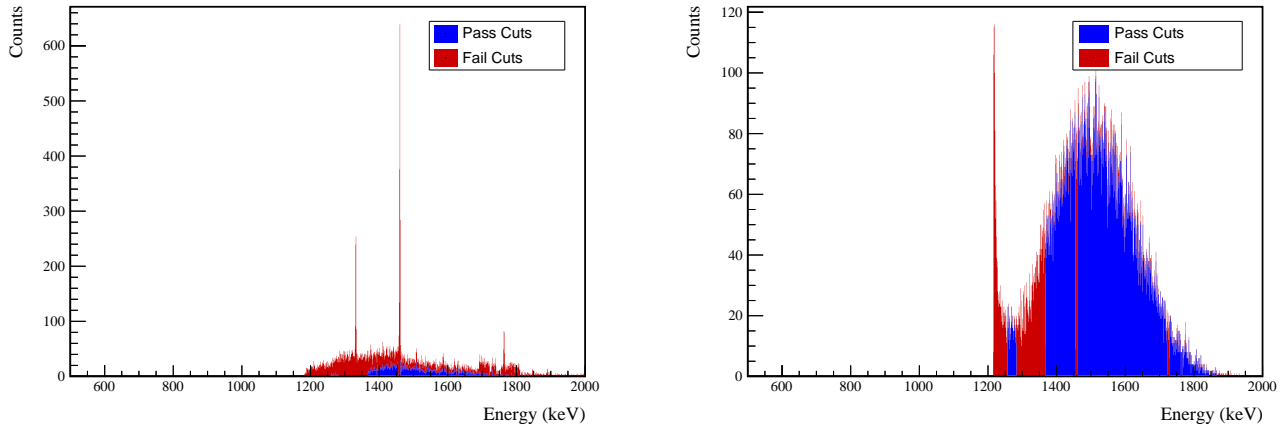


FIG. 58 Effect of 1216 keV peak cuts on sum energy spectra in BG (left) and ES (right) simulations.

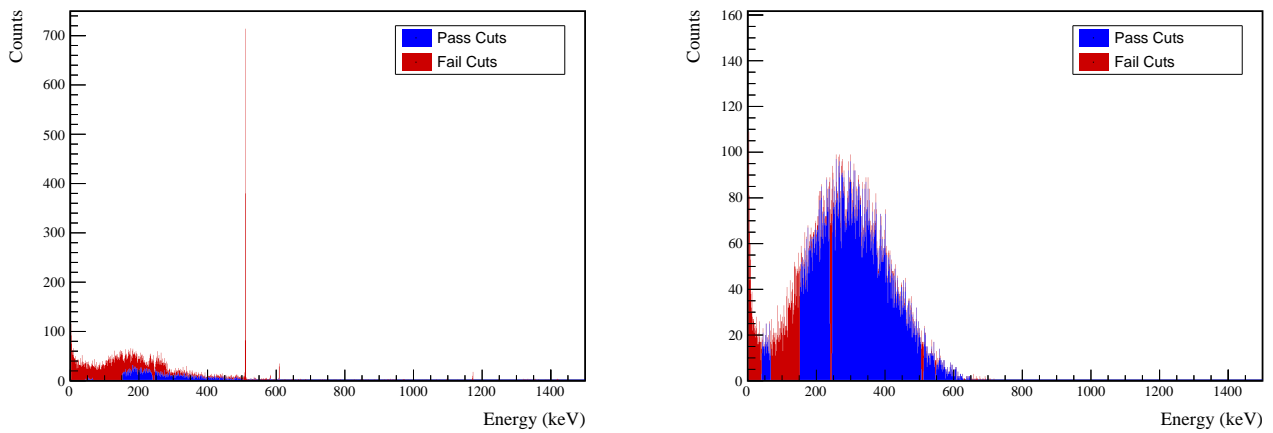


FIG. 59 Effect of 1216 keV peak cuts on coincident energy spectra in BG (left) and ES (right) simulations.



TABLE XVI Table of energy estimation uncertainties for the 1216 keV peak.

DS	E_{peak} (keV)	$\sigma_{f_{fit}}$ (keV)	σ_{drift} (keV)	σ (keV)	$f_{t,f_{fit}}$	$\tau_{f_{fit}}$ (keV)	$\delta_{\mu,f_{fit}}$ (keV)	$\delta_{\mu,NL}$ (keV)	$\delta_{\mu,drift}$ (keV)	$\delta_{\mu,x talk}$ (keV)	$\delta_{\mu,peak}$ (keV)	δ_{μ} (keV)	FWHM	$\delta_{f_{ahm},fit}$ (keV)	$\delta_{f_{ahm,drift}}$ (keV)	$\delta_{f_{ahm,x talk}}$ (keV)	δ_{FWHM} (keV)	$E_{ROI,1}$ (keV)	$E_{ROI,2}$ (keV)	ϵ_{ROI}	$\sigma_{e_{ROI}}$	
DS1	1216.104	0.705	0.137	0.718	0.230	0.945	0.003	0.104	0.005	0.012	0.020	0.107	1.787	0.001	0.039	0.011	0.040	0.023	1214.691	1217.262	0.868	0.008
DS2	1216.104	0.710	0.119	0.720	0.249	0.951	0.003	0.067	0.008	0.012	0.020	0.072	1.803	0.001	0.107	0.011	0.108	0.060	1214.663	1217.262	0.867	0.019
DS3	1216.104	0.715	0.144	0.729	0.224	0.925	0.003	0.026	0.051	0.012	0.020	0.062	1.812	0.001	0.073	0.011	0.074	0.041	1214.679	1217.281	0.872	0.013
DS4	1216.104	0.697	0.167	0.717	0.108	0.746	0.003	0.076	0.022	0.012	0.020	0.083	1.726	0.001	0.106	0.011	0.107	0.062	1214.829	1217.278	0.889	0.021
DS5a	1216.104	0.838	0.185	0.859	0.106	1.316	0.004	0.079	0.012	0.012	0.020	0.083	2.070	0.002	0.055	0.011	0.056	0.027	1214.581	1217.504	0.877	0.009
DS5b	1216.104	0.716	0.161	0.734	0.158	0.963	0.002	0.020	0.024	0.012	0.020	0.039	1.791	0.001	0.125	0.011	0.125	0.070	1214.743	1217.299	0.878	0.023
DS5c	1216.104	0.703	0.185	0.727	0.174	0.932	0.003	0.037	0.066	0.012	0.020	0.079	1.783	0.001	0.162	0.011	0.162	0.091	1214.738	1217.287	0.876	0.030
DS6a	1216.104	0.693	0.095	0.700	0.191	0.873	0.002	0.069	0.055	0.012	0.020	0.092	1.723	0.001	0.041	0.011	0.042	0.025	1214.771	1217.241	0.875	0.009



Cut Name	Cut Description	$\langle \epsilon_{total} \rangle$	$\hat{\epsilon}_{total}$	$\langle \epsilon_{unique} \rangle$	$\hat{\epsilon}_{unique}$	Sacrifice	ΔDP
Enriched Source Cut	Any other detector: isEor	M1: 26.9 %	16.9 ^{+4.5} _{-3.7} %	15.1 %	8.4 ^{+3.6} _{-2.6} %	2.4 %	23%
Detector Cut		M2: 43.9 %	61.9 ^{+9.7} _{-10.9} %	25.8 %	28.6 ^{+8.7} _{-8.7} %	5.8 %	
Multiplicity 2 Cut		M1: 15.3 %	16.9 ^{+4.5} _{-3.7} %	4.0 %	3.6 ^{+2.7} _{-1.6} %	0.1 %	5%
m==2		M2: 11.9 %	9.5 ^{+8.4} _{-4.7} %	3.2 %	0.0 ^{+4.5} _{-0.0} %	0.0 %	
No other detector:	((energy<40.8) (energy>36.6 && energy<15.2) (energy>239.6 && energy<245.8) (energy>605.8 && energy<610.) (energy>605.2 && energy<512.6) (energy>608.8 && energy<610.) (energy>600.8) && isthr)	M1: 34.1 %	38.6 ^{+5.4} _{-5.2} %	10.8 %	8.4 ^{+3.6} _{-2.6} %	0.3 %	14%
Coincident Energy Cut		M2: 25.9 %	14.3 ^{+9.3} _{-6.0} %	9.3 %	4.8 ^{+7.0} _{-2.9} %	0.3 %	
Note:	(sumE<1287.) (sumE<1283. && sumE<1367.4) (sumE>1465.2 && sumE<1462.) (sumE>1721.8 && sumE<1728.6) (sumE>1762. && sumE<1766.) (sumE>1845.6 && sumE<1851.2) (sumE>1866.6)	M1: 40.9 %	38.6 ^{+5.4} _{-5.2} %	10.5 %	4.8 ^{+2.9} _{-1.9} %	0.5 %	12%
Sum Energy Cut		M2: 35.9 %	42.9 ^{+10.9} _{-10.2} %	6.0 %	0.0 ^{+4.5} _{-0.0} %	0.5 %	
Combined Cuts		M1: 77.1 %	65.1 ^{+5.0} _{-5.4} %	—	—	20.1 %	44%
		M2: 79.8 %	81.0 ^{+7.1} _{-9.9} %	—	—	23.8 %	

TABLE XVII Table of cut descriptions and efficiencies for simulated backgrounds and measured data for the 1216 keV peak.

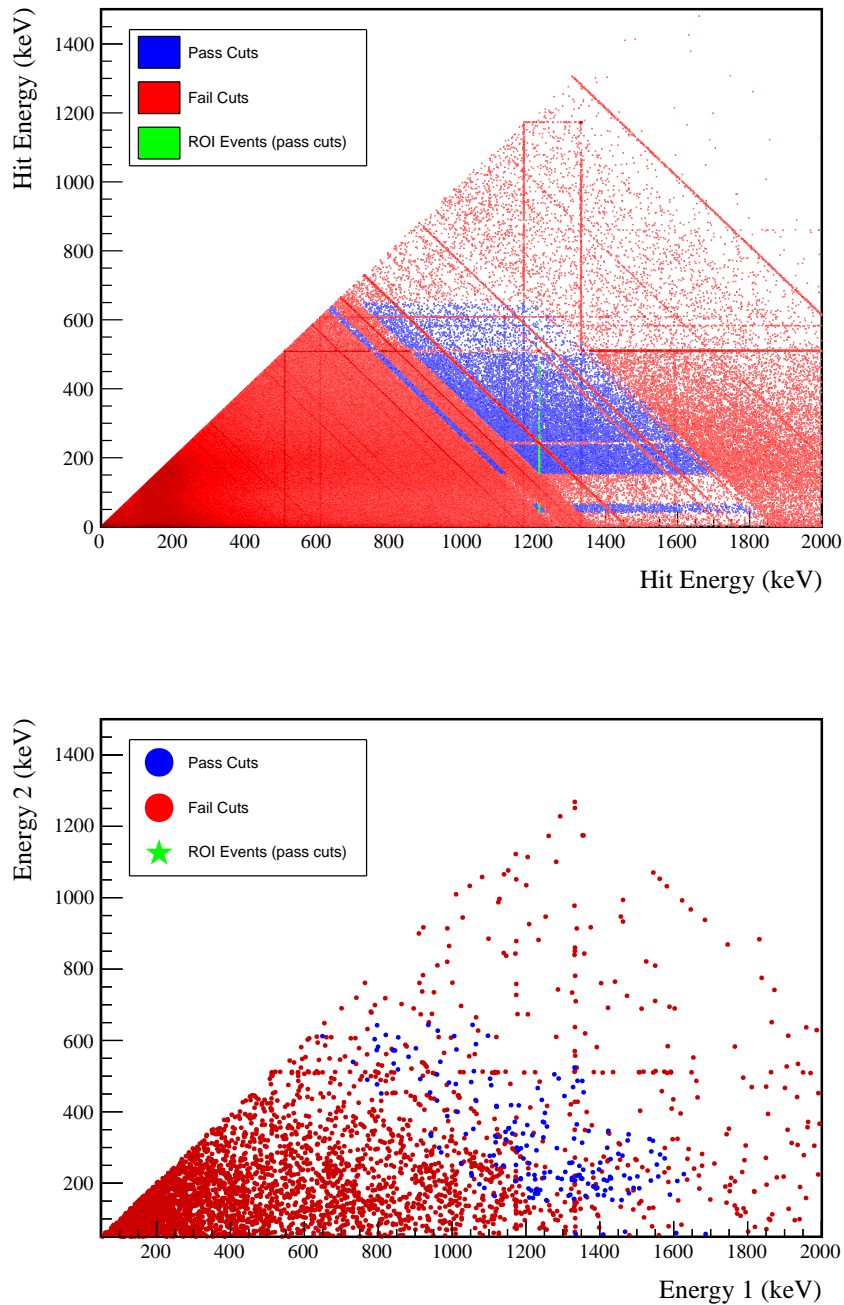
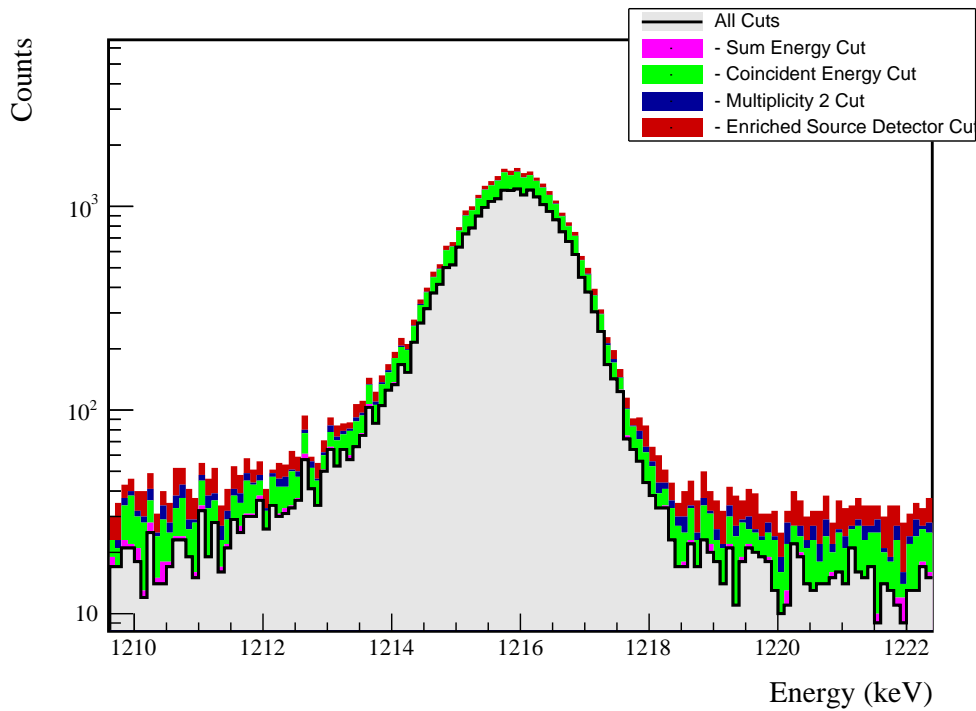


FIG. 60 Simulated (left) and measured (right) multiplicity 2 energy spectrum with sum and coincident energy cuts included for the 1216 keV peak.

FIG. 61 Effect of all cuts applied sequentially on ROI for 1216 keV peak of $2\nu\beta\beta$ to 2_2^+

Source	Module 1 efficiency	Module 2 efficiency
M. S. Event Signature	$0.7 \pm 0.2\%$	$0.3 \pm 0.5\%$
Region of Interest	$87.5 \pm 1.3\%$	$87.5 \pm 1.3\%$
Dead Layer	$73.9 \pm 4.4\%$	$63.6 \pm 6.4\%$
Detector Dead Times	$97.5 \pm 1.1\%$	$98.1 \pm 0.9\%$
Enriched Source Detector Cut	$97.1 \pm <0.1\%$	$93.0 \pm <0.1\%$
Multiplicity 2 Cut	$99.9 \pm <0.1\%$	$100.0 \pm <0.1\%$
Coincident Energy Cut	$99.6 \pm <0.1\%$	$99.6 \pm <0.1\%$
Sum Energy Cut	$99.4 \pm <0.1\%$	$99.4 \pm <0.1\%$
Final Efficiency	$0.43 \pm 0.13\%$	$0.18 \pm 0.25\%$

FIG. 62 Table of detection efficiencies for the 1216 keV peak.

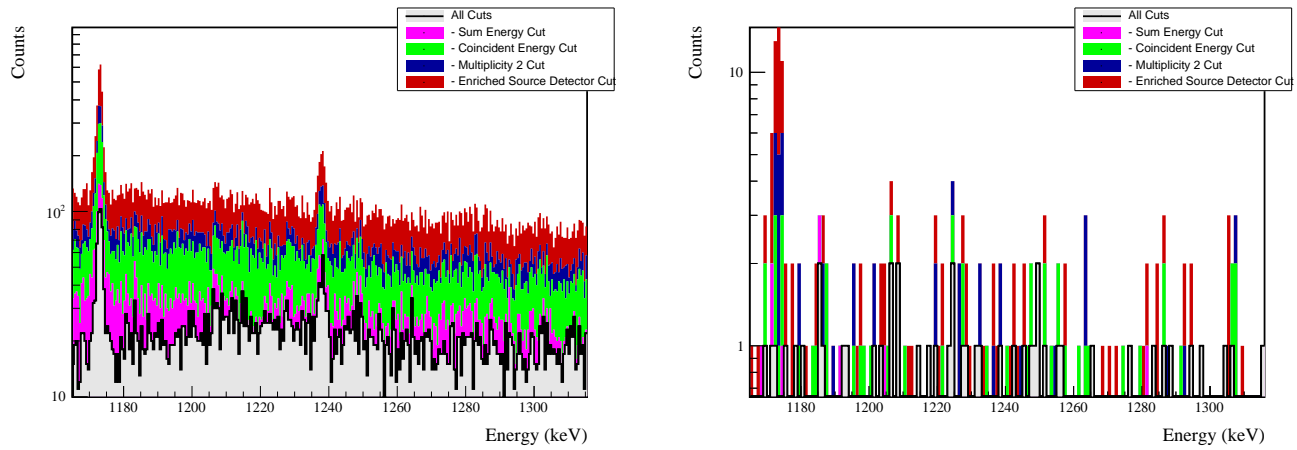
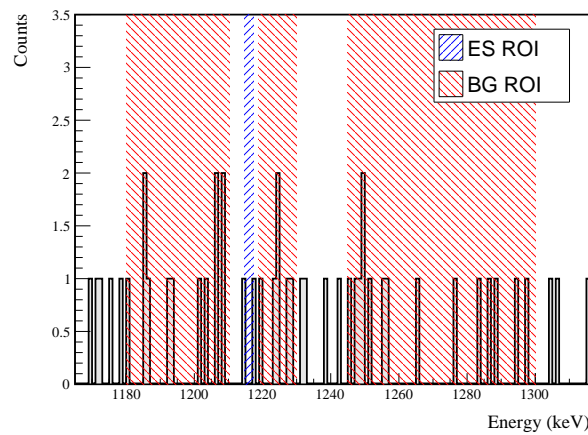
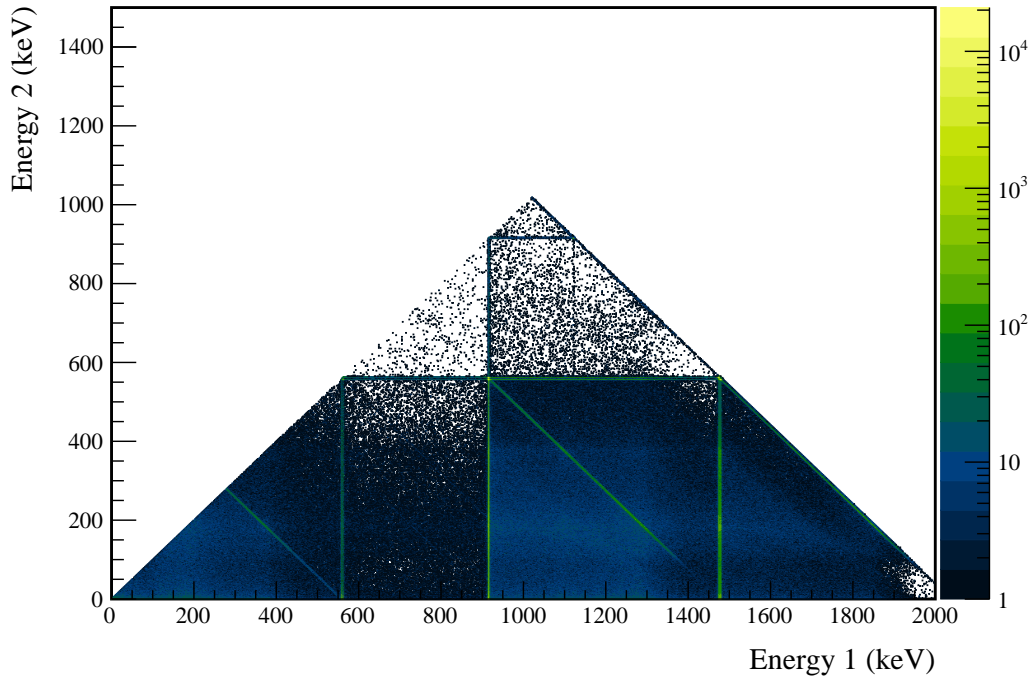


FIG. 63 Effect of all cuts applied to sequentially simulated (left) and measured (right) background data.

FIG. 64 All events after cuts in background (red) and signal (blue) ROIs for 1216 keV peak of $2\nu\beta\beta$ to 2_2^+

581 **Appendix E: $0\nu\beta\beta$ to 0_1^+**

582 Note that both the 559 and 563 keV peaks will be shown together since they use the same sets of cuts.



583 FIG. 65 Simulated multiplicity 2 energy spectrum of the $0\nu\beta\beta$ to 0_1^+ decay mode

584

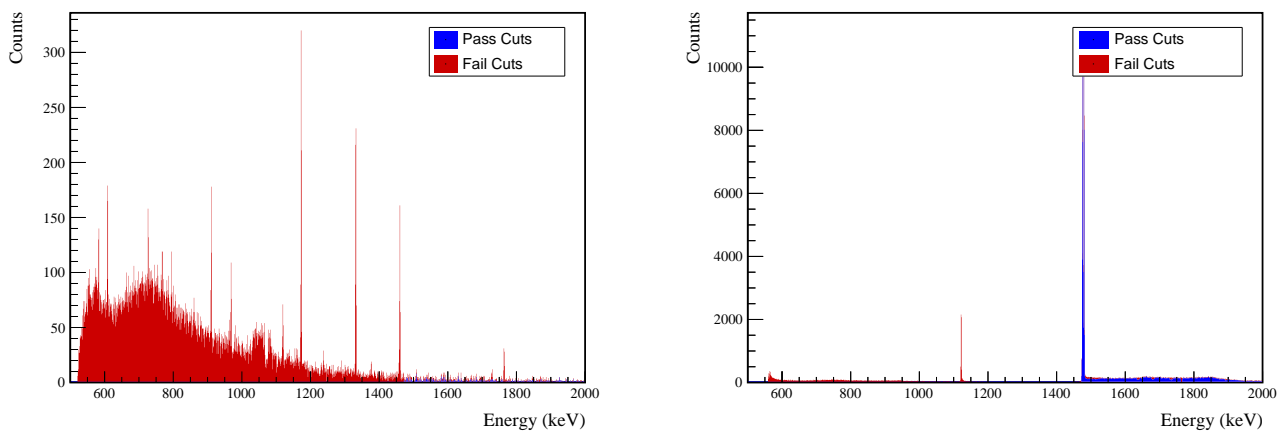


FIG. 66 Effect of 559 and 563 keV peaks cuts on sum energy spectra in BG (left) and ES (right) simulations.



TABLE XVIII Table of energy estimation uncertainties for the 559 and 563 keV peaks.

DS	E_{peak} (keV)	σ_{fit} (keV)	σ_{drift} (keV)	σ (keV)	$f_{t,fit}$ (keV)	τ_{fit} (keV)	$\delta_{\mu,fit}$ (keV)	$\delta_{\mu,NL}$ (keV)	$\delta_{\mu,drift}$ (keV)	$\delta_{\mu,peak}$ (keV)	δ_u (keV)	FWHM (keV)	$\delta_{fwhm,drift}$ (keV)	$\delta_{fwhm,fit}$ (keV)	$\delta_{fwhm,x talk}$ (keV)	δ_{FWHM} (keV)	δ_α	$E_{ROI,1}$ (keV)	$E_{ROI,2}$ (keV)	ϵ_{ROI}	$\sigma_{\epsilon_{ROI}}$	
DS1	559.101	0.460	0.063	0.464	0.230	0.515	0.001	0.104	0.002	0.012	0.005	0.105	1.152	0.001	0.039	0.011	0.040	0.035	558.083	559.935	0.907	0.012
DS2	559.101	0.461	0.055	0.464	0.249	0.515	0.002	0.067	0.004	0.012	0.005	0.068	1.158	0.001	0.107	0.011	0.108	0.093	558.066	559.934	0.910	0.025
DS3	559.101	0.470	0.066	0.474	0.224	0.505	0.001	0.026	0.024	0.012	0.005	0.038	1.174	0.001	0.073	0.011	0.074	0.063	558.071	559.953	0.914	0.017
DS4	559.101	0.455	0.077	0.461	0.108	0.445	0.002	0.076	0.010	0.012	0.005	0.078	1.111	0.001	0.106	0.011	0.107	0.096	558.186	559.943	0.922	0.026
DS5a	559.101	0.560	0.085	0.567	0.106	0.855	0.002	0.079	0.005	0.012	0.005	0.080	1.367	0.002	0.055	0.011	0.056	0.041	557.795	560.129	0.910	0.012
DS5b	559.101	0.469	0.074	0.475	0.158	0.491	0.001	0.020	0.011	0.012	0.005	0.026	1.157	0.001	0.125	0.011	0.125	0.108	558.122	559.962	0.919	0.029
DS5c	559.101	0.460	0.085	0.468	0.174	0.489	0.001	0.037	0.030	0.012	0.005	0.050	1.145	0.001	0.162	0.011	0.162	0.142	558.123	559.948	0.917	0.037
DS6a	559.101	0.456	0.044	0.458	0.191	0.463	0.001	0.069	0.025	0.012	0.005	0.075	1.123	0.000	0.041	0.011	0.042	0.038	558.134	559.928	0.916	0.011
DS1	563.178	0.461	0.064	0.466	0.230	0.518	0.001	0.104	0.002	0.012	0.005	0.105	1.156	0.001	0.039	0.011	0.040	0.035	562.156	564.015	0.907	0.012
DS2	563.178	0.463	0.055	0.466	0.249	0.517	0.002	0.067	0.004	0.012	0.005	0.068	1.162	0.001	0.107	0.011	0.108	0.093	562.139	564.014	0.910	0.025
DS3	563.178	0.471	0.066	0.476	0.224	0.508	0.001	0.026	0.024	0.012	0.005	0.038	1.179	0.001	0.073	0.011	0.074	0.063	562.144	564.033	0.914	0.017
DS4	563.178	0.457	0.077	0.463	0.108	0.447	0.002	0.076	0.010	0.012	0.005	0.078	1.115	0.001	0.106	0.011	0.107	0.096	562.260	564.023	0.922	0.026
DS5a	563.178	0.562	0.086	0.569	0.106	0.858	0.002	0.079	0.006	0.012	0.005	0.080	1.372	0.002	0.055	0.011	0.056	0.041	562.048	564.210	0.910	0.011
DS5b	563.178	0.471	0.074	0.477	0.158	0.494	0.001	0.020	0.011	0.012	0.005	0.026	1.162	0.001	0.125	0.011	0.125	0.108	562.196	564.042	0.919	0.029
DS5c	563.178	0.462	0.086	0.470	0.174	0.492	0.001	0.037	0.030	0.012	0.005	0.050	1.49	0.001	0.162	0.011	0.162	0.141	562.197	564.028	0.917	0.037
DS6a	563.178	0.457	0.044	0.459	0.191	0.465	0.001	0.069	0.026	0.012	0.005	0.075	1.127	0.000	0.041	0.011	0.042	0.038	562.208	564.008	0.915	0.011



Cut Name	Cut Description	$\langle \epsilon_{total} \rangle$	$\hat{\epsilon}_{total}$	$\langle \epsilon_{unique} \rangle$	$\hat{\epsilon}_{unique}$	Sacrifice	ΔDP
Enriched Source Detector Cut	Any other detector: isEar	M1: 23.2 % M2: 42.7 %	27.2 ^{+3.8} _{-7.6} % 62.8 ^{+2.5} _{-7.6} %	0.5 % 0.9 %	0.7 ^{+1.1} _{-0.4} % 7.0 ^{+4.9} _{-3.0} %	1.3 % 3.0 %	13 %
Coincident Energy Cut	No other detector: $((energy < 53) \& (energy > 469.6)$ $\& energy < 526.2) \& (energy > 577.8 \& energy < 552.2) \&$ $(energy > 1074.6 \& energy < 1079.2) \& (energy > 1177.2 \&$ $energy < 1121.6) \& (energy > 170.6 \& energy < 117.2) \&$ $(energy > 121.6 \& energy < 17.6) \& (energy > 175.) \&$ $(energy > 1334.) \& (energy > 1483.) \& (energy > 1331. \& energy < 1334.) \& (energy > 508. \& energy < 522.6) \&$ $(energy > 1385.6) \& 1.isEar)$ Note: $(sumE < 1472.) \& (sumE > 1761.8 \& sumE < 1765.8) \&$ $(sumE > 2042.6)$	M1: 28.8 % M2: 26.9 %	32.0 ^{+4.0} _{-3.7} % 23.3 ^{+3.7} _{-5.8} %	0.8 % 0.5 %	1.4 ^{+1.3} _{-0.7} % 7.0 ^{+4.9} _{-3.0} %	4.5 % 2.9 %	9 %
Sum Energy Cut		M1: 97.1 % M2: 97.6 %	96.6 ^{+1.2} _{-1.8} % 86.0 ^{+4.5} _{-6.7} %	50.9 % 38.0 %	49.0 \pm 4.1 % 27.9 ^{+7.3} _{-6.3} %	12.3 % 15.3 %	243 %
Combined Cuts		M1: 98.4 % M2: 99.1 %	98.6 ^{+1.3} _{-0.7} % 100.0 ^{+0.0} _{-2.3} %	—	—	26.5 % 35.9 %	298 %

TABLE XIX Table of cut descriptions and efficiencies for simulated backgrounds and measured data for the 559 and 563 keV peaks.

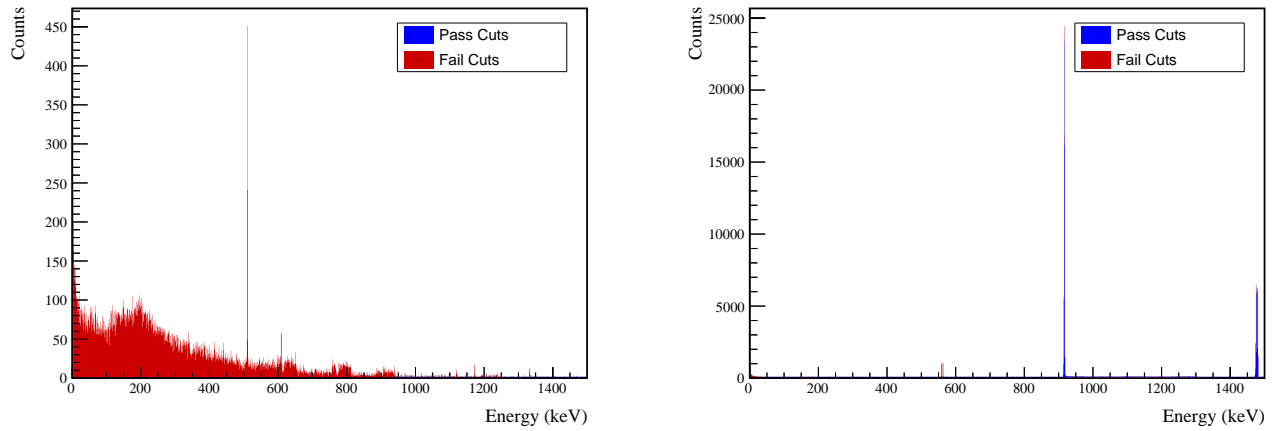


FIG. 67 Effect of 559 and 563 keV peaks cuts on coincident energy spectra in BG (left) and ES (right) simulations.

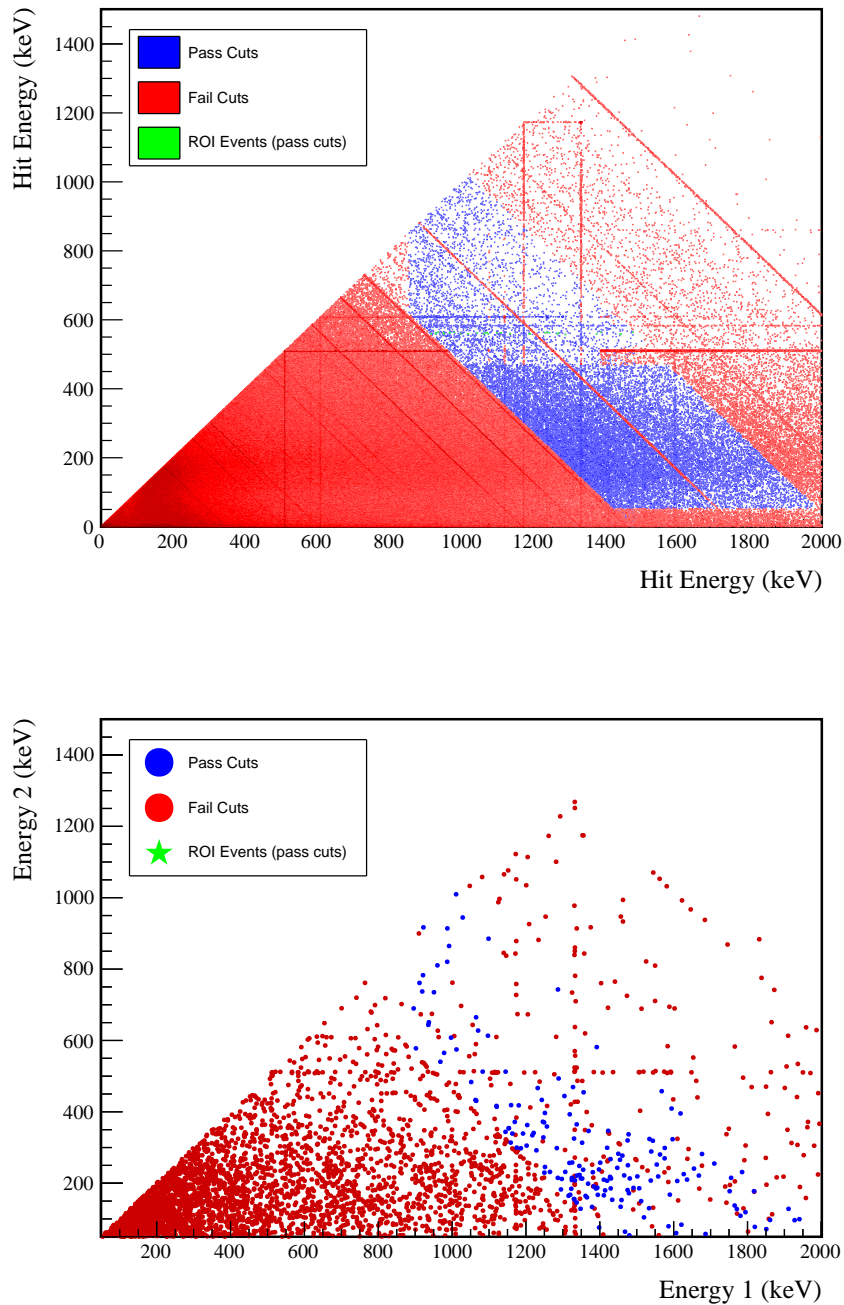


FIG. 68 Simulated (left) and measured (right) multiplicity 2 energy spectrum with sum and coincident energy cuts included for the 559 and 563 keV peaks.

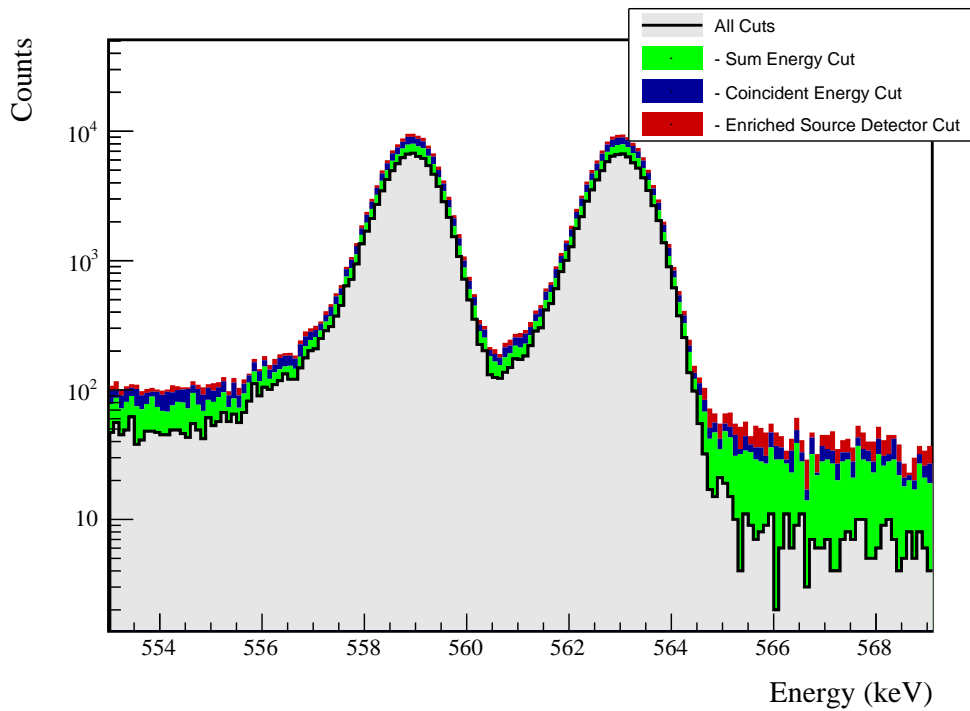


FIG. 69 Effect of all cuts applied sequentially on ROI for 559 and 563 keV peaks of $0\nu\beta\beta$ to 0_1^+

Source	Module 1 efficiency	Module 2 efficiency
M. S. Event Signature	$5.3 \pm 0.2\%$	$2.8 \pm 0.5\%$
Region of Interest	$91.3 \pm 1.1\%$	$91.3 \pm 1.1\%$
Dead Layer	$69.3 \pm 5.2\%$	$60.7 \pm 6.9\%$
Detector Dead Times	$97.6 \pm 1.1\%$	$98.1 \pm 0.9\%$
Enriched Source Detector Cut	$98.3 \pm <0.1\%$	$95.5 \pm <0.1\%$
Coincident Energy Cut	$94.3 \pm 0.3\%$	$95.7 \pm 0.3\%$
Sum Energy Cut	$85.7 \pm 0.3\%$	$80.8 \pm 0.3\%$
Final Efficiency	$3.10 \pm 0.27\%$	$1.34 \pm 0.27\%$

FIG. 70 Table of detection efficiencies for the 559 and 563 keV peaks.

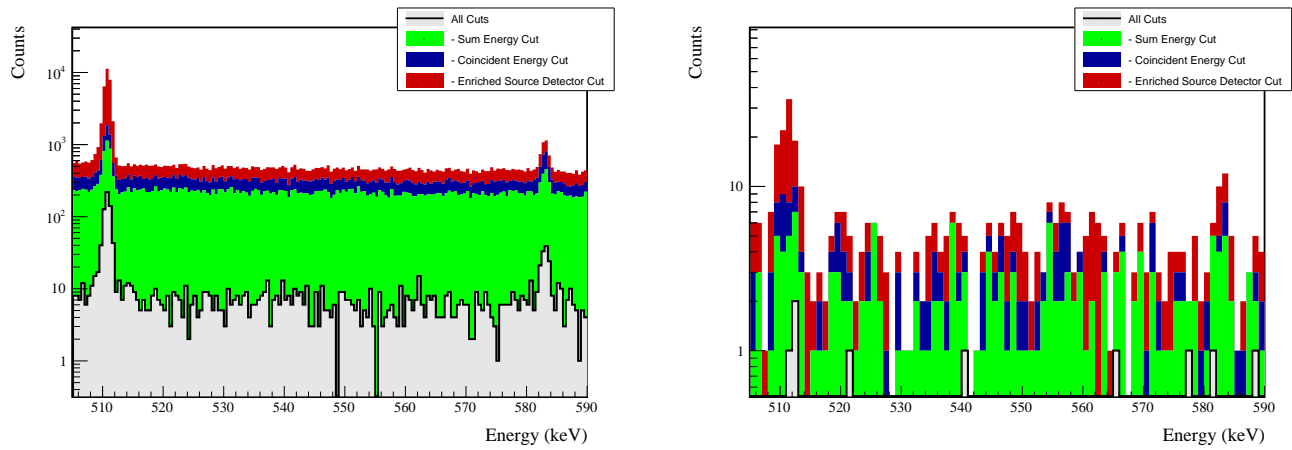
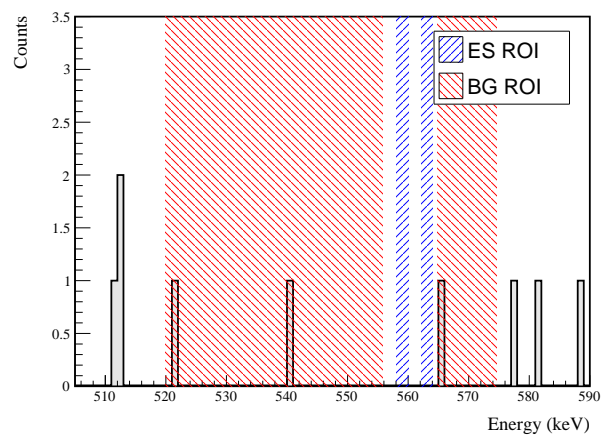


FIG. 71 Effect of all cuts applied to sequentially simulated (left) and measured (right) background data.

FIG. 72 All events after cuts in background (red) and signal (blue) ROIs for 559 and 563 keV peaks of $0\nu\beta\beta$ to 0_1^+

585 **Appendix F: $0\nu\beta\beta$ to 2_1^+**

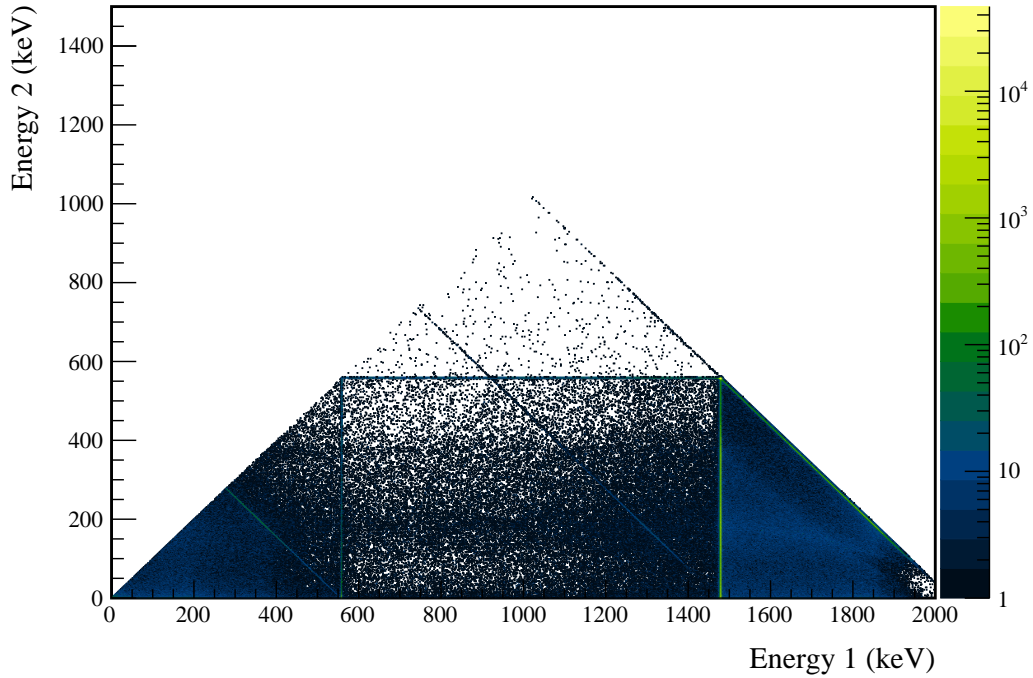


FIG. 73 Simulated multiplicity 2 energy spectrum of the $0\nu\beta\beta$ to 2_1^+ decay mode

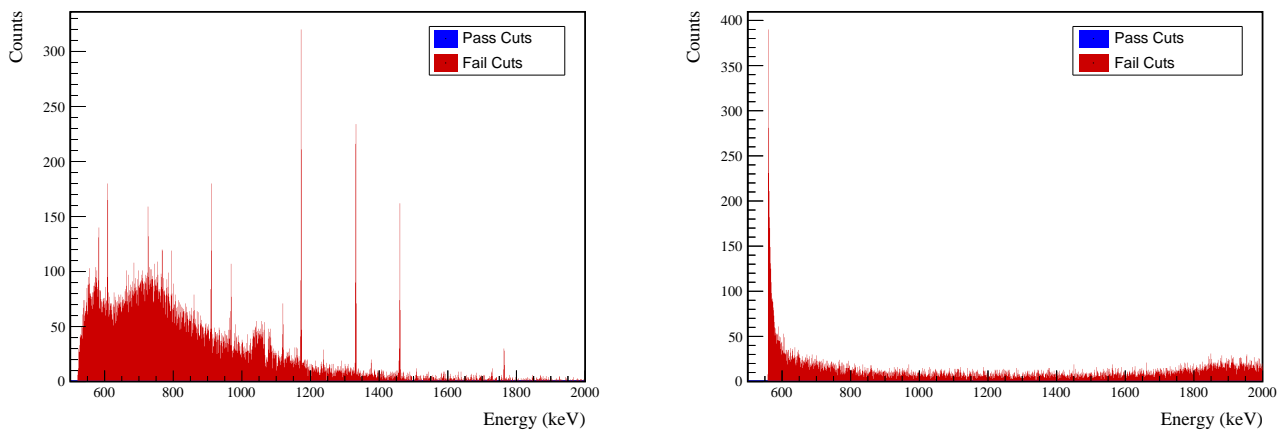


FIG. 74 Effect of 559 keV peak cuts on sum energy spectra in BG (left) and ES (right) simulations.



TABLE XX Table of energy estimation uncertainties for the 559 keV peak.

DS	E_{peak} (keV)	σ_{drift} (keV)	σ_{fit} (keV)	f_{drift}	σ_f (keV)	$f_{t,fit}$ (keV)	$\tau_{f,fit}$ (keV)	$\delta_{\mu,NL}$ (keV)	$\delta_{\mu,drift}$ (keV)	$\delta_{\mu,atalk}$ (keV)	$\delta_{\mu,peak}$ (keV)	δ_u (keV)	FWHM (keV)	$\delta_{fwhm,fit}$ (keV)	$\delta_{fwhm,drift}$ (keV)	$\delta_{fwhm,atalk}$ (keV)	δ_{FWHM} (keV)	δ_α	$E_{ROI,1}$ (keV)	$E_{ROI,2}$ (keV)	ϵ_{ROI}	$\sigma_{\epsilon_{ROI}}$
DS1	559.101	0.460	0.063	0.464	0.230	0.515	0.001	0.104	0.002	0.012	0.005	0.105	1.152	0.001	0.039	0.011	0.040	0.035	558.052	559.959	0.915	0.011
DS2	559.101	0.461	0.055	0.464	0.249	0.515	0.002	0.067	0.004	0.012	0.005	0.068	1.158	0.001	0.107	0.011	0.108	0.093	558.035	559.957	0.917	0.023
DS3	559.101	0.470	0.066	0.474	0.224	0.505	0.001	0.026	0.024	0.012	0.005	0.038	1.174	0.001	0.073	0.011	0.074	0.063	558.039	559.977	0.921	0.016
DS4	559.101	0.455	0.077	0.461	0.108	0.445	0.002	0.076	0.010	0.012	0.005	0.078	1.111	0.001	0.106	0.011	0.107	0.096	558.161	559.966	0.929	0.024
DS5a	559.101	0.560	0.085	0.567	0.106	0.885	0.002	0.079	0.005	0.012	0.005	0.080	1.367	0.002	0.055	0.011	0.056	0.041	557.942	560.158	0.918	0.011
DS5b	559.101	0.469	0.074	0.475	0.158	0.491	0.001	0.020	0.011	0.012	0.005	0.026	1.157	0.001	0.125	0.011	0.125	0.108	558.094	559.986	0.927	0.027
DS5c	559.101	0.460	0.085	0.468	0.174	0.489	0.001	0.037	0.030	0.012	0.005	0.050	1.145	0.001	0.162	0.011	0.162	0.142	558.095	559.972	0.924	0.035
DS6a	559.101	0.456	0.044	0.458	0.191	0.463	0.001	0.069	0.025	0.012	0.005	0.075	1.123	0.000	0.041	0.011	0.042	0.038	558.106	559.951	0.923	0.010



Cut Name	Cut Description	$\langle \epsilon_{total} \rangle$	$\hat{\epsilon}_{total}$	$\langle \epsilon_{unrigue} \rangle$	$\hat{\epsilon}_{unrigue}$	Sacrifice	ΔDP
Enriched Source		M1: 23.2 %	26.5 ^{+3.8} / _{-3.5} %	0.0 %	0.0 ^{+0.7} / _{-0.0} %	2.1 %	
Detector Cut	Any other detector: isBar	M2: 42.7 %	62.8 ^{+7.0} / _{-7.6} %	0.0 %	0.0 ^{+2.3} / _{-0.0} %	4.5 %	-2%
Multiplicity 2 Cut	n==2	M1: 15.4 %	16.3 ^{+3.3} / _{-3.6} %	0.0 %	0.0 ^{+0.7} / _{-0.0} %	0.0 %	0%
Coincident Energy Cut	Any other detector: energy>1472.4 && energy<1483.3	M2: 11.7 %	16.2 ^{+2.8} / _{-6.4} %	0.0 %	0.0 ^{+2.3} / _{-0.0} %	0.0 %	
Combined Cuts		M1: 100.0 %	100.0 ^{+0.0} / _{-0.0} %	62.7 %	59.9 ^{+4.0} / _{-4.1} %	19.0 %	808%
		M2: 100.0 %	100.0 ^{+2.3} / _{-0.0} %	47.8 %	27.9 ^{+7.3} / _{-6.3} %	20.5 %	
		M1: 100.0 %	100.0 ^{+0.7} / _{-0.0} %	—	—	22.9 %	
		M2: 100.0 %	100.0 ^{+0.0} / _{-2.3} %	—	—	27.9 %	994%

TABLE XXI Table of cut descriptions and efficiencies for simulated backgrounds and measured data for the 559 keV peak.

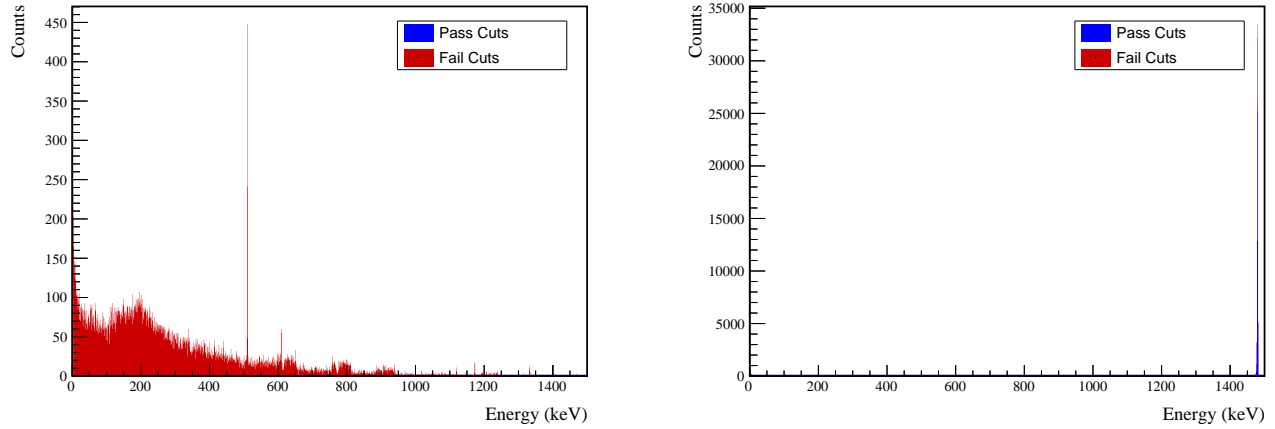


FIG. 75 Effect of 559 keV peak cuts on coincident energy spectra in BG (left) and ES (right) simulations.

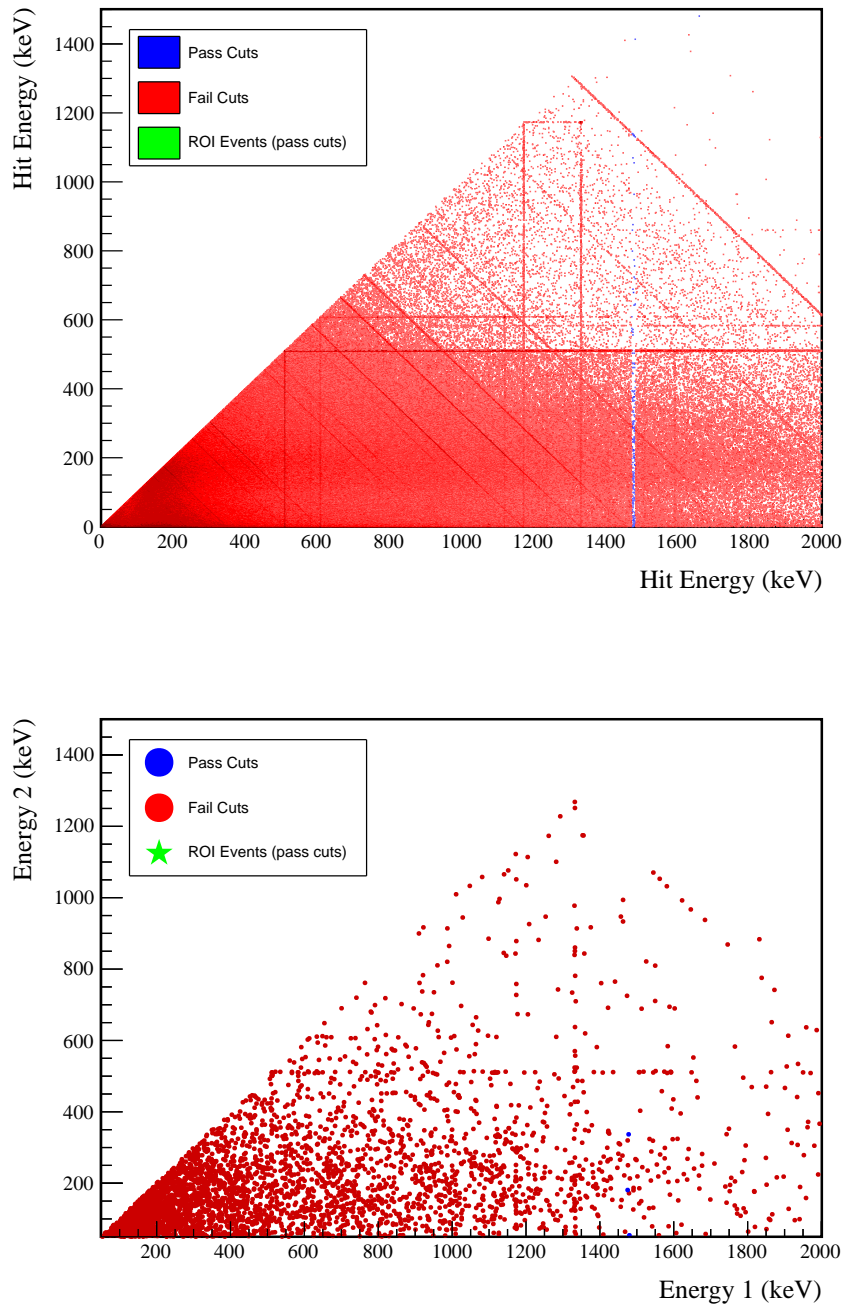
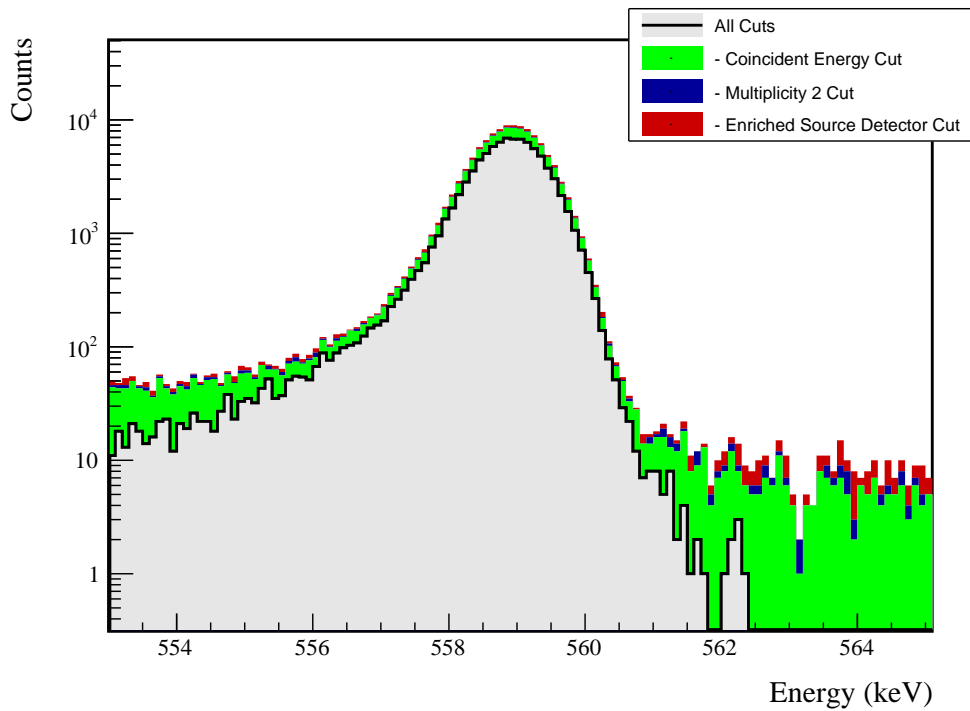


FIG. 76 Simulated (left) and measured (right) multiplicity 2 energy spectrum with sum and coincident energy cuts included for the 559 keV peak.

FIG. 77 Effect of all cuts applied sequentially on ROI for 559 keV peak of $0\nu\beta\beta$ to 2_1^+

Source	Module 1 efficiency	Module 2 efficiency
M. S. Event Signature	$2.7 \pm 0.2\%$	$1.4 \pm 0.5\%$
Region of Interest	$92.1 \pm 1.5\%$	$92.1 \pm 1.5\%$
Dead Layer	$67.8 \pm 5.5\%$	$59.3 \pm 7.1\%$
Detector Dead Times	$97.5 \pm 1.1\%$	$98.0 \pm 0.9\%$
Enriched Source Detector Cut	$97.4 \pm <0.1\%$	$94.1 \pm <0.1\%$
Multiplicity 2 Cut	$100.0 \pm <0.1\%$	$100.0 \pm <0.1\%$
Coincident Energy Cut	$80.3 \pm 0.3\%$	$77.8 \pm 0.3\%$
Final Efficiency	$1.64 \pm 0.18\%$	$0.70 \pm 0.25\%$

FIG. 78 Table of detection efficiencies for the 559 keV peak.

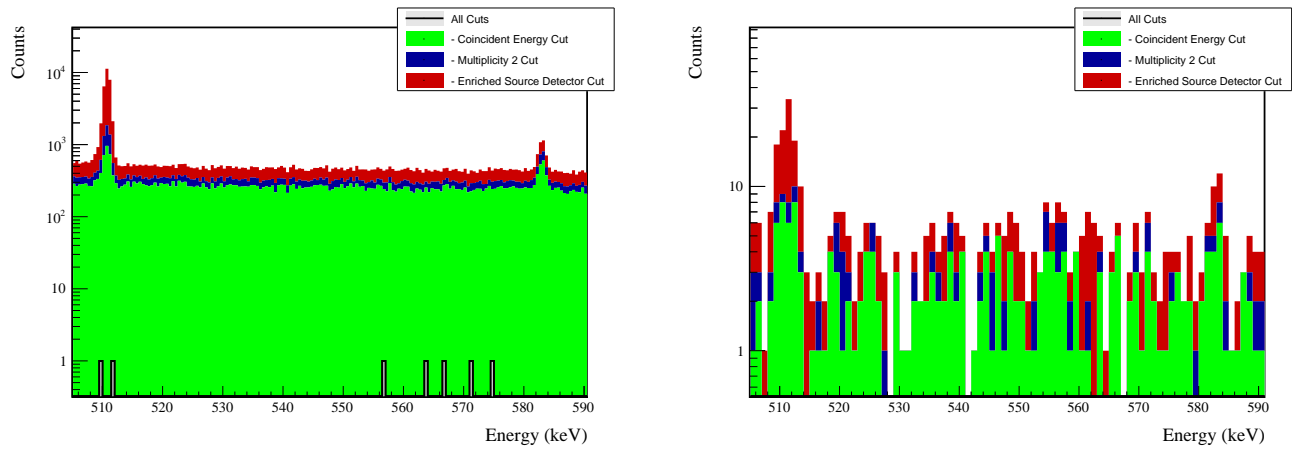
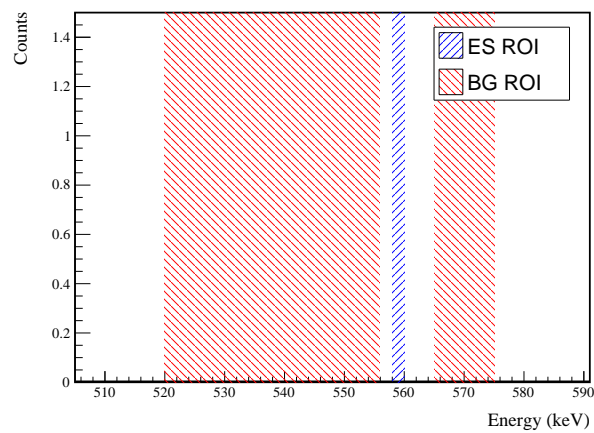


FIG. 79 Effect of all cuts applied to sequentially simulated (left) and measured (right) background data.

FIG. 80 All events after cuts in background (red) and signal (blue) ROIs for 559 keV peak of $0\nu\beta\beta$ to 2_1^+

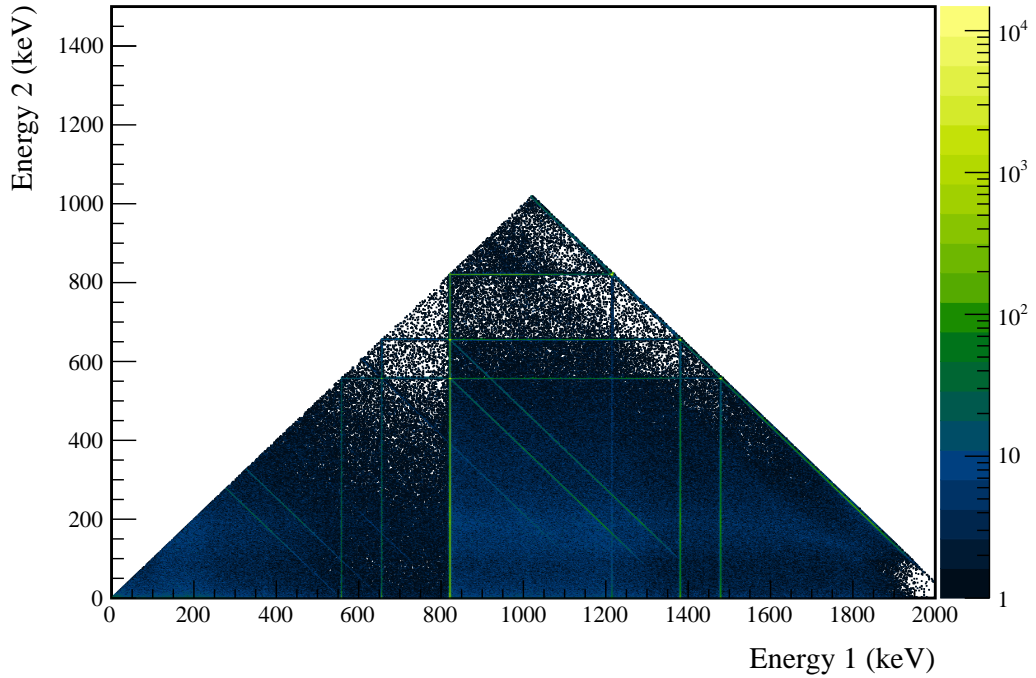
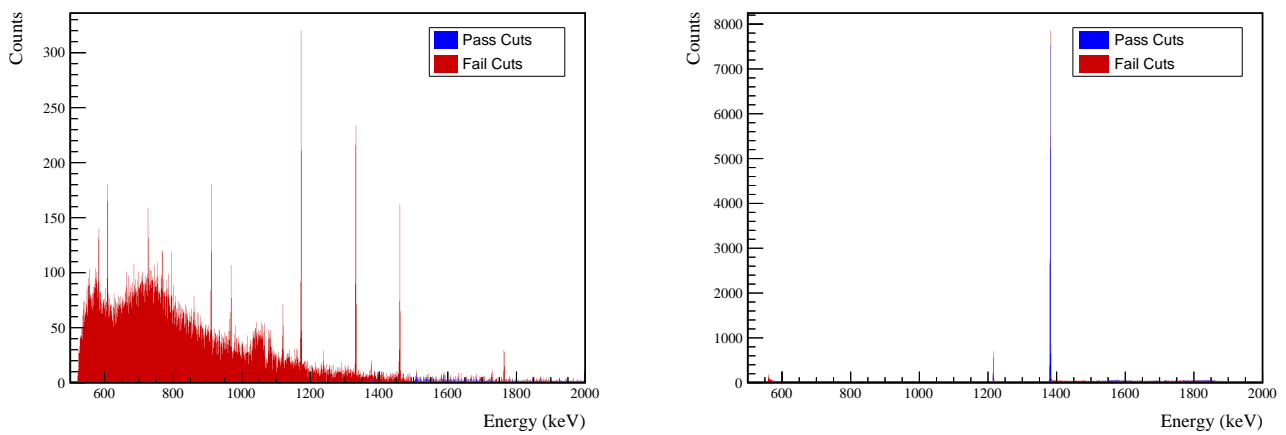
586 **Appendix G: $0\nu\beta\beta$ to 2_2^+** FIG. 81 Simulated multiplicity 2 energy spectrum of the $0\nu\beta\beta$ to 2_2^+ decay mode587 **1. 559 keV peak**

FIG. 82 Effect of 559 keV peak cuts on sum energy spectra in BG (left) and ES (right) simulations.



TABLE XXII Table of energy estimation uncertainties for the 559 keV peak.

DS	E_{peak} (keV)	σ_{drift} (keV)	σ_{fit} (keV)	σ (keV)	$f_{t,fit}$	$\tau_{f,fit}$ (keV)	$\delta_{\mu,drift}$ (keV)	$\delta_{\mu,NL}$ (keV)	$\delta_{\mu,fit}$ (keV)	$\delta_{\mu,xtalk}$ (keV)	δ_u (keV)	FWHM (keV)	$\delta_{fwhm,fit}$ (keV)	$\delta_{fwhm,drift}$ (keV)	$\delta_{fwhm,xtalk}$ (keV)	δ_{FWHM} (keV)	δ_α	$E_{ROI,1}$ (keV)	$E_{ROI,2}$ (keV)	ϵ_{ROI}	$\sigma_{e_{ROI}}$	
DS1	559.101	0.460	0.063	0.464	0.230	0.515	0.001	0.104	0.002	0.012	0.005	0.105	1.152	0.001	0.039	0.011	0.040	0.035	558.084	559.935	0.907	0.012
DS2	559.101	0.461	0.055	0.464	0.249	0.515	0.002	0.067	0.004	0.012	0.005	0.068	1.158	0.001	0.107	0.011	0.108	0.093	558.067	559.933	0.909	0.025
DS3	559.101	0.470	0.066	0.474	0.224	0.505	0.001	0.026	0.024	0.012	0.005	0.038	1.174	0.001	0.073	0.011	0.074	0.063	558.072	559.952	0.913	0.017
DS4	559.101	0.455	0.077	0.461	0.108	0.445	0.002	0.076	0.010	0.012	0.005	0.078	1.111	0.001	0.106	0.011	0.107	0.096	558.187	559.942	0.922	0.026
DS5a	559.101	0.560	0.085	0.567	0.106	0.885	0.002	0.079	0.005	0.012	0.005	0.080	1.367	0.002	0.055	0.011	0.056	0.041	557.976	560.128	0.910	0.012
DS5b	559.101	0.469	0.074	0.475	0.158	0.491	0.001	0.020	0.011	0.012	0.005	0.026	1.157	0.001	0.125	0.011	0.125	0.108	558.123	559.962	0.919	0.029
DS5c	559.101	0.460	0.085	0.468	0.174	0.489	0.001	0.037	0.030	0.012	0.005	0.050	1.145	0.001	0.162	0.011	0.162	0.142	558.124	559.948	0.917	0.037
DS6a	559.101	0.456	0.044	0.458	0.191	0.463	0.001	0.069	0.025	0.012	0.005	0.075	1.123	0.000	0.041	0.011	0.042	0.038	558.135	559.927	0.915	0.011



Cut Name	Cut Description	$\langle \epsilon_{total} \rangle$	$\hat{\epsilon}_{total}$	$\langle \epsilon_{unique} \rangle$	$\hat{\epsilon}_{unique}$	Sacrifice	ΔDP
Enriched Source Detector Cut	Any other detector: isEar	M1: 23.2 % M2: 42.7 %	26.5 ^{+3.8} _{-2.5} % 62.8 ^{+2.0} _{-7.6} %	0.5 % 0.9 %	0.7 ^{+1.1} _{-0.4} % 7.0 ^{+4.9} _{-3.0} %	1.4 % 3.3 %	10%
Coincident Energy Cut	No other detector: (((energy<65.6) (energy>504.4 && energy<516.4) (energy>591.4 && energy<637.8) (energy>841.8 && energy<866.6) (energy>1074.6 && energy<1175.4) (energy>110.6 && energy<175.) (energy>1205. && (energy>1208.6) && energy<175.) (energy>1482.6) && energy<1531. && energy>1331. && isbar) ((energy<44.8) (energy>507.8 && energy>524.6) (energy>1375.4) && iisEar) && energy<1214.) (sumE<1216.2 && sumE<1377.6) (sumE>1383.6 && sumE<1495.8) (sumE>1761.8 && sumE<1765.8) (sumE>2041.6))	M1: 25.2 % M2: 24.4 %	29.9 ^{+3.9} _{-3.6} % 25.6 ^{+2.2} _{-6.0} %	0.6 % 0.4 %	2.0 ^{+1.5} _{-0.9} % 7.0 ^{+4.9} _{-3.0} %	3.1 % 1.8 %	5%
Sum Energy Cut	Note:	M1: 97.1 % M2: 97.6 %	95.9 ^{+1.3} _{-2.0} % 86.0 ^{+2.0} _{-4.5} %	54.4 % 40.3 %	51.7 ^{+4.1} _{-6.0} % 25.6 ^{+7.2} _{-6.0} %	18.3 % 20.4 %	192%
Combined Cuts		M1: 98.3 % M2: 99.0 %	98.6 ^{+0.7} _{-1.3} % 100.0 ^{+0.0} _{-2.3} %	—	—	31.5 % 40.6 %	226%

TABLE XXIII Table of cut descriptions and efficiencies for simulated backgrounds and measured data for the 559 keV peak.

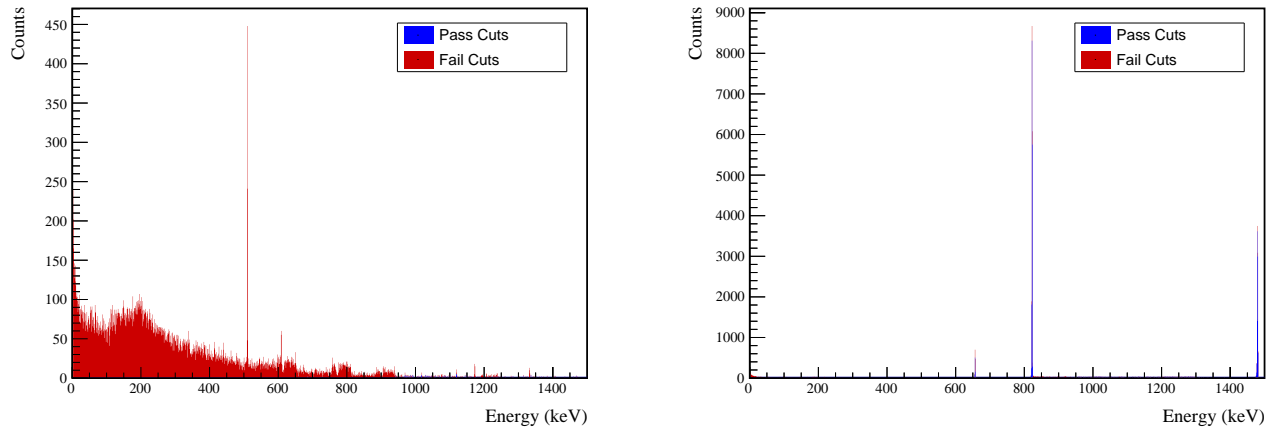


FIG. 83 Effect of 559 keV peak cuts on coincident energy spectra in BG (left) and ES (right) simulations.

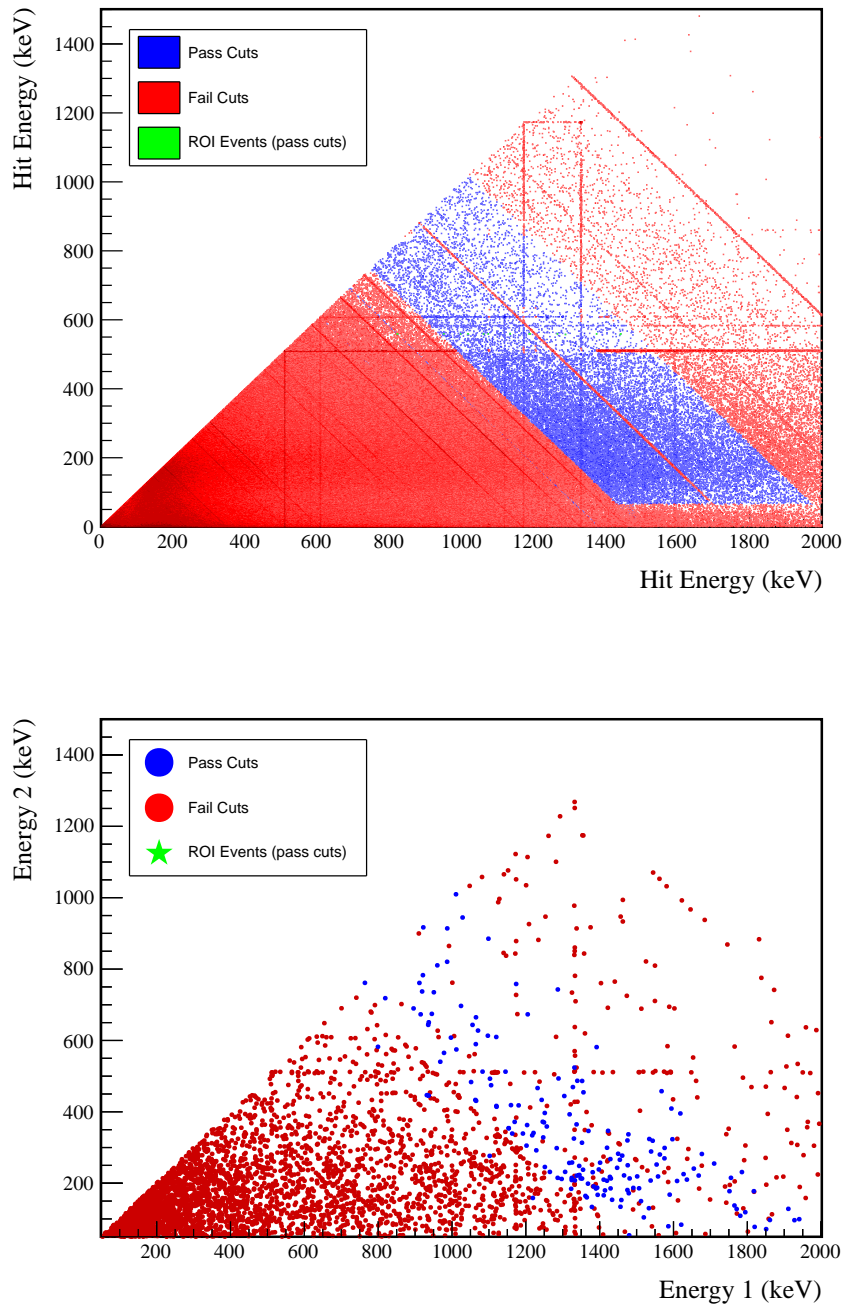
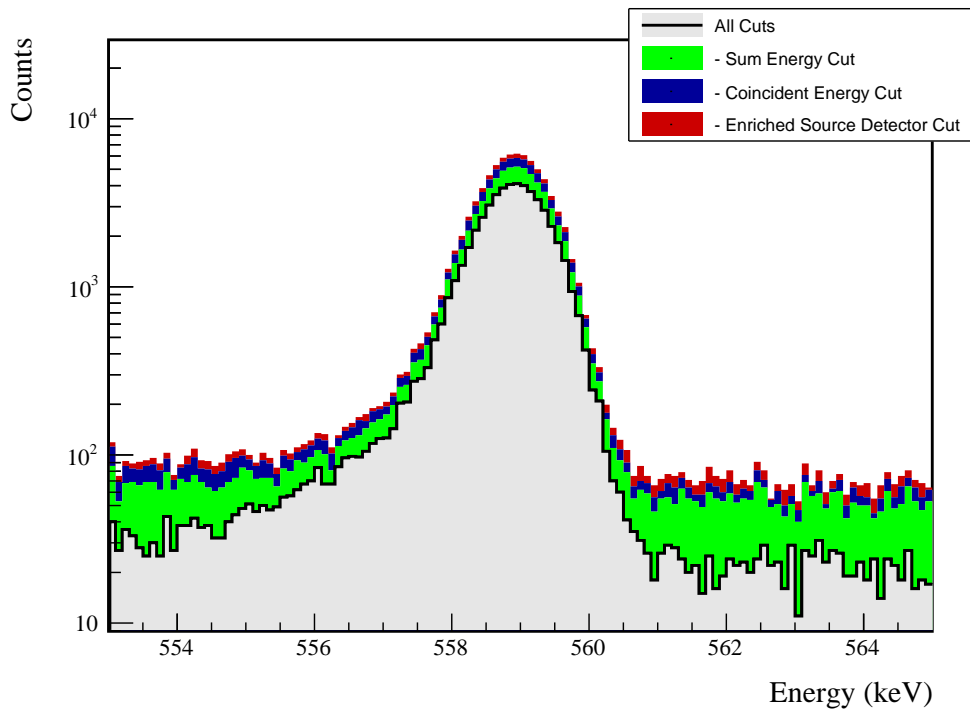


FIG. 84 Simulated (left) and measured (right) multiplicity 2 energy spectrum with sum and coincident energy cuts included for the 559 keV peak.

FIG. 85 Effect of all cuts applied sequentially on ROI for 559 keV peak of $0\nu\beta\beta$ to 2_2^+

Source	Module 1 efficiency	Module 2 efficiency
M. S. Event Signature	$1.8 \pm 0.2\%$	$0.9 \pm 0.5\%$
Region of Interest	$91.3 \pm 1.6\%$	$91.3 \pm 1.6\%$
Dead Layer	$68.5 \pm 5.4\%$	$60.3 \pm 7.0\%$
Detector Dead Times	$97.6 \pm 1.1\%$	$98.1 \pm 0.9\%$
Enriched Source Detector Cut	$98.0 \pm <0.1\%$	$94.7 \pm <0.1\%$
Coincident Energy Cut	$95.7 \pm 0.3\%$	$97.1 \pm 0.3\%$
Sum Energy Cut	$78.9 \pm 0.3\%$	$74.5 \pm 0.3\%$
Final Efficiency	$0.98 \pm 0.14\%$	$0.42 \pm 0.21\%$

FIG. 86 Table of detection efficiencies for the 559 keV peak.

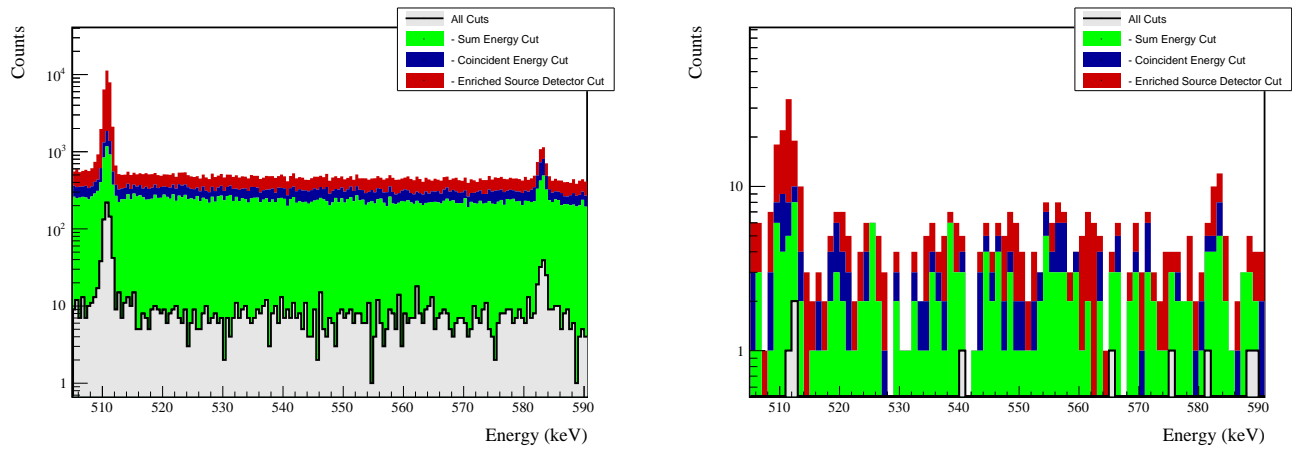
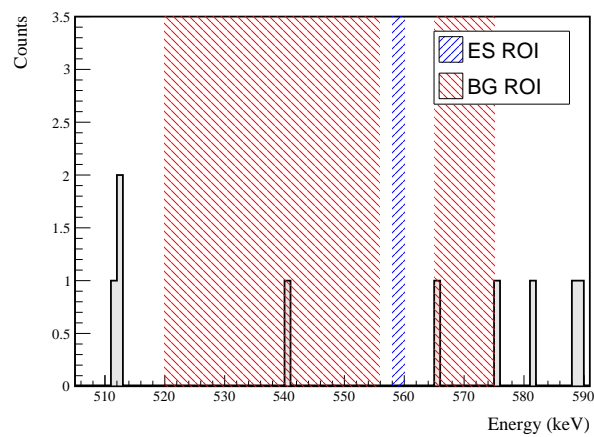


FIG. 87 Effect of all cuts applied to sequentially simulated (left) and measured (right) background data.

FIG. 88 All events after cuts in background (red) and signal (blue) ROIs for 559 keV peak of $0\nu\beta\beta$ to 2_2^+

588 2. 657 keV peak

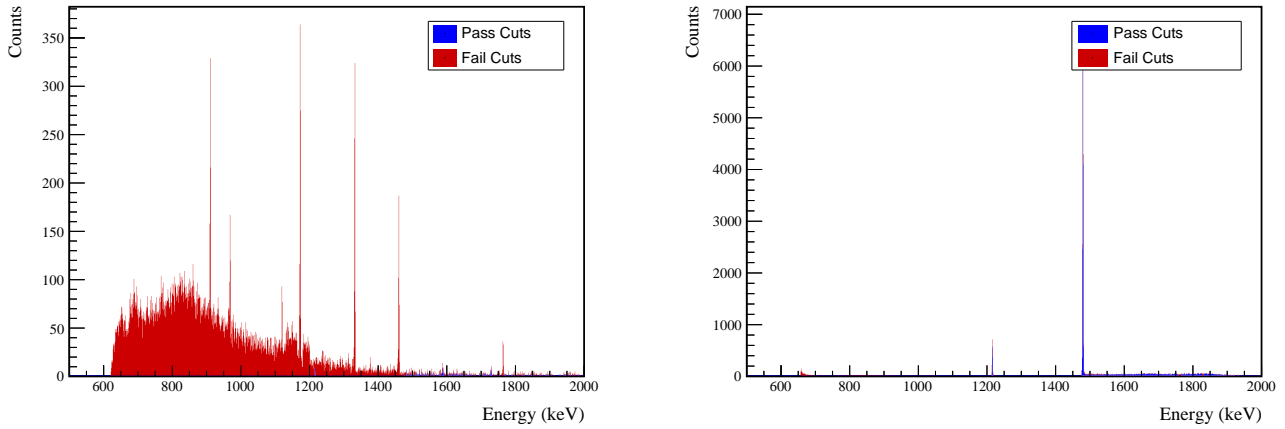


FIG. 89 Effect of 657 keV peak cuts on sum energy spectra in BG (left) and ES (right) simulations.

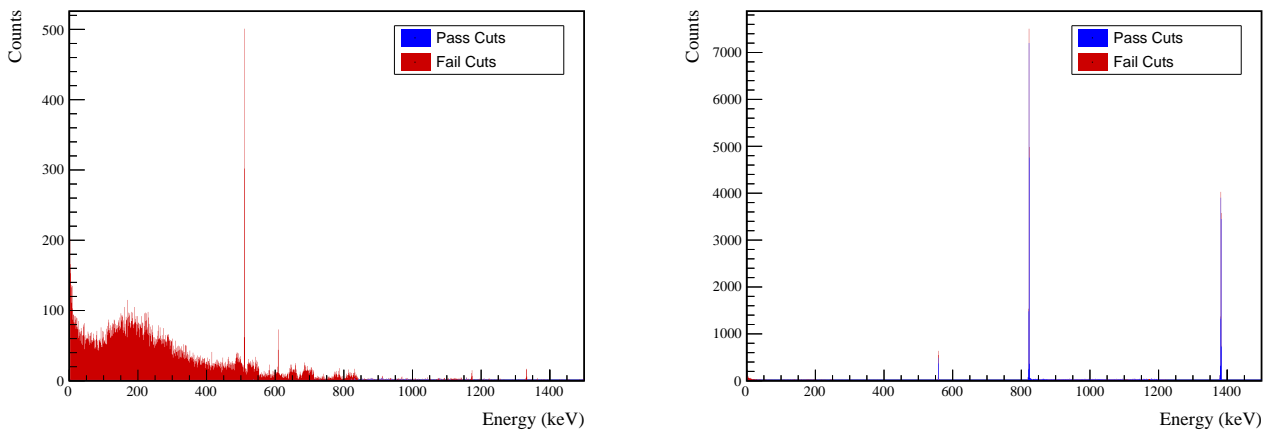


FIG. 90 Effect of 657 keV peak cuts on coincident energy spectra in BG (left) and ES (right) simulations.



TABLE XXIV Table of energy estimation uncertainties for the 657 keV peak.

DS	E_{peak} (keV)	σ_{fit} (keV)	σ_{drift} (keV)	σ (keV)	$f_{t,fit}$	$\tau_{f,fit}$ (keV)	$\delta_{\mu,fit}$ (keV)	$\delta_{\mu,NL}$ (keV)	$\delta_{\mu,drift}$ (keV)	$\delta_{\mu,xtalk}$ (keV)	δ_u (keV)	FWHM (keV)	$\delta_{fwhm,fit}$ (keV)	$\delta_{fwhm,drift}$ (keV)	$\delta_{fwhm,xtalk}$ (keV)	δ_{FWHM} (keV)	δ_α	$E_{ROI,1}$ (keV)	$E_{ROI,2}$ (keV)	ϵ_{ROI}	$\sigma_{e_{ROI}}$	
DS1	657.041	0.500	0.074	0.505	0.230	0.579	0.002	0.104	0.003	0.012	0.005	0.105	1.256	0.001	0.039	0.011	0.040	0.032	656.019	657.882	0.883	0.013
DS2	657.041	0.502	0.064	0.506	0.249	0.580	0.002	0.067	0.005	0.012	0.005	0.068	1.263	0.001	0.107	0.011	0.108	0.085	656.002	657.881	0.885	0.026
DS3	657.041	0.510	0.078	0.516	0.224	0.568	0.002	0.026	0.026	0.012	0.005	0.040	1.278	0.001	0.073	0.011	0.074	0.058	656.007	657.899	0.889	0.018
DS4	657.041	0.493	0.090	0.501	0.108	0.490	0.002	0.076	0.076	0.012	0.005	0.078	1.207	0.001	0.106	0.011	0.107	0.088	656.120	657.890	0.899	0.028
DS5a	657.041	0.606	0.100	0.614	0.106	0.924	0.002	0.079	0.006	0.012	0.005	0.080	1.481	0.002	0.055	0.011	0.056	0.038	655.915	658.075	0.887	0.012
DS5b	657.041	0.509	0.087	0.517	0.158	0.562	0.001	0.020	0.013	0.012	0.005	0.027	1.259	0.001	0.125	0.011	0.125	0.100	656.056	657.909	0.895	0.031
DS5c	657.041	0.500	0.100	0.510	0.174	0.555	0.002	0.037	0.035	0.012	0.005	0.053	1.247	0.001	0.162	0.011	0.162	0.130	656.057	657.896	0.893	0.040
DS6a	657.041	0.495	0.051	0.497	0.191	0.524	0.001	0.069	0.030	0.012	0.005	0.076	1.221	0.001	0.041	0.011	0.042	0.035	656.070	657.874	0.891	0.012



Cut Name	Cut Description	$\langle \epsilon_{total} \rangle$	$\hat{\epsilon}_{total}$	$\langle \epsilon_{unique} \rangle$	$\hat{\epsilon}_{unique}$	Sacrifice	ΔDP
Enriched Source Detector Cut	Any other detector: isEsr No other detector: (((energy<59.) (energy>422.6 && energy<562.4 && energy>616.6) (energy>776.8 && energy<529.4) (energy>159.6 && energy<1175.) (energy>159.6 && energy<1175.) (energy>133.2) (energy>308. && energy>133.2) (energy>384.8) && isEsr) ((energy<52.2) (energy>491.6 && energy<554.8) (energy>1248.) && :isEsr) (sumE<1214.8) (sumE>1216.8 && sumE<1475.2) (sumE>1757.6 && sumE<1766.) (sumE>2042.6) (sumE>2042.6))	M1: 23.9 % M2: 43.7 %	25.2 ^{+3.9} _{-3.5} % 60.4 ^{+6.8} _{-7.2} %	0.6 % 1.2 %	3.7 ^{+2.0} _{-1.3} % 4.2 ^{+3.9} _{-2.1} %	1.4 % 3.7 %	1.2 %
Coincident Energy Cut	M1: 30.4 % M2: 29.1 %	25.2 ^{+3.9} _{-3.5} % 16.7 ^{+6.0} _{-4.7} %	0.8 % 0.6 %	2.2 ^{+1.7} _{-1.0} % 2.1 ^{+3.2} _{-1.3} %	4.9 % 3.2 %	4.9 % 3.2 %	7%
Sum Energy Cut	M1: 96.9 % M2: 97.0 %	88.9 ^{+2.4} _{-3.0} % 91.7 ^{+3.2} _{-4.9} %	49.8 % 36.9 %	48.9 ^{+4.3} _{-4.3} % 27.1 ^{+6.8} _{-5.9} %	11.6 % 13.6 %	11.6 % 13.6 %	207%
Combined Cuts	M1: 98.5 % M2: 99.0 %	94.8 ^{+2.3} _{-1.6} % 97.9 ^{+1.3} _{-3.2} %	— —	— —	25.7 % 34.9 %	25.7 % 34.9 %	255%

TABLE XXV Table of cut descriptions and efficiencies for simulated backgrounds and measured data for the 657 keV peak.

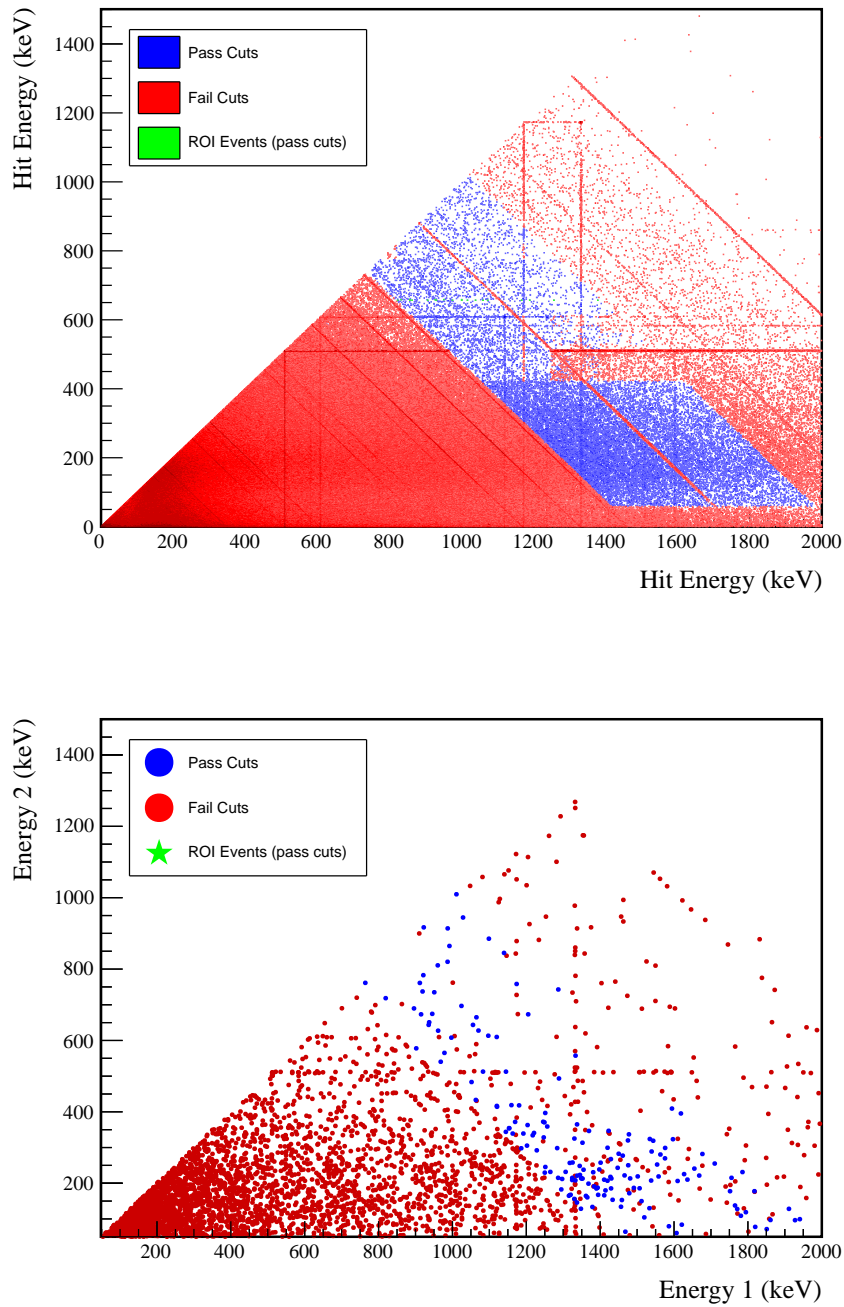
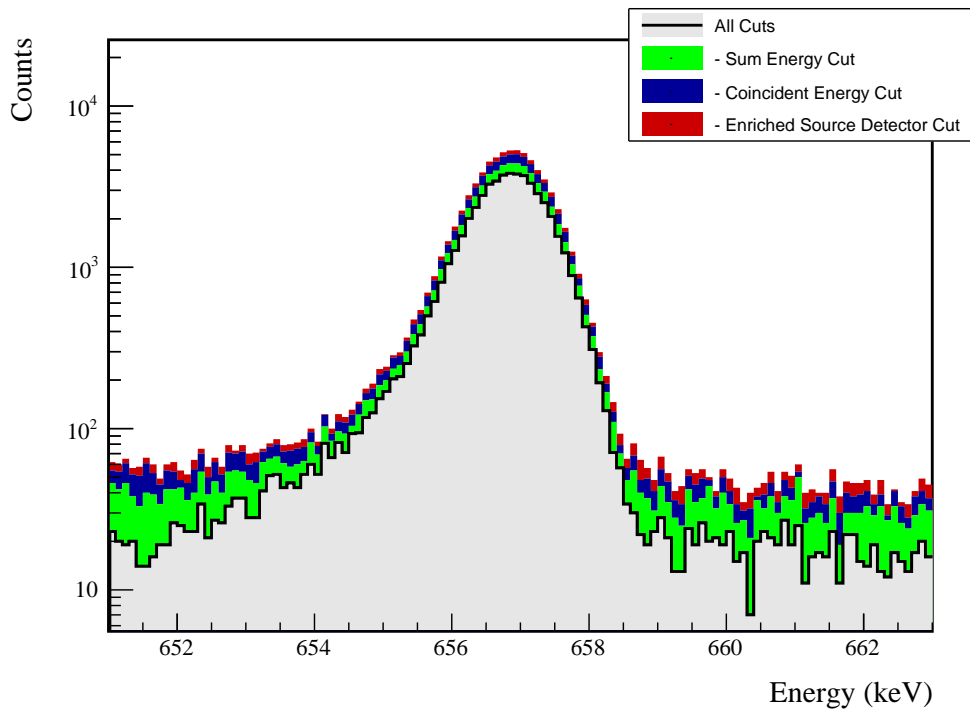


FIG. 91 Simulated (left) and measured (right) multiplicity 2 energy spectrum with sum and coincident energy cuts included for the 657 keV peak.

FIG. 92 Effect of all cuts applied sequentially on ROI for 657 keV peak of $0\nu\beta\beta$ to 2_2^+

Source	Module 1 efficiency	Module 2 efficiency
M. S. Event Signature	$1.6 \pm 0.2\%$	$0.8 \pm 0.5\%$
Region of Interest	$89.0 \pm 1.7\%$	$89.0 \pm 1.7\%$
Dead Layer	$69.6 \pm 5.2\%$	$61.1 \pm 6.8\%$
Detector Dead Times	$97.6 \pm 1.1\%$	$98.1 \pm 0.9\%$
Enriched Source Detector Cut	$98.2 \pm <0.1\%$	$94.6 \pm <0.1\%$
Coincident Energy Cut	$93.9 \pm 0.3\%$	$95.3 \pm 0.3\%$
Sum Energy Cut	$86.5 \pm 0.3\%$	$82.8 \pm 0.3\%$
Final Efficiency	$0.95 \pm 0.14\%$	$0.41 \pm 0.23\%$

FIG. 93 Table of detection efficiencies for the 657 keV peak.

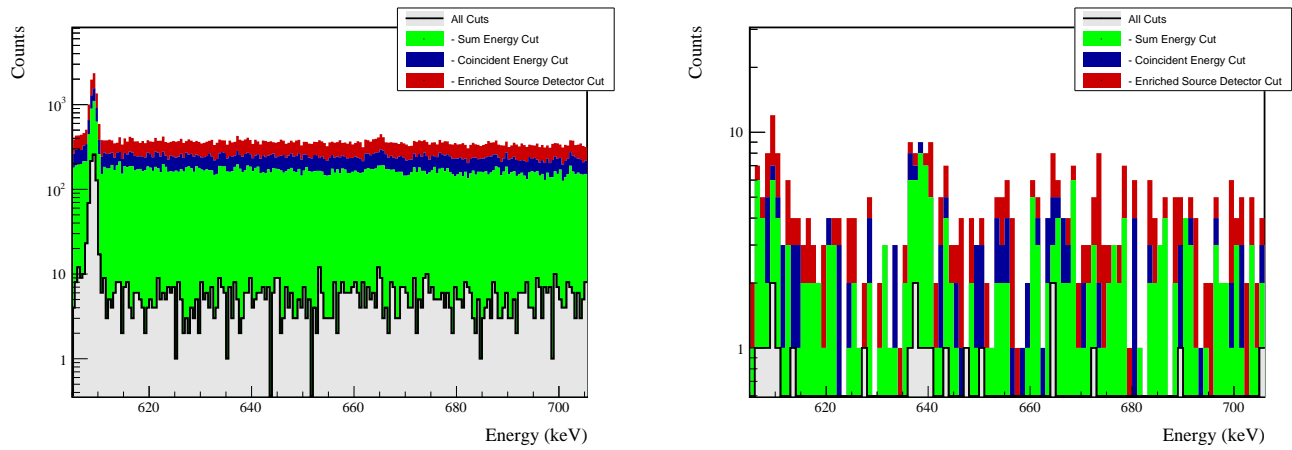
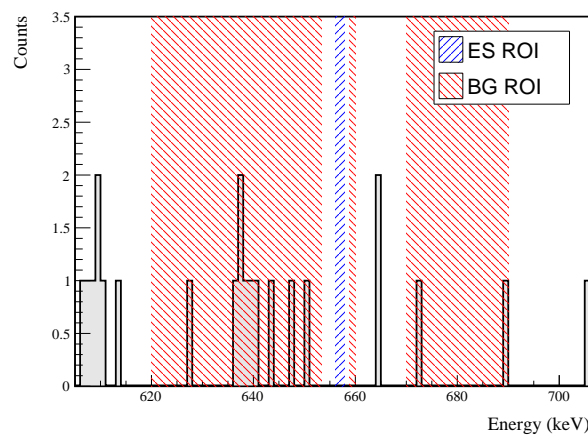


FIG. 94 Effect of all cuts applied to sequentially simulated (left) and measured (right) background data.

FIG. 95 All events after cuts in background (red) and signal (blue) ROIs for 657 keV peak of $0\nu\beta\beta$ to 2_2^+



589 3. 1216 keV peak

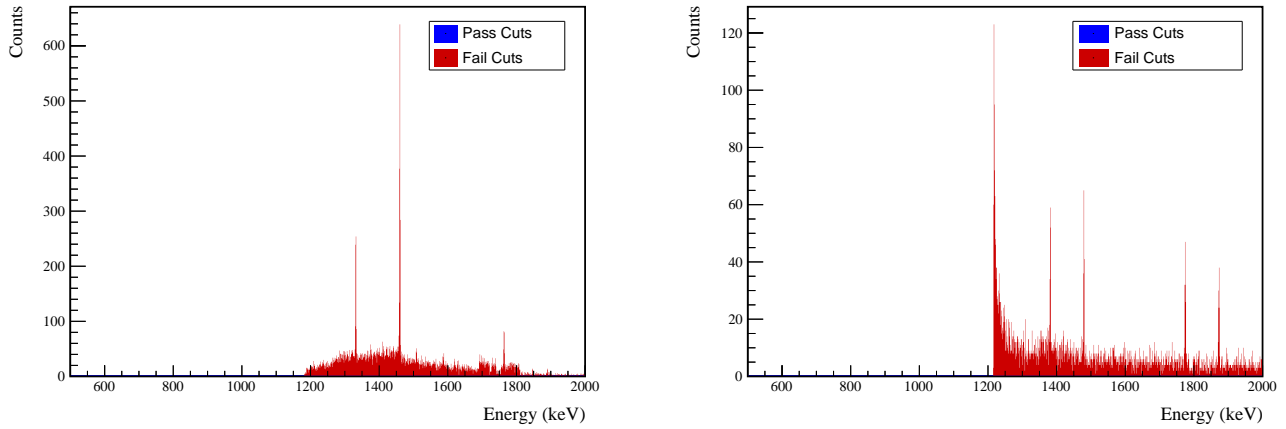


FIG. 96 Effect of 1216 keV peak cuts on sum energy spectra in BG (left) and ES (right) simulations.

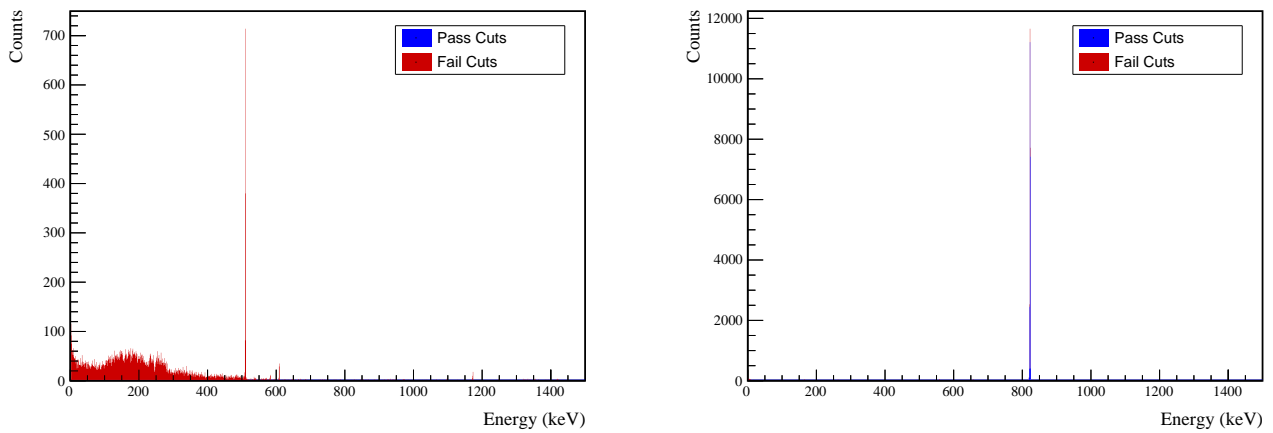


FIG. 97 Effect of 1216 keV peak cuts on coincident energy spectra in BG (left) and ES (right) simulations.



TABLE XXVI Table of energy estimation uncertainties for the 1216 keV peak.

DS	E_{peak} (keV)	σ_{fit} (keV)	σ_{drift} (keV)	σ (keV)	$f_{t,fit}$	τ_{fit} (keV)	$\delta_{\mu,NL}$ (keV)	$\delta_{\mu,drift}$ (keV)	$\delta_{\mu,xtalk}$ (keV)	$\delta_{\mu,peak}$ (keV)	δ_μ (keV)	FWHM	$\delta_{fwhm,fit}$ (keV)	$\delta_{fwhm,drift}$ (keV)	$\delta_{fwhm,xtalk}$ (keV)	δ_{FWHM} (keV)	δ_α	$E_{ROI,1}$ (keV)	$E_{ROI,2}$ (keV)	ϵ_{ROI}	$\sigma_{e_{ROI}}$	
DS1	1216.104	0.705	0.137	0.718	0.230	0.945	0.003	0.104	0.005	0.012	0.020	0.107	1.787	0.001	0.039	0.011	0.040	0.023	1214.426	1217.449	0.914	0.006
DS2	1216.104	0.710	0.119	0.720	0.249	0.951	0.003	0.067	0.008	0.012	0.020	0.072	1.803	0.001	0.107	0.011	0.108	0.060	1214.387	1217.449	0.914	0.014
DS3	1216.104	0.715	0.144	0.729	0.224	0.925	0.003	0.026	0.051	0.012	0.020	0.062	1.812	0.001	0.073	0.011	0.074	0.041	1214.416	1217.470	0.917	0.010
DS4	1216.104	0.697	0.167	0.717	0.108	0.746	0.003	0.076	0.022	0.012	0.020	0.083	1.726	0.001	0.106	0.011	0.107	0.062	1214.621	1217.461	0.932	0.015
DS5a	1216.104	0.838	0.185	0.859	0.106	1.316	0.004	0.079	0.012	0.012	0.020	0.083	2.070	0.002	0.055	0.011	0.056	0.027	1214.323	1217.722	0.921	0.007
DS5b	1216.104	0.716	0.161	0.734	0.158	0.963	0.002	0.020	0.024	0.012	0.020	0.039	1.791	0.001	0.125	0.011	0.125	0.070	1214.506	1217.487	0.922	0.017
DS5c	1216.104	0.703	0.185	0.727	0.174	0.932	0.003	0.037	0.066	0.012	0.020	0.079	1.783	0.001	0.162	0.011	0.162	0.091	1214.497	1217.474	0.921	0.022
DS6a	1216.104	0.693	0.095	0.700	0.191	0.873	0.002	0.069	0.055	0.012	0.020	0.092	1.723	0.001	0.041	0.011	0.042	0.025	1214.535	1217.422	0.920	0.006



Cut Name	Cut Description	$\langle \epsilon_{total} \rangle$	$\hat{\epsilon}_{total}$	$\langle \epsilon_{unique} \rangle$	$\hat{\epsilon}_{unique}$	Sacrifice	ΔDP
Enriched Source	Any other detector: isEnr	M1: 26.9 %	16.9 ^{+4.5} / _{-3.7} %	0.0 %	0.0 ^{+1.2} / _{-0.0} %	2.0 %	-2%
Detector Cut		M2: 43.9 %	61.9 ^{+9.8} / _{-10.9} %	0.0 %	0.0 ^{+4.5} / _{-0.0} %	4.3 %	
Multiplicity 2 Cut	m==2	M1: 15.3 %	16.9 ^{+4.5} / _{-3.7} %	0.0 %	0.0 ^{+1.2} / _{-0.0} %	0.0 %	0%
		M2: 11.9 %	9.5 ^{+8.4} / _{-4.7} %	0.0 %	0.0 ^{+4.5} / _{-0.0} %	0.0 %	
Coincident Energy Cut	Any other detector: energy>817.7 && energy<826.4	M1: 100.0 %	100.0 ^{+0.0} / _{-1.2} %	59.6 %	68.7 ^{+4.8} / _{-5.3} %	18.7 %	555%
Combined Cuts		M2: 100.0 %	100.0 ^{+0.0} / _{-4.5} %	46.6 %	33.3 ^{+10.8} / _{-9.3} %	17.9 %	
		M1: 100.0 %	100.0 ^{+0.0} / _{-1.2} %	—	—	25.2 %	
		M2: 100.0 %	100.0 ^{+0.0} / _{-4.5} %	—	—	28.7 %	669%

TABLE XXVII Table of cut descriptions and efficiencies for simulated backgrounds and measured data for the 1216 keV peak.

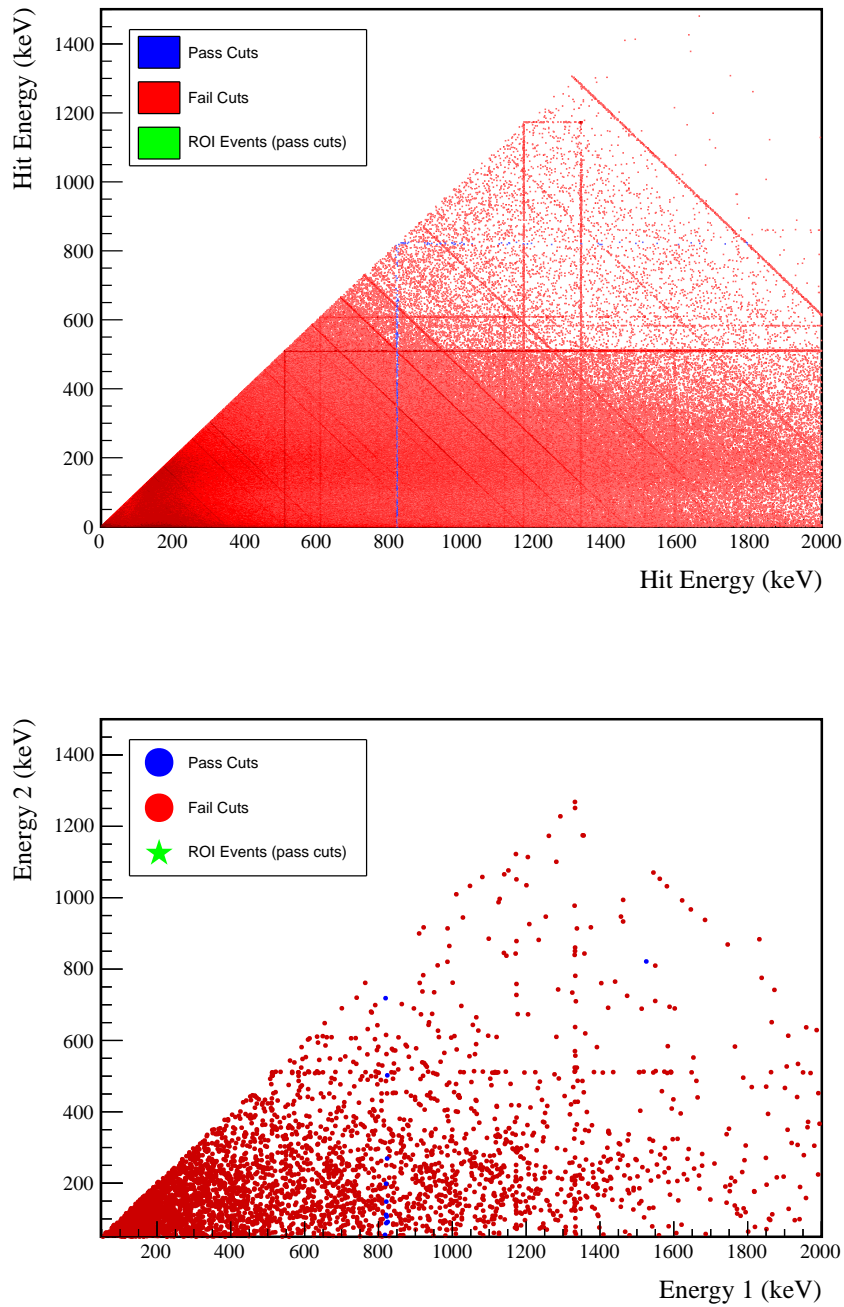
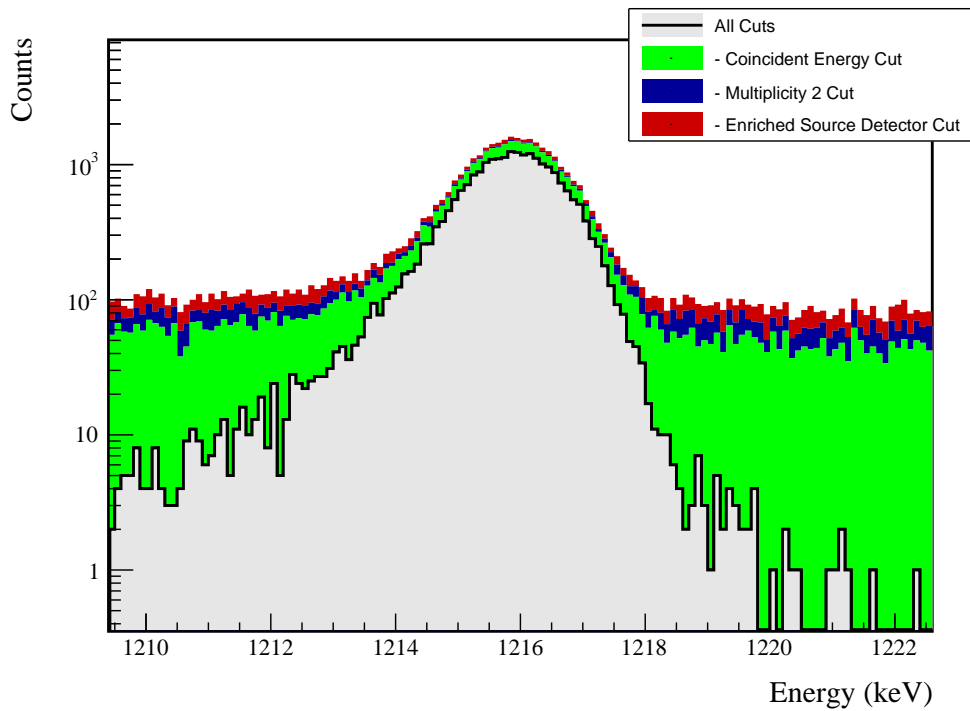


FIG. 98 Simulated (left) and measured (right) multiplicity 2 energy spectrum with sum and coincident energy cuts included for the 1216 keV peak.

FIG. 99 Effect of all cuts applied sequentially on ROI for 1216 keV peak of $0\nu\beta\beta$ to 2_2^+

Source	Module 1 efficiency	Module 2 efficiency
M. S. Event Signature	$0.8 \pm 0.2\%$	$0.4 \pm 0.5\%$
Region of Interest	$92.0 \pm 0.9\%$	$92.0 \pm 0.9\%$
Dead Layer	$68.8 \pm 5.3\%$	$61.2 \pm 6.8\%$
Detector Dead Times	$97.5 \pm 1.1\%$	$98.0 \pm 0.9\%$
Enriched Source Detector Cut	$97.3 \pm <0.1\%$	$94.3 \pm <0.1\%$
Multiplicity 2 Cut	$100.0 \pm <0.1\%$	$100.0 \pm <0.1\%$
Coincident Energy Cut	$80.0 \pm 0.3\%$	$79.9 \pm 0.3\%$
Final Efficiency	$0.44 \pm 0.12\%$	$0.19 \pm 0.24\%$

FIG. 100 Table of detection efficiencies for the 1216 keV peak.

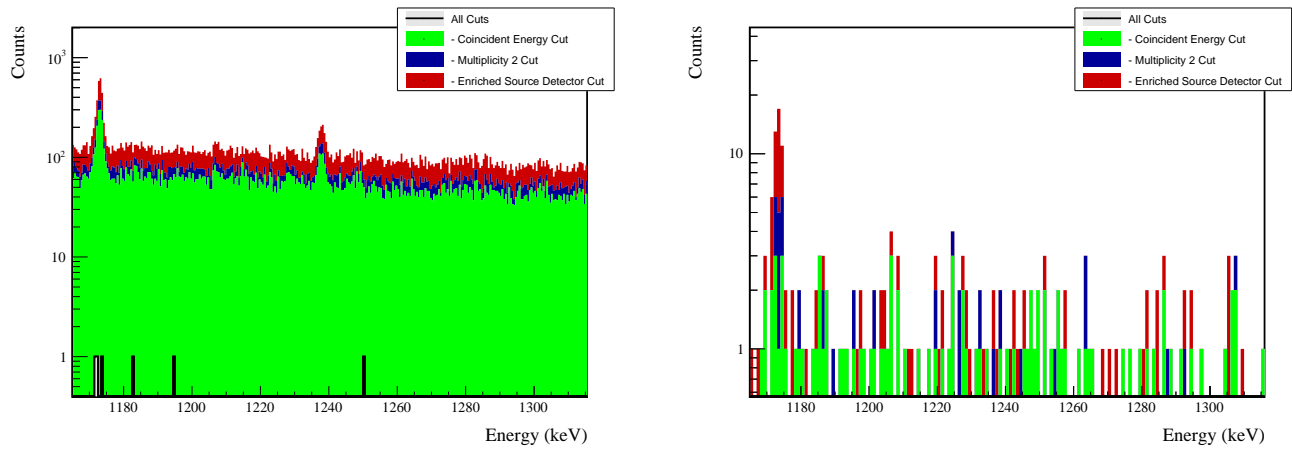


FIG. 101 Effect of all cuts applied to sequentially simulated (left) and measured (right) background data.

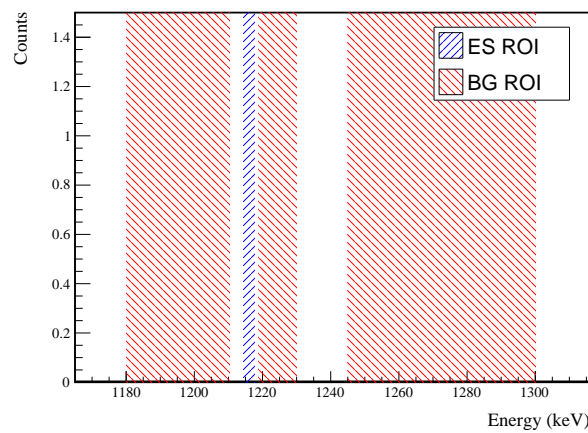


FIG. 102 All events after cuts in background (red) and signal (blue) ROIs for 1216 keV peak of $0\nu\beta\beta$ to 2_2^+